Optimisation of Electroless Co-deposited Solid Oxide Fuel Cell Electrodes

by

Nkem O.E. Nwosu (B.Sc, M.Sc)

A thesis submitted in partial fulfilment of the requirements
of Edinburgh Napier University, for the award of
Doctor of Philosophy

June 2013

DECLARATION

I hereby declare that this work has been carried out in its entirety by me at Edinburgh Napier University. Neither the thesis nor the original work has been previously submitted to this or any other university for the award of a higher degree.

_____ Nkem Nwosu
(Candidate)

_____ Date

Dedication

…..to my beautiful wife, best friend and pillar, Julian, and my amazing children, Melanie and Ashley, who fill me with joy and happiness.

ACKNOWLEDGMENTS

My sincere gratitude goes to Edinburgh Napier University and the Scottish Funding Council for sponsoring this project. Being a recipient of a university studentship and a Scottish Overseas Research Student Award (SORSAS) ensured that I was financially stable during the project.

Mr Alan Davidson who supervised my work and Mr Colin Hindle who gave me advice on a continuous basis are acknowledged for the time, patience and diligence they extended towards me.

In addition to thanking Dr Callum Wilson and Dr Neil Shearer for their ever willingness to assist me with any difficulty I experienced during my time in the laboratory, the invaluable trainings and support provided by Mrs Lynn Chalmers on how to use practically every equipment in the laboratory cannot go without mention. To Lynn, I truly say thank you very much.

My utmost gratitude goes to Chief C.J. Umeadi for his unflinching support during this project. His dominant role in ensuring that all the necessary non-academic prerequisites were in place prior to, and during the project, is truly acknowledged.

Finally, to God who made this project a possibility. Without his works in a mysterious and miraculous way, my undertaking of this project would not have been possible at all.

ABSTRACT

Research already carried out on the use of the recently patented electroless nickel ceramic codeposition technique as a method of manufacturing solid oxide fuel cell (SOFC) electrodes has thus far indicated that, while functional electrodes can be manufactured by the technique, for optimum performance of the cell, amplification of the ceramic content of the coatings is still required**.**

By mainly employing external agents such as surface active agents (surfactants) and magnetic fields (in a bid to aid ceramic particle stability), this research focused on the prospect of increasing the ceramic content of cermets co-deposited for use as SOFC electrodes. A total of 137 co-deposited samples were produced from different bath compositions.

As a prelude to the study, the interactions between the ceramic powders used (yttria stabilised zirconia (YSZ) / lanthanum strontium manganate (LSM)) and the medium for the deposition process – the electroless nickel solution, were investigated by zeta potentiometry and ultraviolet-visible spectroscopy techniques. The results obtained from the studies led to a variation of a series of fundamental plating factors such as the ceramic bath loading and particle size of the powders. While the former was found to yield the highest ceramic content in the coating at a bath loading of 50 g/l, variation of latter notably produced mixed results.

With the introduction of surfactants, it was noted that above the surfactant's (sodium dodecyl sulphate) critical micelle concentration, the incorporation of ceramic particles (YSZ) into the nickel matrix steadily increased to as much as 60 volume %. An inverse relationship was though found to exist between the coating thickness and the surfactant's bath concentration.

Uniform coatings were found to be associated with low magnetic field strengths while although increased magnetic field strengths positively resulted in the amplification of particle incorporation into the coating, a lack of cohesion between the coating and the substrate – as indicated by coating flake-off, was observed at such strengths. It is suggested that because the magnetic flux was more dominant than the normally ionic plating mechanism, the particles co-deposited under the influence of a high magnetic field were relatively unstable after the coating process.

Since LSM is alkaline in nature this work confirms that future research on the application of electroless nickel ceramic co-deposition as a method of manufacturing SOFC cathodes, be focused on the use of alkaline electroless nickel baths rather than the acidic solutions, which better suite YSZ particles.

CONTENTS

DECLARATION ii

DEDICATION iii

ACKNOWLEDGMENTS iv

ABSTRACT v

CONTENTS vi

LIST OF FIGURES xii

LIST OF TABLES xvii

LIST OF SYMBOLS xix

ABBREVIATED TERMS xx

1. General Introduction 1

1.0 Introduction 2

2. Literature review 6

2.1 Overview of solid oxide fuel cell technology 7

2.2 Components of a solid oxide fuel cell 12

2.2.1 Electrolyte 12

2.2.2 Anode 14

2.2.3 Cathode 15

2.2.4 Interconnect 17

2.3 Structure of electrodes 18

2.4 Current and emerging methods of electrode manufacture 19

2.4.1 Screen printing 19

2.4.2 Chemical vapour deposition 21

2.4.3 Laser reactive deposition 22

2.4.4 Electrophoretic deposition 24

2.4.5 Freeze drying 25

2.5 Cell testing 25

2.5.1 Four point conductivity test 26

2.5.2 Electrochemical Impedance Spectroscopy 27

3. Electroless nickel co-deposition as a method of manufacturing SOFC electrodes: Evolution, process and characterisation 29

3.0 Introduction 30

3.1 Substrate preparation and the co-deposition process 31

3.2 Factors influencing the ECD process 35

3.2.1 Bath additives 35

3.2.2 Potential Hydrogen (pH) 37

3.3.3 Plating temperature 38

3.3 Pre and post co-deposition characterisation techniques 38

3.3.1 Pre co-deposition 38

3.3.1.1 Ultra violet visible spectrophotometry 38

3.3.1.2 Zeta potentiometry 42

3.3.2 Post co-deposition 43

3.3.2.1 Optical and scanning electron microscopy 43

3.3.2.2 Energy Dispersive X-ray Analysis 44

3.3.2.3 Mercury intrusion porosimetry (MIP) 44

3.3.2.4 Atomic force microscopy 45

4. Potential plating aids: Surfactants and magnets 47

4.0 Introduction 48

4.1 Surface active agents (surfactants) 48

4.1.1 Rudiments of surface active agents (surfactants) 48

4.1.2 Essential criteria for surfactant selection 49

4.1.3 Surfactant selection 50

4.1.3.1 Synthesis of block co-polymer surfactant, PMMA/ PS 53

4.2 Magnets 59

4.2.1 Magnetic properties of LSM particles 60

4.2.1.1 Magnetic susceptibility of selected LSM powders 62

4.3 Other variables considered 62

4.3.1 Bath loading 62

4.3.2 Particle size 63

4.3.3 Rate of agitation 63

5. Experimental work – Part I: Preliminary assessments 64

5.0 Introduction 65

5.1 Electroless nickel solution – ceramic particle 65

5.1.1 Assessment by ultraviolet visible spectrophotometry 65

5.1.1.1 Sample preparation 65

5.1.1.2 Analysis 68

5.1.1.3 Result of EN solution – ceramic particles PPR experiment 69

5.1.2 Zeta potential assessment of YSZ & LSM particles in an EN solution 70

5.2 Electroless nickel solution – ceramic particles – surfactants 72

5.2.1 Zeta potential assessments: Influence of surfactants 74

5.3 Conclusions 75

6. Experimental work – Part II: Co-deposition **77**

6.0 Introduction 78

6.1 Experimental materials 78

6.1.1 Substrate 78

6.1.2 Ceramic powder 79

6.1.3 Pre-treatment chemicals 80

6.1.3.1 Cuprolite 80

6.1.3.2 Pre-catalyst 80

6.1.3.3 Catalyst 82

6.1.3.3.1 Stability of the catalyst 83

6.1.3.4 Niplast at 78 85

6.1.4 Plating solutions 85

6.1.4.1 Acidic electroless nickel solution 86

6.1.4.2 Alkaline electroless nickel solution 86

6.2 Post co-deposition sample preparation and characterisation equipment 89

6.3 Co-deposition 89

6.3.1 Determination of suitable ceramic bath loading for the coating Process 89

6.3.1.1 Control run 90

6.3.1.1.1 Result I: Plain coatings 90

6.3.1.2 Nickel/YSZ co-deposition 91

6.3.1.2.1 Result II: Co-deposition of nickel/YSZ in free-from external agents EN solutions 92

6.3.1.2.2 Inference 96

6.3.1.3 Nickel/LSM co-deposition 97

6.3.1.3.1 Result III: Co-deposition of nickel/LSM in free-from external agents EN solutions 97

6.3.1.4 Effect of LSM on the pH of acidic EN solution 99

6.3.1.4.1 EN/LSM pH study 1 101

6.3.1.4.2 EN/LSM pH study 2 102

6.3.1.4.3 EN/LSM pH study 3 102

6.3.1.4.4 Chemistry of LSM 103

6.3.1.5 Alkaline LSM plating 103

6.3.2 Influence of surfactants 107

6.3.2.1 Design of experiment 107

6.3.2.2 Result IV: Effect of SDS on the composition of electroless nickel -YSZ coating 108

6.3.2.3 Favourable effect(s) of SDS incorporation on SOFC electrodes manufactured by ECD 111

6.3.2.3.1 Composition 111

6.3.2.3.2 Surface morphology 113

6.3.2.4 Unfavourable effect(s) of SDS incorporation on SOFC electrodes manufactured by ECD 115

6.3.2.4.1 Coating thickness 115

6.3.2.4.2 Coating coherence 118

6.3.3 Influence of a magnetic field 119

6.3.3.1 Magnetic orientation of YSZ 119

6.3.3.2 Co-deposition of LSM particles under the influence of a magnetic field 120

6.3.3.2.1 Experimental setup 120

6.3.3.2.2 Experimental procedure and rationale 121

6.3.3.3 Findings 122

6.3.3.4 Coating adhesion and composition versus magnetic field strength 124

6.3.3.5 Agitation rate and magnetic field 126

6.3.3.5.1 Result V: Effect of agitation rate on the nature of coatings manufactured under the influence of a magnetic field 127

6.3.3.6 Effect of alkaline baths 129

6.3.3.7 Effect of powder composition 131

6.3.3.8 Effect of plating duration 131

6.3.3.9 Effect on surface topography 132

7. Conclusion 134

8. Contribution to knowledge 139

9. Future work 140

10. Publications 142

REFERENCES 143

APPENDIX A 147

APPENDIX B 151

APPENDIX C 154

LIST OF FIGURES

Figure Number	Title	Page
1	Schematic representation of (a) a case containing a stack of cells and (b) a unit cell comprising an anode, cathode and electrolyte.	9
2	Representation of basic SOFC inputs and outputs	10
3	Schematic representation of fuel flow and a planner stack assembly	10
4	Schematic representation of tubular SOFC	11
5	Illustration of a monolithic SOFC	11
6	YSZ/ ScSZ conductivity against % yttria/ scandia doping at 1000^{o}C	13
7	Scanning electron micrograph of a commercial SOFC electrolyte	14
8	Image of a Presco model 465 semi automatic screen printer	20
9	Scanning electron micrograph of a screen printed commercial cathode showing high porosity network	20
10	CVD deposition rate as a function of temperature	21
11	Sticking probability as a function of substrate aspect ratio	22
12	Schematic representation of laser reactive deposition (LRD)	23
13	Schematic diagram of cell configuration for EPD of YSZ on an LSM or LSM-YSZ substrate	24
14	Conductivity vs. temperature plot of a four point probe tested commercial SOFC cathode	27
15	Deposition as a factor of time	33
16	Stages of electroless nickel-ceramic co-deposition process	34
17	Effect of hypophosphite reducing agent concentration on Ni-P alloy composition	36
18	Acidic slotonip 1850 electroless nickel solution	40
19	Schematic representation of the green octahedral hexaquonickel ion ($[Ni(H_2O)_6]^{+2}$)	40
20	UV-Vis spectra of slotonip 1850 electroless nickel plating solution	41
21	Simplified schematic representation of a single surfactant molecule	48
22	Surfactant concentration vs critical micelle concentration and surface tension	50
23	Chemical structure of a dissociated sodium dodecyl sulphate molecule	51

24	Molecular structure of polyethylene	52
25	Molecular structure of (a) polystyrene and (b) polymethyl methacrylate	52
26	Image of a five neck condenser vessel with constituents	54
27	Image of dried polymethyl methacrylate/ poly styrene	55
28	I.R Spectrometry of polymethyl methacrylate	56
29	I.R Spectrometry of poly styrene co-polymer	57
30	I.R Spectrometry of polymethyl methacrylate/ poly styrene co-polymer	58
31	Illustration of particle attraction to the substrate	59
32	Crystallographic structure of Lanthanum Strontium Manganate showing A- , B- and X sites	60
33	Illustration of (a) La, Sr, Mn and O ionic interaction and (b) Mn-O electron orbital exchange typical of the double exchange mechanism	61
34	Schematic representation of the possible effect of particle size on particle incorporation during electroless nickel ceramic co-deposition	63
35	Dominant peak of acidic UV–VIS spectra of acidic electroless nickel solution	66
36	Absorption of electroless nickel solution at 392.8nm	67
37	Images of the electroless nickel solution (a) before and after the introduction of (b) YSZ and (c) LSM powders	68
38	Schematic representation of Beer Lambert law showing incident light beam, precipitated particles and particles in suspension	68
39	Sedimentation patterns of both LSM and YSZ particles in an acidic electroless nickel solution	69
40	Absorption vs. time plot of YSZ particles in deionised water	70
41	Size distribution of YSZ particles in water and EN solution	72
42	Effect of PMMA/PS and SDS on YSZ and LSM dispersion stability	73
43	Absorption as a function of time for an EN solution containing YSZ particles and various concentrations of SDS surfactant	73
44	Absorption as a function of time for an EN solution containing LSM particles and various concentrations of SDS surfactant	74
45	Zeta potential of YSZ particles in an EN solution containing various concentrations of SDS surfactant	75
46	Image of an alumina tile used for the co-deposition process	79
47	Field emission scanning electron micrograph of ceramic particles	81

48	Energy dispersive x-ray spectrum of LSM_{20} powder	81
49	Image of catalyst solution (a) freshly made up and (b) after 120hours of exposure to air	83
50	UV-Vis spectra of catalyst solution (a) freshly made up and (b) expired	84
51	Transformation of (a) green octahedral hexaquonickel ions to (b) blue nickel-ammonia complex with increasing ammonium hydroxide concentration	88
52	(a) Image of an EN coating produced from a solution devoid of any ceramic in the bath and (b) photo micrograph of the coating showing its cross sectional view	91
53	Image of electroless nickel coatings produced from (a) bath SC 1 (b) bath SC 2 (c) bath SC 3	93
54	Photo micrographs of the cross section of electroless nickel – YSZ coatings produced from baths (a) SC 1 (b) SC 2 (c) SC 3	95
55	Relationship of YSZ bath concentration, coating thickness and ceramic content In the coating	96
56	SEM micrograph of electroless Ni - LSM_{20} coatings produced from bath SC 5	98
57	EDXA spectra of electroless Ni - LSM_{20} coating from bath SC 5	98
58	SEM micrograph of electroless Ni - LSM_{20} after 15 minutes. Coatings were produced from bath SC 5	100
59	EDXA spectrum of electroless Ni - LSM_{20} after 15 minutes. Coatings were produced from bath SC 5	100
60	SEM micrograph of a plain electroless nickel plating produced from bath SC 10 (x1000 magnification)	104
61	SEM micrograph of an electroless nickel - LSM plating produced from bath SC 15 (x1000 magnification)	105
62	SEM micrograph of an electroless nickel - LSM plating produced from bath SC 15 (x5220 magnification)	105
63	EDXA spectrum of electroless Ni - LSM_{20} coating from bath SC 15	106
64	SEM micrograph of a plain electroless nickel plating produced from bath SC 15 (x18 magnification)	106
65	EDXA spectrum of electroless Ni -1µM YSZ - 0.3 g/l SDS coating from bath SC 16	110
66	EDXA spectrum of electroless Ni - 1µM YSZ - 0.6 g/l SDS coating from bath SC 17	110
67	EDXA spectrum of electroless Ni - 1µM YSZ - 0.9 g/l SDS coating from bath SC 18	110

68	Composition of Ni -1µm YSZ coatings with various concentrations of SDS	111
69	Composition of Ni- 5µm YSZ coatings with various concentrations of SDS	112
70	Illustration of the effect of critical micelle concentration (CMC) on coating composition	113
71	SEM micrograph of Ni - 1 µm YSZ - 0.3 g/l SDS coatings from bath SC 16	114
72	SEM micrograph of Ni - 1 µm YSZ - 0.6 g/l SDS coatings from bath SC 17	114
73	SEM micrograph of Ni - 1 µm YSZ - 0.9 g/l SDS coatings from bath SC 18	114
74	Influence of SDS on the coating thickness of Ni – 1µm YSZ coatings	116
75	Influence of SDS on the coating thickness of Ni – 5µm YSZ coatings	116
76	Schematic diagram of surfactant aided hydrogen evolution	117
77	Photo micrograph of an Ni - 1µm YSZ - 0.6g/l SDS coating.	118
78	Adsorption isotherm of FC surfactant	119
79	Experimental setup for magnetic Ni – LSM co-deposition process	121
80	Side (a) and aerial (b) views of a substrate immersed in an electroless Ni – LSM coating	123
81	EDXA spectrum of an acidic electroless Ni – LSM coating deposited from bath SC 24	124
82	EDXA spectrum of an acidic electroless Ni – LSM coating deposited from bath SC 26.	125
83	Image of an acidic electroless nickel – LSM coating deposited under the Influence of a 200 mT magnetic field. (a) Just coated (b) after washing, drying and rubbing	125
84	Typical relationship between the coating composition, bond strength and strength of magnetic field used during the co-deposition process	126
85	Image of acidic electroless nickel – LSM coating manufactured under 65mT magnetic field strength at an agitation speed of 300 rpm	128
86	Image of acidic electroless nickel – LSM coating manufactured under 65 mT magnetic field strength at an agitation speed of 400 rpm	128
87	Image of acidic electroless nickel – LSM coating manufactured under 65 mT magnetic field strength at an agitation speed of 500 rpm	128
88	Image of 2 alkaline electroless nickel – LSM coatings manufactured under the influence of 200 mT magnetic field strength	130

89	AFM topographical scan of the surface an AD 96 alumina tile	132
90	AFM topographical scan of the surface a plain electroless nickel coating – bath SC10	132
91	AFM topographical scan of the surface an Ni-LSM coating from bath SC 27	133
92	AFM topographical scan of the surface an Ni-LSM coating from bath SC 29	134
93	AFM topographical scan of the surface an Ni-LSM coating from bath SC 32	134

LIST OF TABLES

Table Number	Title	Page
1	Common fuel cell types	8
2	Stability of particles in relation to zeta potential	43
3	Extract of polymer reactivity ratios	53
4	Zeta potential of LSM and YSZ particles in deionised water and electroless nickel solutions	71
5	Composition of alkaline plating bath	87
6	Setup I: Experimental matrix for the study of the effect of bath loading on the composition of electroless nickel – YSZ coatings	92
7	Composition of electroless nickel – YSZ coatings	94
8	Thickness of electroless nickel – YSZ coatings as a function of YSZ bath concentration	96
9	Setup II: Experimental matrix for the study of the effect of bath loading on the composition of electroless nickel – LSM coatings	97
10	pH of EN solution as a function of bath composition	101
11	Influence of LSM on the pH of an acidic electroless nickel solution	102
12	Setup III: Experimental matrix for the study of the effect of bath loading on the com position of alkaline electroless nickel – LSM coatings	103
13	Composition of alkaline electroless nickel – LSM coatings	104
14	DoE I: Experimental setup for surfactant (SDS) incorporated coatings	108
15	Composition of electroless nickel – 1µm YSZ – SDS coatings	109
16	Composition of electroless nickel – 5µm YSZ – SDS coatings	109
17	Setup IV: Experimental setup for acidic electroless Ni-LSM coating under the influence of a magnet	122
18	Composition of acidic electroless nickel – LSM coatings under the influence of a magnetic field	124

19 Setup V: Experimental setup for alkaline electroless ni-LSM coating under the influence of a magnet 129

20 Composition of alkaline electroless nickel – LSM coatings manufactured under the influence of a magnetic field 130

21 Variation of the composition of alkaline electroless nickel – LSM coatings with time. Solutions subjected to 65mT magnetic field strength 131

22 Effect of magnetic field on the average surface roughness of alkaline electroless nickel – LSM coatings 133

LIST OF SYMBOLS

ρ	Resistivity
R	Resistance
$\emptyset$	Conductivity
V	Voltage
I	Current
E_0	Standard cell voltage
$V_o^{\cdot\cdot}$	Vacancies
K	Gas permeability factor
A	Absorption
ξ	Molar absorptivity
c	Concentration
b	Cell path length
ζ	Zeta potential
R_a	Surface roughness
r	Reactivity ratio
I_o	Incident radiation
I_1	Emergent radiation

ABBREVIATED TERMS

AFM	Atomic force microscopy
CCCL	Cathode current collecting layer
COSHH	Control of substances hazardous to health
D.I	De-ionised
ECD	Electroless nickel ceramic co-deposition
EDXA	Energy dispersive x-ray analysis
EN	Electroless nickel
ENP	Electroless nickel plating
EPD	Electrophoretic deposition
FC	Fluorinated alkyl quaternary ammonium iodides
HLB	Hydrophile – lipophile balance
IEP	Iso-electric point
LSM	Lanthanum strontium manganate
mT	Milli tesla
Ni	Nickel
PMMA	Polymethyl methacrylate
PPR	Particle precipitation ratio
PPS	Potassium per-sulphate
PS	Polystyrene
Ra	Average roughness
SC	Solution composition
SDS	Sodium dodecyl sulphate
SEM	Scanning electron microscope
SOFC	Solid oxide fuel cell
TPB	Triple phase boundary
YSZ	Yttria stabilised zirconia

Chapter 1

General Introduction

The aims and objectives of this research are detailed in this chapter. The pertinent problem is stated and a general overview of the project as well as a brief insight into the methodology is discussed.

1.0 Introduction

Alternative energy technologies such as fuel cells have continued to positively contribute to the quest to increase the world's overall energy supply from renewable sources. In line with progress in the field, electroless co-deposition of ceramic and nickel (ECD) recently emerged as a method of manufacturing solid oxide fuel cell (SOFC) electrodes (Davidson & Waugh, 2008).

Simply requiring a source of energy to liberate chelated metal ions existing in an electroless nickel (EN) solution, the technique has been shown to have a much faster rate of production and lower energy consumption than traditional SOFC electrode manufacturing processes. In addition to its lower cost of production providing an opportunity for the SOFC technology to meet the stringent target of $400 per kW (equivalent to the cost of the most efficient gas turbines and diesel generators (Krotz, 2002)), the total elimination of a high energy sintering stage completely allows for the eradication of some sintering-associated defects such as cell warpage (Nozawa et al., 2008). Furthermore, the non-formation of Lanthanum Zirconate ($La_2Zr_2O_7$) – a resultant high temperature reaction material between the common electrolyte and cathode materials, Yttria stabilised zirconia (YSZ) and Lanthanum strontium manganate (LSM), (Mitterdorfer & Gauckler, 1998; Tsai & Barnett, 1996; Millar et al., 2008) additionally comprehensively highlights the array opportunities availed by the technique .

Of much importance and continuously attracting interest in the ECD process is the ability to control the composition of electrodes manufactured by the technique. The composition of SOFC electrodes very distinctively, directly influences the integrity and performance of an SOFC. A high metal content in the coating often promotes cell cracking while too low a nickel content and a correspondingly high ceramic presence can compromise cell efficiency

and performance. Problems of cell de-lamination, a dire consequence of a mismatch between the co-efficient of thermal expansion of SOFC components, is another issue which can arise from inappropriate composition of SOFC component parts.

To this end, as part of the work of Waugh in 2009, the influence of surface roughness and ceramic bath loading on the characteristics of SOFC electrodes manufactured by ECD was studied. The researcher found that a relationship existed between the ceramic bath loading and the composition of electrodes manufactured by the technique. Further to the work of Waugh, was that of Baba in 2010 where the optimum conditions required for the achievement of a low metal content and porosity in anodes manufactured by the ECD technique was investigated. The ceramic bath loading, plating solution pH, particle size and the method of agitation were variables evaluated in that study. The researcher reported in the conclusion that the necessary combination required to achieve a low nickel to ceramic ratio was to mechanically agitate large ceramic particle sizes of 10 μm in an electroless nickel bath of 4.9 pH (Baba, 2010).

In furtherance to these studies, the aim of this research is to;

i) With the aid of external agents, attempt to further increase and optimise the ceramic content of cermets co-deposited for use as SOFC electrodes and,

ii) Confirm the viability of using the process to deposit cathodes.

Two types of external agents, surfactants and magnets were used in the study. In the former, increased particle dispersion was expected to augment particle incorporation into the coating while in the latter, higher ceramic concentration near the surface of the substrate was sought after as a means of boosting particle incorporation into the nickel matrix.

Surfactants, short for surface active agents are compounds that migrate to surfaces (condensed phase and a gas phase) or interfaces (two condensed phases) due to their polar – non polar nature. Their resultant adhesion to particles through electrostatic interactions or steric stabilisation mechanism, which often results in particle dispersion, is a property utilised in this project to stabilise the YSZ or LSM particles in the electroless nickel solution. In addition to the possible formation of a semi nickel barrier which might reduce the metal content of the coating, the use of surfactants may also serve another purpose of acting as pore formers after being burnt off. Quite promising and observed in the work of Chen et al. (2002) is that surfactants may also very usefully perform another role of enhancing the deposition rate of the process due to its observed nature of preventing evolved hydrogen bubbles from masking the surface of the substrate.

Magnetophoresis is the movement of magnetic particles in a fluid under the influence of a magnetic field. With LSM being ferromagnetic, the possibility of increasing the concentration of ceramic particles around the substrate by magnetically attracting the particles to the region where the substrate is suspended, it is believed, will aid particle incorporation. This assumption is based on the fact that since the ECD process operates on the principle of ceramic entrapment in the nickel matrix, a higher concentration of the particles around the substrate – if located around the magnet, will translate to increased ceramic content in the co-deposit.

To assist in the development of experimental matrices, the underlying interactions between the ceramic particles (YSZ & LSM) and the electroless nickel plating solutions were studied at the outset. Essentially, this involved the determination of particle zeta potentials and their corresponding precipitation ratios which would indicate their disposition and tendency to be dispersed – if at all – in the electroless nickel plating solution.

The results and conclusions from experiments conducted are detailed in this thesis which has been structured in the following manner:-

Chapter 2 focuses on the rudiments of SOFC technology and its component parts. In addition to highlighting some traditional and emerging methods of manufacturing SOFC electrodes, a few methods of assessing the performance of SOFC electrodes, are elucidated upon.

Chapter 3 presents the intricacies of electroless nickel plating – the platform on which ECD operates. Factors influencing the deposition process as well as some equipment and tools required to characterise both the electroless nickel solution and its resultant co-deposits, form the core of issues discussed in the section. The dynamics of the external agents, on which the research is largely based upon, is presented in chapter 4.

Chapter 5 details the results of experiments carried out to establish the interaction between the external agents, the ceramic particles and the electroless nickel solution. In particular, the work undertaken and detailed in the section provided the basis for the formulation of suitable experimental matrices that would best achieve the desired results in the research. Chapter 6 outlines the nature of materials used in the research work, influence of the external agents on coatings obtained and the co-deposits suitability for use as SOFC electrodes based their composition.

Chapter 7 concludes the findings while chapter 8 presents the contribution of the work to knowledge. Suggestions and recommendations for future work which may further yield more positive results are proposed and discussed in chapter 9. In chapter 10, a list of all related publications to date is provided.

Chapter 2

Literature review

The theory of fuel cells and their related manufacturing processes is discussed in this chapter. After a review of the dynamics of solid oxide fuel cells (SOFC), some basic properties of SOFC electrodes as well as a number of traditional and emerging techniques of manufacturing the device are discussed prior to an overview of some methods of evaluating an SOFC's performance.

2.1 Overview of solid oxide fuel cell technology

A solid oxide fuel cell (SOFC) is an electro-chemical device that generates electricity from the direct oxidation of a fuel. It relies on the affinity of hydrogen for oxygen of which when they combine, yield water vapour and electrons (equation 2.1).

$$2H_2 + O_2 \longrightarrow 2H_2O \qquad (2.1)$$

(E_0 (V) at 1000K = 0.997)

Where E_0 is the standard cell voltage. SOFC's operate at relatively high temperatures of between 600^{o}C and 1000^{o}C. While those operating at temperatures of as low as 600^{o}C are generally referred to as intermediate temperature SOFC's, those in the higher category are known as high temperature SOFC's. The high operating temperature of an SOFC not only bestows upon it a high tolerance of different types of fuels such as methane, but also enables the cell to function without a catalyst which is often required in lower temperature fuel cells such as the polymer electrolyte fuel cell (PEMFC) and phosphorus acid fuel cell (PAFC). Table 1 provides a list of the most common types of fuel cells available. Other types though, such as the microbial fuel cell, zinc air fuel cell and regenerative fuel cell also exit and are also of research interest.

A unit SOFC – several of which is referred to as a stack – consists of four basic components. A dense electrolyte, two porous electrodes (an anode and a cathode), and an interconnect charged with the role of conveying electrons to an external circuit (Figure 1). To produce electricity, air is inflowed at the cathode as a source of an oxidant – oxygen. At the electrolyte-cathode boundary, known as the triple phase boundary (TPB) (since air is also in

Table 1. Common fuel cell types

Fuel cell type	**Electrolyte**	**Operating temperature (^{o}C)**	**Catalyst**	**Electrical efficiency**
Phosphoric acid	Liquid phosphoric acid in a lithium aluminium oxide matrix	150 – 200	Yes	36 – 42%
Polymer electrolyte membrane	Solid polymer membrane	80 – 100 Typically 80	Yes	40 – 60%
Alkaline	Potassium hydroxide solution in water	~100	Yes	60 – 70%
Direct methanol	Solid polymer membrane	50 – 100	Yes	Up to 40%
Molten carbonate	Solution of lithium, sodium and or potassium carbonates soaked in a matrix.	~ 650	Yes	50 – 60%

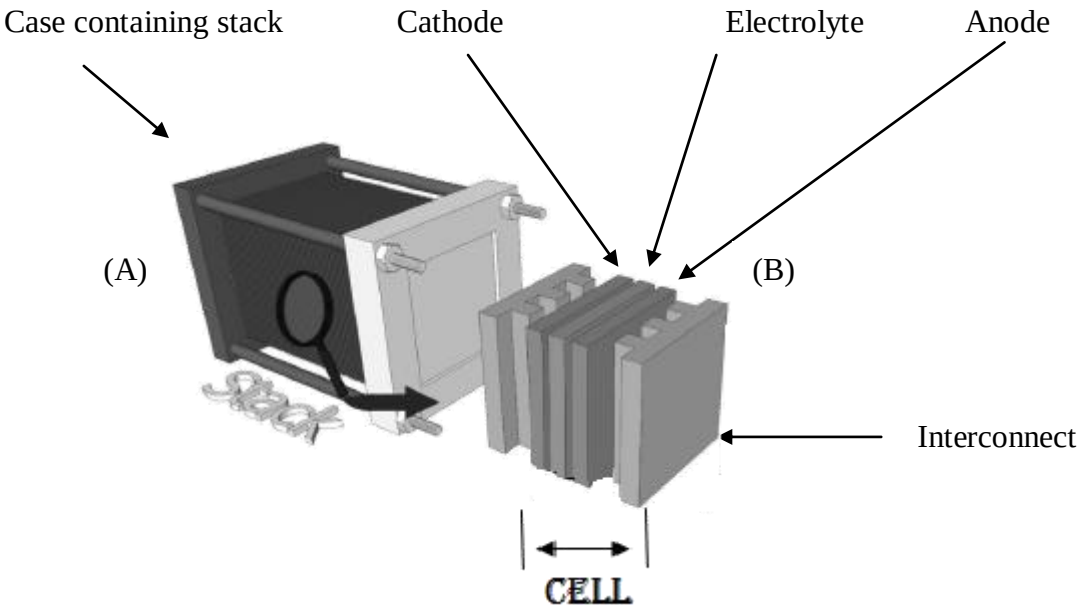

Figure 1 – Schematic representation of (a) a case containing a stack of cells and (b) a unit cell comprising an anode, cathode, electrolyte and interconnect.

contact with both materials), oxygen molecules are catalytically reduced to ions by electrons present in the region (equation 2.2).

$$O_2 + 4e^- \longrightarrow 2O^{2-} \qquad (2.2)$$

The oxygen ions thereafter diffuse into the electrolyte and due to a concentration gradient, travel across the electrolyte to the anode region through oxygen vacancies in the material. At the anode-electrolyte interface, hydrogen which simultaneously passes through the anode reacts with oxygen ions arriving at the boundary. Along with water being yielded as a by-product, electrons are produced. Figure 2 is an illustration of the basic inputs and outputs of an SOFC.

When fuel types such as methane or butane are used, water, CO_2 and electrons constitute the output from the cell (equation 2.3). As mentioned earlier, contamination of the cell by compounds such as carbon monoxide does not occur.

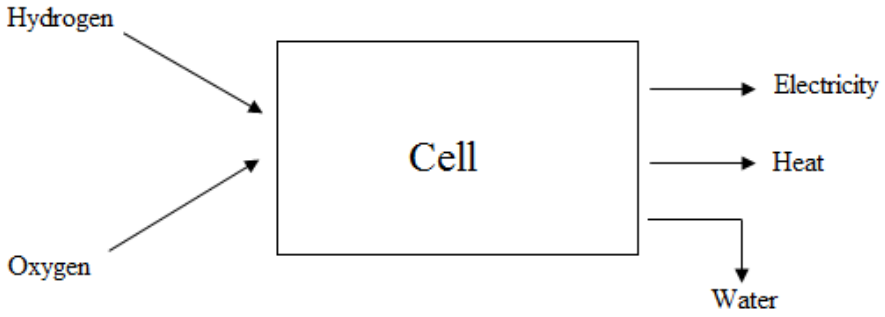

Figure 2 – Representation of basic SOFC inputs and outputs.

$$CH_4 + 4O^{2-} \longrightarrow 2H_2O + CO_2 + 8e^- \qquad (2.3)$$

(E_0 (V) at 1000K = 1.039)

Because power produced by a cell is typically in the range of 1W, cells are generally stacked (Figure 3) to increase the output.

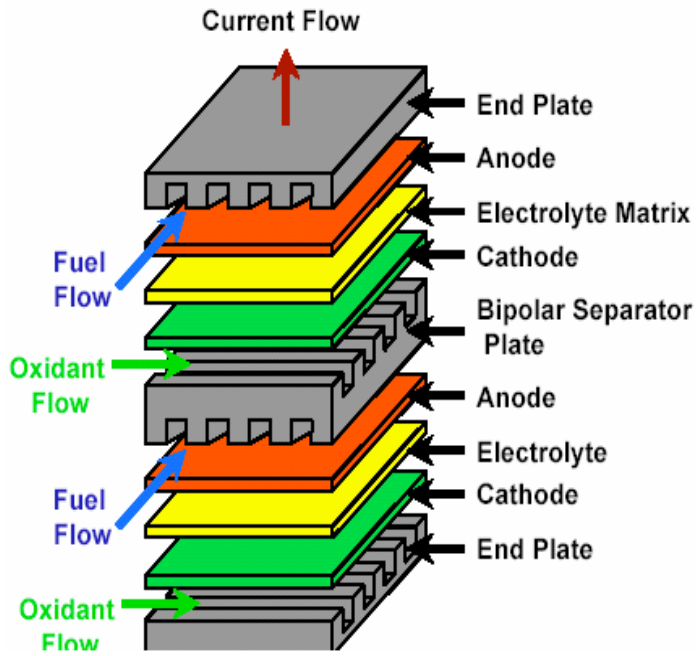

Figure 3 – Schematic representation of fuel flow and a planer stack assembly. *Source: Case Western Reserve University*.

Today, there are three distinct configurations of solid oxide fuel cells. Planar (Figure 3), tubular (Figure 4) and monolithic design (Figure 5).

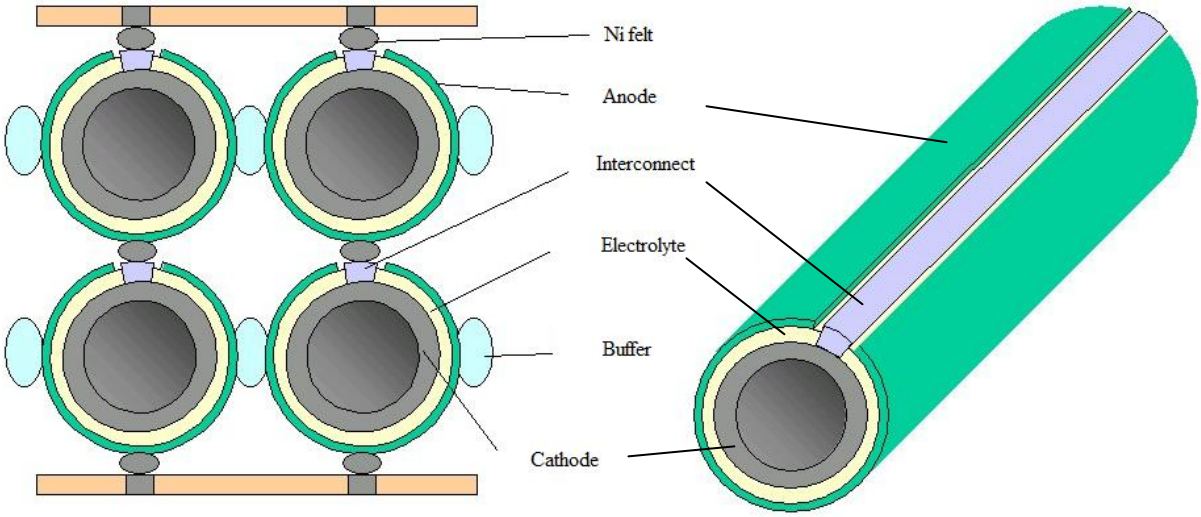

Figure 4. Schematic representation of tubular SOFC. *Image from http://www.aki.che.tohoku.ac.jp*

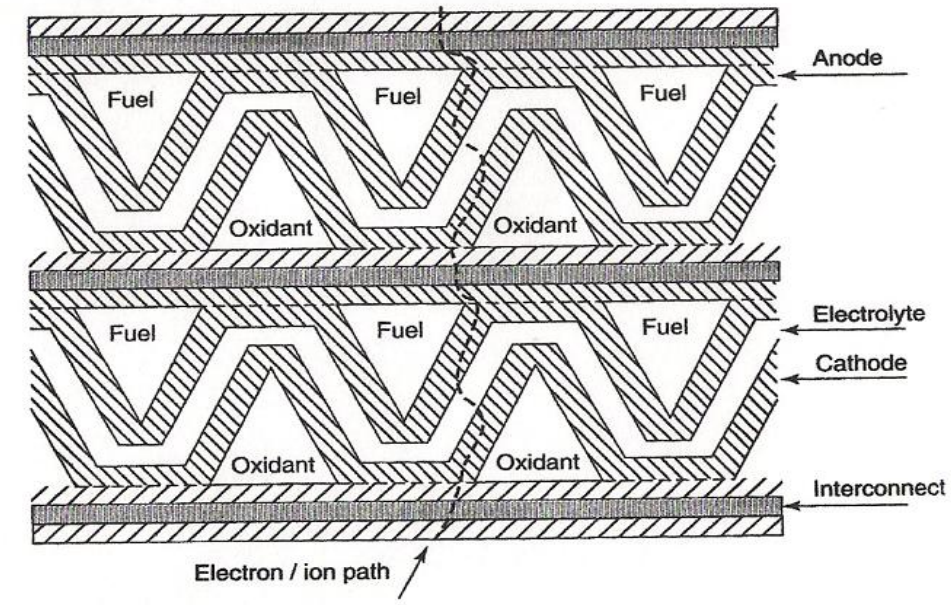

Figure 5. Illustration of a monolithic SOFC (Xianguo, 2006)

All SOFC configurations have a trade-off in terms of advantages and disadvantages. For example, though the planar is the easiest to manufacture, problems associated with ensuring that the unit cells are properly sealed in order to avoid gas leakage which can lead to exposure of flammable gases, exist. While the gas exposure problem can be eliminated with the tubular design, tubular SOFC's are relatively more difficult to manufacture and have a higher intrinsic electrical resistance due to a larger electrolyte surface area that can result in a reduction of the cell's efficiency.

2.2 Components of a solid oxide fuel cell

2.2.1 Electrolyte

The electrolyte provides the medium for the transportation of oxygen ions between the electrodes. Due to the elevated operating temperature of SOFC's and the stringent requirements that materials to serve as an electrolyte must satisfy, hard ceramic oxides that can withstand such high temperatures and conditions become the materials of choice. In fact the name of the device – solid oxide fuel cell, directly originates from the use of such solid materials.

A material that can be chosen to serve as an electrolyte must fulfil conditions such as high ionic conductivity, no electronic conductivity and stability in oxidising and reducing environments. Several materials have been suggested to serve as SOFC electrolytes, however the stringent conditions to be met has continuously eliminated a majority of them. Lanthanum strontium gallium manganate (LaSrGaMnO) and scandia stabilized zirconia (ScSZ), initially strongly recommended in the industry to serve as electrolyte materials, are amongst a recent batch that have been generally discouraged due to stability related issues (Fergus, 2006). Yttria Stabilised Zirconia (YSZ), a ceramic in which yttria prevents the crystal structure of zirconia from changing from its most conductive cubic fluorite phase to a lower tetragonal

phase, continues to remain the material of choice for the purpose. With yttria also creating oxygen vacancies in zirconia's crystal structure at the rate of one oxygen vacancy per mole of yttria introduced into zirconia's lattice, conductivities of about 0.1 $S.cm^{-1}$ at 1000°C, 0.02 $S.cm^{-1}$ at 800°C and 0.008 $S.cm^{-1}$ at 700°C can be typically attained with the material.

Although YSZ is currently the most widely used electrolyte material in SOFC technology, certain drawbacks still beclouds its usage. Firstly, the ionic conductivity of the material generally drops off with decreasing temperature and at temperatures above 1500°C, transits into an electron conductor which ultimately short circuits the cell (Hawkes et al., 2006). Furthermore it is well known that the level of yttria doping into zirconia's crystal lattice affects the performance of the material. Beyond 8% yttria doping, the ionic conductivity of the material drops. A plot of the ionic conductivity of zirconia as a function of the level of yttria doping is shown in Figure 6 (Fergus, 2006). The effect of doping zirconia with the oxide of another rare earth metal scandium, is also shown in the plot.

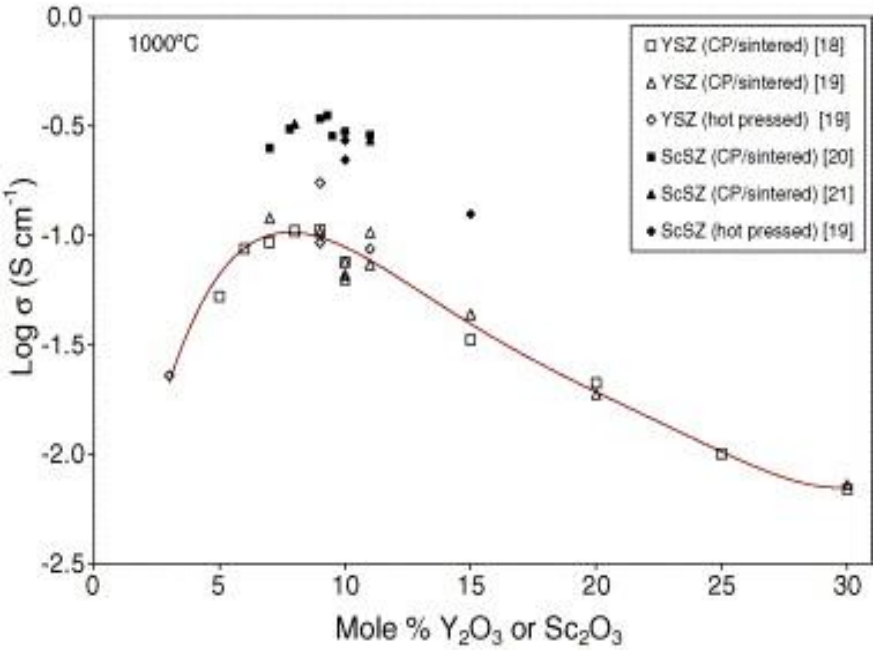

Figure 6. YSZ/ ScSZ conductivity against % yttria/ scandia doping at 1000°C (Fergus, 2006). The ionic conductivity can be seen to rise with increased doping before tailing off beyond about 8% yittria or scandia doping.

To help reduce inherent resistances presented by an electrolyte material, the thickness of SOFC electrolytes is normally not more than 40 microns. In fact if an appreciable output from the SOFC is sought, it is imperative that the total travel distance of the ions across the electrolyte is reduced to the barest minimum since ions are much larger than electrons and thus more difficult to conduct. In general, an SOFC electrolyte must be dense and fully compact to avoid gas losses. This is essential as any gas leakage within the cell will greatly reduce its efficiency. Figure 7 shows a scanning electron micrograph of a commercial SOFC electrolyte.

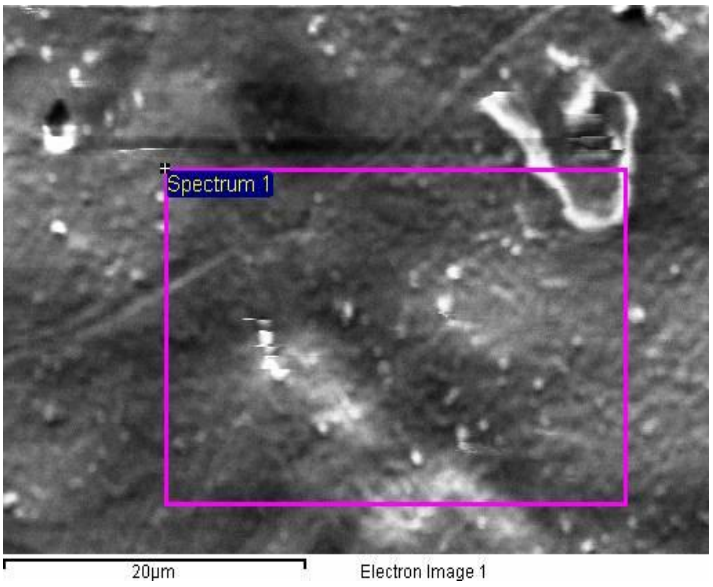

Figure 7. Scanning electron micrograph of a commercial SOFC electrolyte (x3000 magnification). The image confirms the characteristic dense nature of an SOFC electrolyte – even at micrometer level.

2.2.2 Anode

The anode, which is the positive terminal of an SOFC, essentially provides reaction sites for fuel oxidation. It also enables electrons generated within the cell to be transported to the

circuit. In order to ensure optimum electron conduction, a material to adequately serve as an anode must at the very minimum possess adequate electronic conductivity. It must also be stable in a reducing environment and adequately porous to allow for appropriate gas flow.

Due to its availability, affordability, good conductivity (143,000 $S.cm^{-1}$) and stability in a reducing environment, nickel, a group 2 face-centred-cubic transition metal, is often a common choice of material for the anode. It effectively acts as a catalyst for hydrogen oxidation and directly aids reformation of hydrocarbon fuels such as methane for direct use in SOFC's. However downsides such as the operating temperature of SOFC's being in the region of sintering of the material and a large difference between its coefficient of thermal expansion (13.3×10^{-6}/C) and that of YSZ (10×10^{-6}/C), has seen the anode material regularly made up of a composite of nickel and the respective electrolyte material – commonly YSZ. Another seeming disadvantage of nickel is that it encourages the formation of carbon from the hydrocarbon fuels that deposits on its surface. If the carbon deposit is not controlled, its formation on the electrode's surface will not only cover the electrochemically active sites but also encourage the mechanism metal dusting (Choi, 2007) which may ultimately destroy the anode (Singhal, 2007).

When SOFC's are anode supported, the thickness of anodes may be as much as ~0.7mm (Shao et al., 2004).

2.2.3 Cathode

The cathode is known as the negative electrode due to the inward flow of electrons. Although it must like the anode possess good conductivity and be compatible with the electrolyte, its highly oxidising environment requires any material to serve the purpose to be at the minimum, stable in such an atmosphere. The Kroger – vink notation in equation 2.4, typically depicts the reaction that takes place at the active TPB, i.e., the region where the electrolyte, cathode

$$\frac{1}{2} O_2 (g) + 2e' + V_o^{\cdot\cdot} \rightarrow O_o^{\cdot} \quad (2.4)$$

material and air meet. Vacancies (V_o), that exist in the electrolyte, enable oxygen ions (O_o), obtained from the reduction of oxygen molecules (O_2) in air by the electrons (e'), to be mobile. Within the cathode, a 25 to 40μm thick layer known as the cathode current collecting layer (CCCL) is specifically charged with electron collection while another layer, a composite between the cathode and the electrolyte, is known as the cathode layer or simply 'C-layer' (Jørgensen, 2001).

A wide range of materials, mostly perovskite ceramics with the $A_mB_nX_p$ structure, have been investigated to serve as SOFC cathodes. Whilst they meet different requirements, certain shortfalls have made some of them unacceptable. For example, although lanthanum strontium cobaltites ($La_xSr_{1-x}CoO_3$) with high ionic conductivities (as high as 1 $S.cm^{-1}$) have shown to possess the highest number of oxygen vacancies which indicates high rates of surface oxygen exchange, the matter of their coefficient of thermal expansion being much higher (20.5×10^{-6} K^{-1} – 25.0×10^{-6} K^{-1} at 800°C) than that of the common SOFC electrolyte (YSZ) presents a major challenge for use of the materials (Datta et al., 2008; Ullmann et al., 2000). Another material, Lanthanum strontium cobaltite ferrite (LSCF) has also shown potential. However, it's observed reaction with zirconia to form unwanted insulating phases – when the latter is used as an electrolyte, remains an obstacle for its use. Chiba et al. investigated the material lanthanum nickel ferrite ($LaNi_{1-x}Fe_xO_3$) and found that when nickel was doped at the A-site to the tune of 40 mole fraction i.e. x=0.4, the material exhibited a similar structure to $LaNiO_3$ and boasted a very high conductivity of 580 $S.cm^{-1}$ at 800°C (Chiba et al., 1999). However it was discouragingly found that the material was relatively unstable at high temperatures and decomposed to a ruddlesden popper structure – La_2NiO_4 (Lanthanum nickelate) – which

although displays relatively high oxygen tracer diffusion and surface exchange coefficients (Skinner & Kilner, 2000; Boehm et. al., 2005), possesses very low conductivity.

Strontium doped lanthanum manganate ($La_{1-x}Sr_xMnO_3$), a black ceramic powder denoted as LSM, has thus far emerged as the best candidate material for use as an SOFC cathode. Though the material is only capable of attaining an electronic conductivity of about 180 $S.cm^{-1}$ (approximately 1/3 of that of $LaNi_{1-x}Fe_xO_3$ previously mentioned), its stability in oxidising environments and possession of a coefficient of thermal expansion (CTE) (12.0×10^{-6}/C) that is compatible with that of the common electrolyte YSZ, amongst other reasons, continues to make it the material of choice.

2.2.4 Interconnect

The interconnect serves as a link between cells, multiplying in series the electricity generated by each cell to produce a combined total output. A material serving as an interconnect must meet certain conditions. Unreactivity with other components of the cell and stability in both oxidising and reducing environments are essential. Porosity is undesired as it could reduce effective conductivity of electrons and also expose the oxidising area to the reducing ends. To maintain the integrity of the cell, the material must also have similar thermal expansion rates as other cell materials they are attached to.

Although ceramics have coped with this function, for reason of cost, metallic alloys have been researched and have continued to show promise. The most popular choice for SOFC's that employ YSZ as an electrolyte is doped chromites of lanthanum with $LaCrO_3$ formula. Elements used to improve interconnect conductivity by doping, include but are not limited to calcium, magnesium and rare earth metal strontium (Yeong-Shyung Chou, 1999).

2.3 Structure of electrodes

Electrodes must at a minimum allow for unrestrictive travel of reactant gases to the TPB. Achieved by creating pores or void spaces, adequate control of these pores when formed is essential for efficient operation of a cell. Very small pores provide barriers to gas diffusion while very large pores result in a reduction of the electronic conductivity of the cell. For example, a typical cathode material such as LSM, with a composition $La_{0.5}Sr_{0.5}MnO_3$, can possess electronic conductivity values of as high as 294 $S.cm^{-1}$ at 1000^{o}C. With porosity, this often drops to as low as 100 $S.cm^{-1}$ (Xianguo, 2006). The optimum porosity value is 30% of the volume of the electrode.

It is worthy of note though that effective transportation of gases to the TPB does not stop at creating pores to allow its passage. If the pores are not accessible i.e. pores are agglomerated at a particular area or inclusions are present, then the gases will still not have easy access (impermeable).

The gas permeability factor k is represented by the equation 2.5 where ΔV is the volume of

$$K = \frac{I}{\Delta p} - \frac{\Delta v 2 p 2}{\Delta t}(p1 + p2)\Delta p \qquad (2.5)$$

gas travelling through the cathode during a certain period of time denoted by Δt for a known pressure drop Δp. The pressure drop here Δp, is the difference between the initial and final pressure of the gas.

A build up of gases due to non passage is known as concentration polarisation (CP) or overvoltage and seriously undermines the efficiency of a cell.

2.4 Current and emerging methods of electrode manufacture

SOFC components can be manufactured by various techniques such as chemical vapour deposition, physical vapour deposition, electrostatic spray deposition, sputter deposition and screen printing. While some such as screen printing are traditional and widely used even in several other industries, newer techniques have continued to emerge.

A common denominator amongst most types of SOFC manufacturing processes though is the requirement for products obtained to be sintered as part of the manufacturing process. Although unarguably a crucial step, the step presents several challenges – one of which is a high energy requirement that translates to exorbitant costs (Appendix A). Horne et al., 2007, Karakoussi et al. 2001 and Hart and colleagues, 2000, have all reported that the sintering step creates the largest environmental impact due to the energy used during the process and nature of organic compounds expelled during binder burnout.

Where sintering is not required or the problems associated with it circumventable, many SOFC manufacturing techniques also tend to have other issues to address. These include but are not limited to difficulty in obtaining good post manufacture composition homogeneity, unsuitability for mass production and difficulty for component reproducibility. A few of these techniques are discussed in detail below.

2.4.1 Screen printing

Also known as silk screening, the art of screen printing involves the deposition of an ink onto a substrate material through a screen. The process can be manual or semi automatic. Inks used in the manufacture of SOFC electrodes by screen printing generally consist of suitable binders, a solvent and fine ceramic powders (YSZ or LSM depending on which electrode is being manufactured). Largely made of either stainless steel or polypropylene, the size of the screen often ensures that the required particle size and porosity are maintained during coating.

Upon completion of the deposition process which takes place on a vacuum work plate as shown in Figure 8, the end product is dried. Before sintering of the coating is carried out to

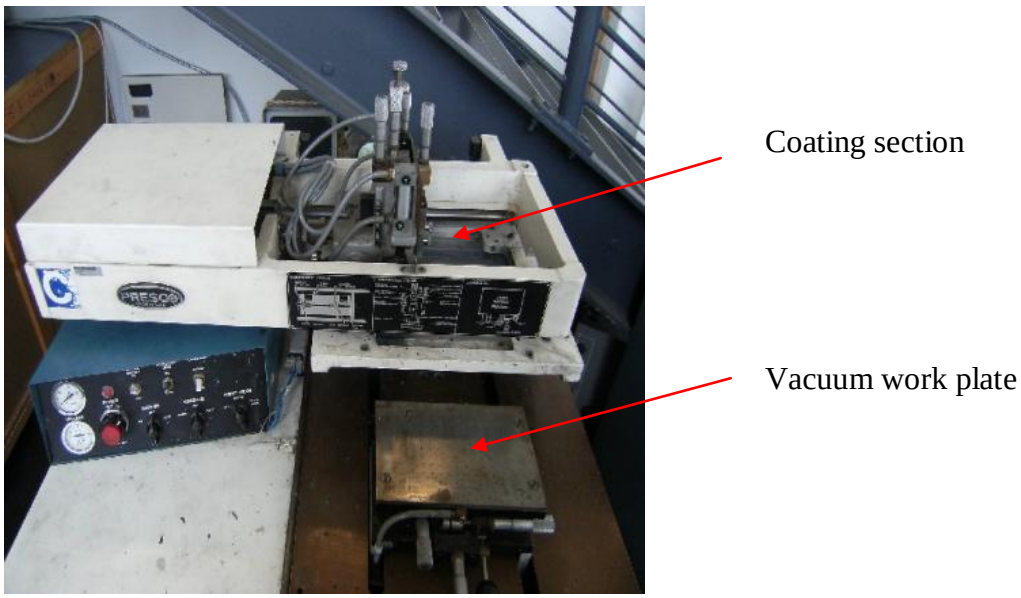

Figure 8. Image of a Presco model 465 semi automatic screen printer. Similar equipments commonly find use for the deposition of SOFC components

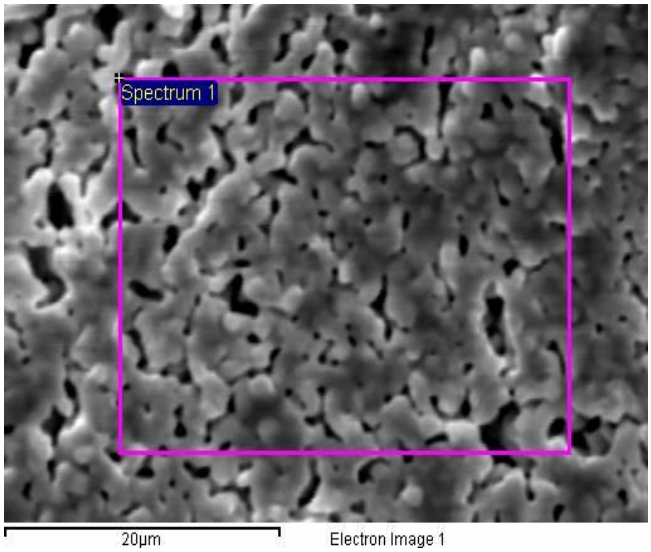

Figure 9. Scanning electron micrograph of a screen printed commercial cathode showing high porosity network.

ensure that the required porosity is achieved, the vehicle ink used during the deposition process is also burnt off to prevent entrapment of gases in the coating. Figure 9 shows an SEM micrograph of a screen printed commercial cathode.

2.4.2 Chemical vapour deposition

Chemical vapour deposition (CVD) presents a gaseous method of manufacturing SOFC components. The process relies on gas precursors which combine to yield densely non-porous deposits. For the manufacture of a typical electrolyte e.g. YSZ, chlorides of zirconium and yttrium are allowed to flow over the outer surface of a porous electrode (say the cathode), while oxygen is passed along the inside. Subsequent interactions between the gases results in the formation of YSZ at the surface, which closes off the surface porosity whilst ensuring a good reaction area for the TPB. Because oxygen which travels through the layer of already formed YSZ still meets both chlorides of Yttrium and Zirconium, the electrolyte layer continues to grow thus forming an evenly dense material in the process.

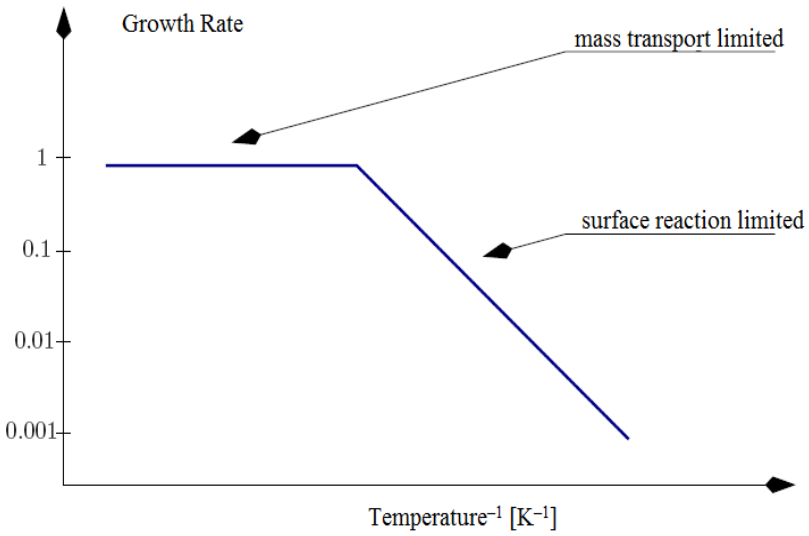

Figure 10. CVD deposition rate as a function of temperature. http://www.iue.tuwien.ac.at /phd/holzer/node41.html

Though the method boasts of high levels of purity, as well as being a process that can be controlled, its operating and initial capital costs can be very high. Furthermore, the fact that key variables associated the process – such as mass transportation and surface reaction that can greatly reduce the rate of deposition associated with the process, are strongly influenced by temperature (Figure 10) is worthy of note during the manufacturing process. Bonding to the substrate is also affected by the geometry of the substrate as depicted in Figure 11.

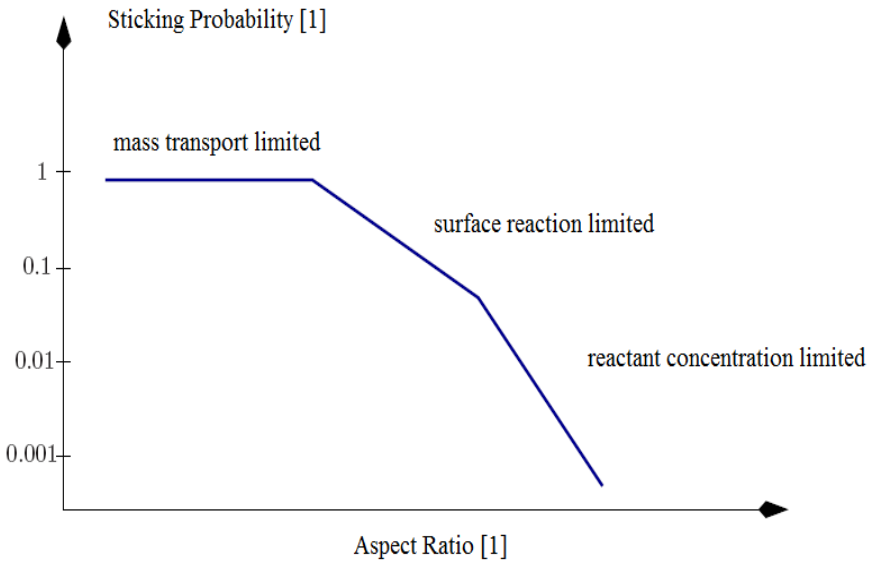

Figure 11. Sticking probability as a function of substrate aspect ratio.http:/www.iue.tuwien.ac.at/phd/holzer/node41.html.

2.4.3 Laser reactive deposition

Laser reactive deposition (LRD), introduced by Horne et al, belongs to a cohort of newly devised SOFC manufacturing techniques. Aided by reactions which occur in an LRD reactor, the process which relies on laser pyrolysis (LP) has been suggested to improve the efficiency of SOFC component part manufacture by replacing processes such as powder synthesis, modification and batching which occur in traditional techniques. The process as shown in Figure 12 utilises deionised water as a solvent and nitrates of respective deposition materials

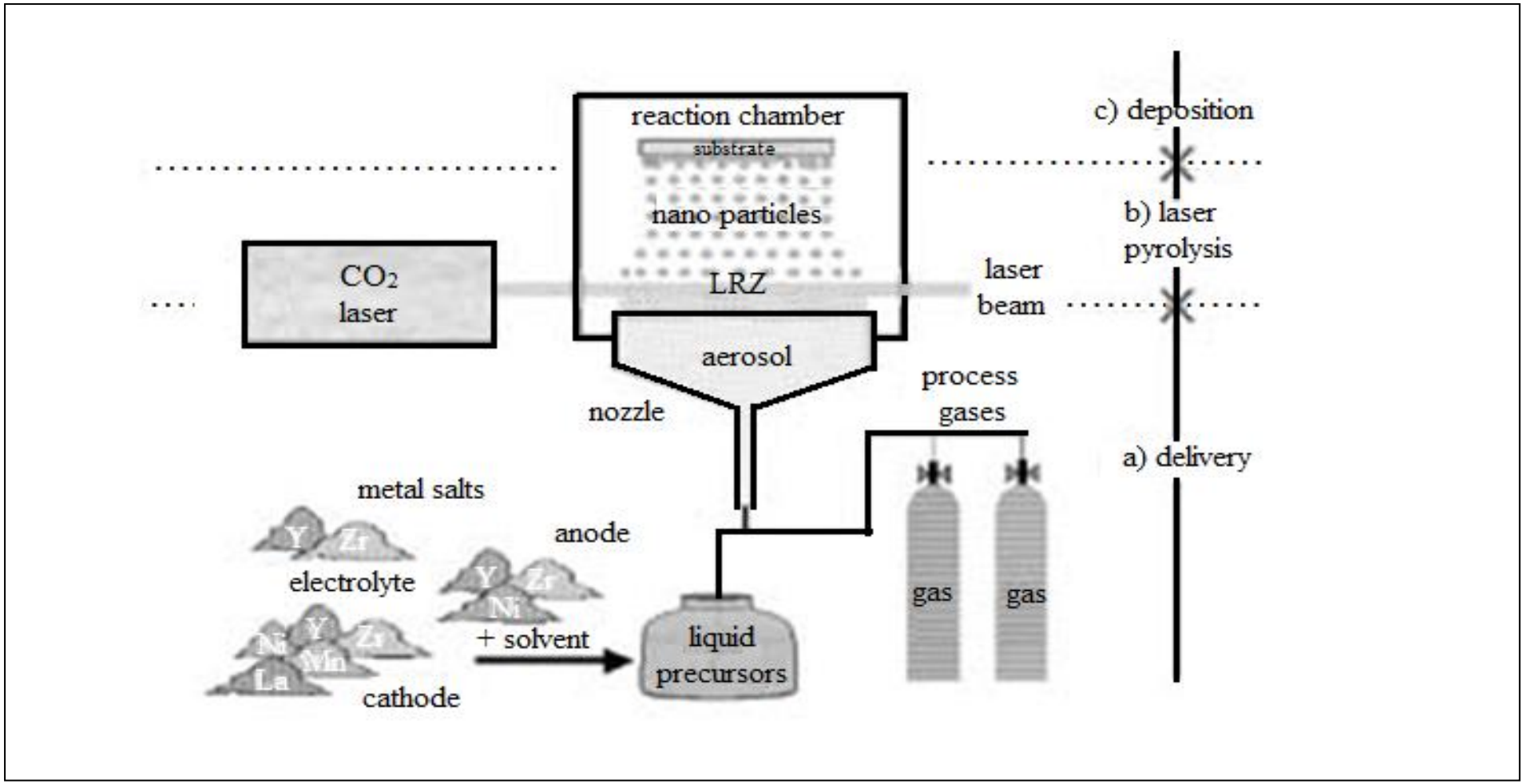

Figure 12. Schematic representation of laser reactive deposition (LRD) (Horne et al. 2007).

e.g. zirconyl nitrate and yttrium nitrate for the electrolyte. The aqueous solutions are converted from a liquid stream to an aerosol by an atomiser. The aerosol is then delivered to the reactor where by LP, the precursors are converted into submicron or nanoscale particles. Conditions in a laser reactive zone (LRZ) are engineered in such a manner that the newly formed particles are entrained in a spent process gas flow field and directed into contact with a deposition surface (Horne et. al., 2007). The process generally allows for variation of attainable thicknesses.

2.4.4 Electrophoretic deposition

Electrophoretic deposition (EPD) operates on the principles of electrophoresis. Electrophoresis is the mobility of charged particles under the influence of an electric current. The method involves the deposition of charged particles onto a conductive surface such as LSM. For the deposition of an electrolyte onto a cathode for example, YSZ powders are

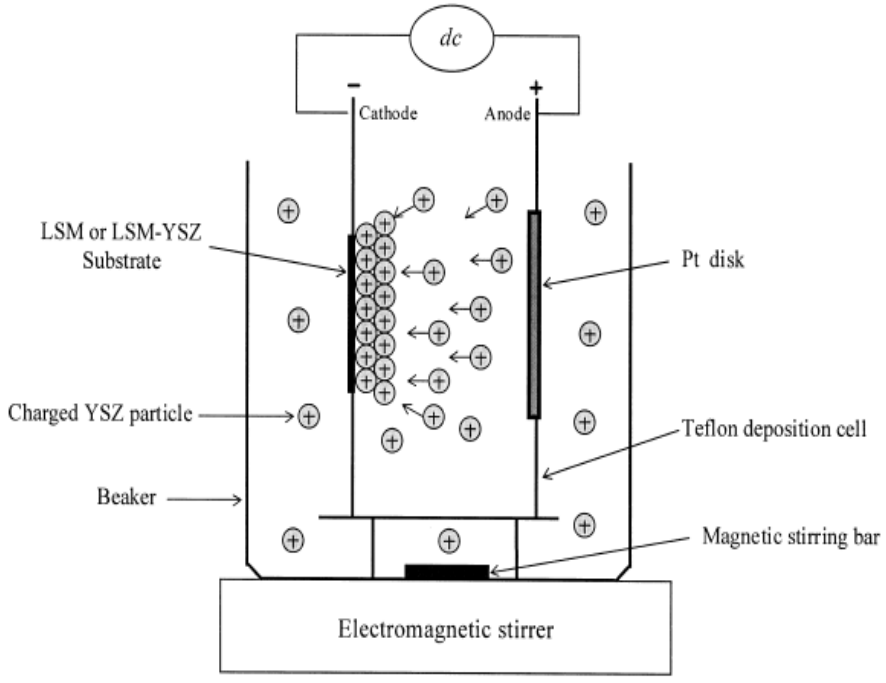

Figure 13. Schematic diagram of cell configuration for EPD of YSZ on an LSM or LSM-YSZ substrate (Chen & Liu. 2000).

dispersed with iodine in solvents such as acetylacetone, ethanol or a mixture of both. Under an applied DC field, the charged YSZ particles move towards and deposit on the LSM cathode (Figure 13).

While it has been acknowledged to be a cost effective process, the resultant thickness of the coating often varies with several factors such as voltage, concentration and the nature of the solvent. Cracking of the deposit and poor adhesion to the substrate are also amongst other issues that surround the process.

2.4.5 Freeze drying

Freeze drying is an emerging SOFC electrode manufacturing technique. It involves dipping an electrolyte into a slurry e.g Ni/YSZ, before freeze drying the combination immediately afterwards. The ice which forms on the part is sublimed out and because water dissolves in a smooth and steady manner, creates pores that are neatly aligned and allow for efficient transportation of gases to and from the electrolyte/electrode interface.

Due to the possibility of creating effective porosity while avoiding the likelihood of cracking which occasionally occurs when pore formers are burnt off during the manufacture of SOFC electrodes by a slurry process (J-W. Moon, 2003), interest in this process has continued to grow.

2.5 Cell testing

Cell testing is an essential part of SOFC manufacture. Intrinsic properties of the components of the cell such as their level of conductivity as well as their limitations are evaluated with the aim of determining or improving the performance of the device. Several techniques exist for this purpose - some of which are;

2.5.1 Four point conductivity test

Good electronic conductivity is a highly desired property of SOFC electrode materials. A four point conductivity test, also known as the four point probe (FPP) test, is often used to measure the resistivity of SOFC electrodes. The test essential determines the extent of permittance of electron flow through the electrode at various temperatures.

It involves the use of 4 probes where electric current passed through 2 outer probes, induces a voltage in the 2 inner probes. The relationships,

$$\rho = \frac{RA}{L} \tag{2.6}$$

$$R = \frac{V}{I} \tag{2.7}$$

$$\rho = \left(\frac{\pi}{\ln(2)}\right)\left(\frac{V}{I}\right) \tag{2.8}$$

where ρ denotes resistivity, R resistance, A cross sectional area and L the material's length, are used to calculate the material's resistivity which in turn using the relationship

$$\emptyset = \frac{1}{\rho} \tag{2.9}$$

where Ø represents conductivity, enables the calculation of the material's conductivity. Figure 14 shows how the conductivity of a commercial cathode varies with temperature when examined by FPP. The slope is directly indicative of a conductive ceramic unlike a metal which would possess a negative slope.

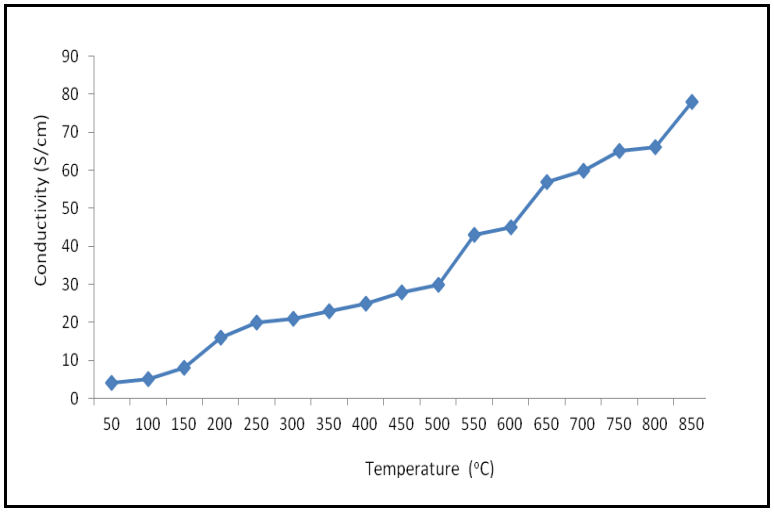

Figure 14. Conductivity vs temperature plot of a four point probe tested commercial SOFC cathode

2.5.2 Electrochemical Impedance Spectroscopy

Successful evaluation of the performance or limitations of a cell requires the ability to adequately model how the key components of the cell will affect or contribute to its operation. Electrochemical impedance spectroscopy (EIS) is a reliable diagnostic tool that can be used for SOFC performance evaluation. The technique conveniently allows for the three fundamental sources of voltage loss in fuel cells – charge transfer activation, ion and electron transport losses and mass transfer losses – to be isolated and studied.

Key cell components or physiochemical processes are converted to equivalent circuit models wherein they are represented by a network of resistors, capacitors and inductors. Conductive pathways for ion and electron transfer (i.e. ionic conductivity by the electrolyte or electronic conductivity by the electrodes) are represented by resistors while polarisation due to space-charge such as at the double layer or adsorption/desorption at an electrode, are represented by capacitors and inductors.

Typical EIS fuel cell test results normally relate the magnitude of impedance in the cell or phase angle to the frequency of a small AC signal imposed on it during testing. A bode plot

depicts this. The capacitive and inductive characters of the cell are also assessed against the real impedance of the cell under what is represented by the complex plane or Nyquist plot.

Obtaining EIS data during an SOFC test involves linking up a working, counter and reference electrode to a frequency response analyser.

Chapter 3

Electroless nickel co-deposition as a method of manufacturing SOFC electrodes: Evolution, process and characterisation

This chapter lays emphasis on the novel technique, electroless nickel ceramic co-deposition, on which platform the manufacturing process in this research is based upon. Methods of characterising both the electroless nickel solution and the coatings obtained from the plating process (i.e. the resultant electrode in the case of fuel cell applications) are also outlined in this section.

3.0 Introduction

First applied by Davidson and Waugh (2009) in SOFC technology, electroless nickel co-deposition (ECD) is a method of simultaneously depositing a ceramic and metal, nickel, onto a substrate without an electric current. It operates on the electroless nickel plating (ENP) platform – an autocatalytic plating process that is well known to produce coatings with superior corrosion and wear resistance properties. Although Brenner & Riddell (1950) are credited with developing the ENP process, Odekerken who while attempting to improve the corrosion resistance of nickel chromium electrodeposits, applied an intermediate layer of alumina (Al_2O_3) and poly vinyl chloride (PVC) within a metal matrix, is widely acknowledged as the earliest demonstrator of particulate matter incorporation by ENP (Odekerken, 1966). As the process does not rely on electricity for deposition to occur, reduction of the metal, nickel, is entirely achieved by a reducing agent. Sodium hypophosphite, hydrazine and the borohydride ion are some commonly used reducing agents. Typical reactions that occur during the process, including the evolution of hydrogen and co-deposition of phosphorus (depending on type of reducing agent used) are detailed as follows (Gutzeit, 1959);

$$(H_2PO_2)^- + H_2O \longrightarrow (H_2PO_3)^- + 2H^+ + e^- \quad (3.1)$$

$$Ni^{2+} + 2e^- \longrightarrow Ni \quad (3.2)$$

$$2H^+ + 2e^- \longrightarrow H_2 \quad (3.3)$$

$$(H_2PO_2) + 2H^+ + e^- \longrightarrow P + 2H_2O \quad (3.4)$$

The process starts in catalytically sensitive areas on the surface of a substrate before auto-catalytically growing in an isotropic pattern (Marton & Schlesinger, 1968). Ceramic particles present in the region closest to the surface of the substrate are engulfed in the metal matrix

during the growth process. The result is the formation of a cermet coating. Because ceramics (such as the electrolyte material – YSZ), generally possess passive surfaces with poor catalytic properties, a pre-treatment stage consisting of different steps is generally required before plating can be carried out.

3.1 Substrate preparation and the co-deposition process

Dependent on several factors such as the nature of material being coated (e.g conductive or non-conductive), sample preparation during ECD largely varies. When materials like ceramics (e.g. YSZ) – which mostly possess passive surfaces, are to be coated by the technique, the sample generally passes through 4 pre-treatment stages. As the very first step, the substrate is degreased to remove unwanted materials from its surface and prevent contamination from loose dirt particles getting dragged in during the co-deposition process. Alkaline cleaners such as acetone or methanol, or even soap are often adopted for this stage. In the experimental part of this work, Cuprolite X-96 DP supplied by Alfachimici Italy, was employed as the cleaner. To use the chemical, the solution was first brought to temperature ($56 – 60^{o}C$) before the substrate was introduced into it. To ensure that the entire surface of the immersed substrate was effectively cleaned, a mechanical stirrer was utilised as a source of agitation and the cleaning operation was always carried out over a 15 minute period.

Upon completion of the cleaning step, the sensitisation and activation steps – required to provide catalytic activity on the surface of the substrate, follow. These steps are of particular importance as they ensure that the surface of the substrate is the preferential surface for nickel to deposit onto.

To sensitise the surface, the substrate is dipped in a pre-catalyst solution containing stannous chloride ($SnCl_2$) as the main ingredient. This step is carried out at room temperature.

Activation of the substrate's surface is subsequently carried out by immersing the substrate into a catalyst – a stannous chloride/ palladium chloride ($SnCl_2/PdCl_2$) acidic colloidal solution, of which for this research was supplied by Alfachimi under the trade name Uniphase php. The fact that palladium (Pd) requires longer deposition times than Sn, may explain why unlike the pre-catalyst dipping which is carried out at room temperature, the catalyst dip is carried out for the same length of time (15 minutes) but at a higher temperature of between 36 and 40^{o}C. Palladium (Pd) is subsequently adsorbed onto the surface of the substrate as Pd^{2+} (Natividad et al., 2004).

Proprietary Niplast at 78 (Alfachimici, Italy), with HCl as its main constituent, is often used as the last pre-treatment stage. The substrate is immersed in the solution between 36 to 40^{o}C for 15 minutes. Besides etching the surface of the substrate which improves the mechanical interlocking bonding between the coating and the substrate, Niplast at 78 is used to ensure loose catalyst particles are not dragged in during the plating process.

It is worthy to note that each step is followed by rinsing the substrate with de-ionised water. This is especially necessary before the plating step as the presence of pre-treatment chemicals can alter the pH of the plating solution (Aleksinas, 1990) which may in some cases affect certain dynamics such as the rate of deposition.

The plating aspect of ECD involves initially heating the plating solution to a specific temperature (which is dependent on the type of the solution being used i.e. alkaline or acidic). Once the plating temperature is achieved, which can be 89^{o}C for acidic EN solutions or as low as 24^{o}C for alkaline EN solutions, the ceramic powder is poured into the plating solution before the substrate is immersed in the mixture. This sequence of ceramic powder introduction before the substrate is immersed is one that for SOFC manufacture must be adhered to. This is because as electroless nickel plating is typically a barrier coating, if the

substrate is introduced before the ceramic powder, plating will initiate on the substrate with the formation of a completely non-porous nickel layer consequent. In terms of SOFC, this will result in a complete starvation of gases to the TPB.

To ensure uniform dispersion of ceramic powder(s) in the solution – a condition critical for particle incorporation in the nickel matrix – the ceramic particles are often agitated by either a magnetic stirrer or a mechanical stirrer depending on the inherent properties of the particles. Plating time can range from ½ hour to 3 hours. Since the process relies on the reduction of metal ions before the adhesion of zero-valent nickel metal to the substrate, the consequent steady depletion of nickel ions in the plating solution with time eventually unavoidably results in an observable decrease in the nickel/ceramic deposition rate onto the substrate (Figure 15).

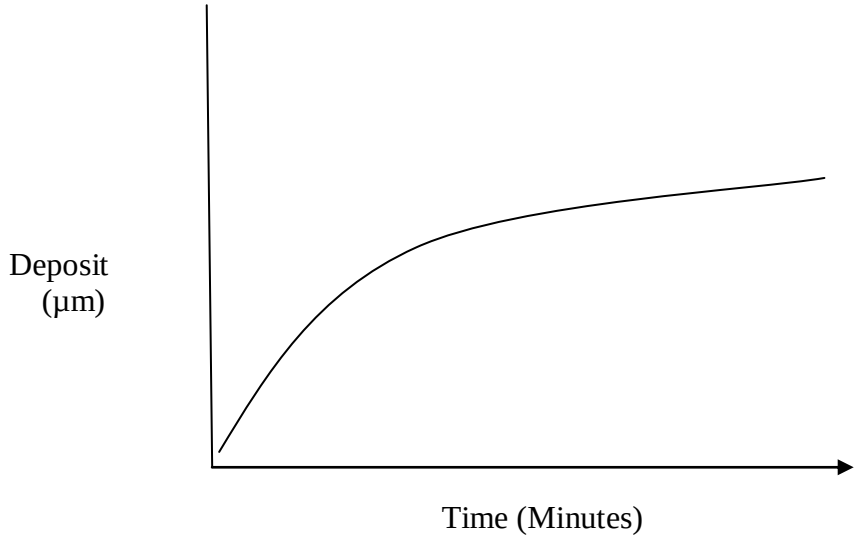

Figure 15. Deposition as a factor of time

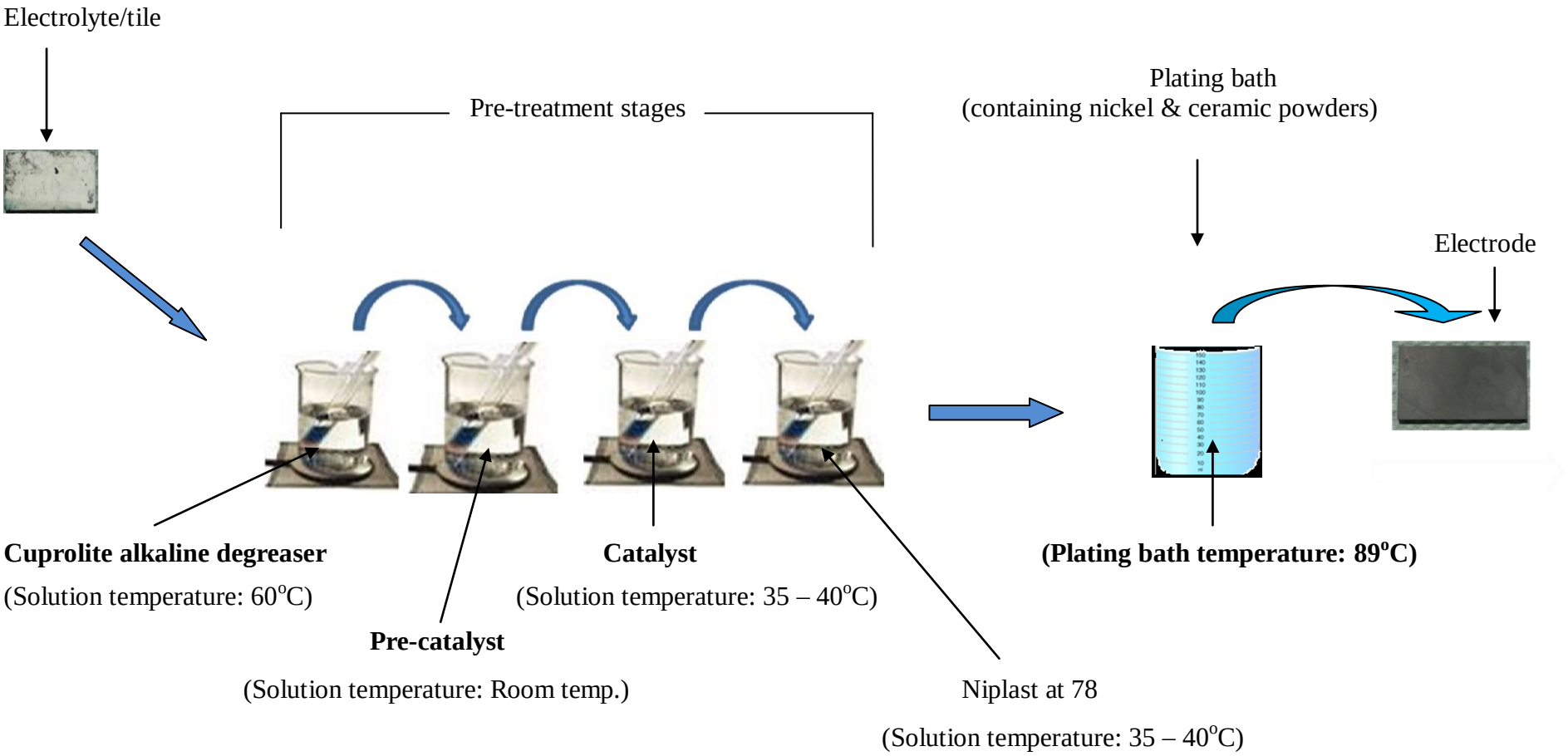

Figure 16. Stages of electroless nickel-ceramic co-deposition process (Nwosu, 2010). Illustration shows the ceramic tile (electrolyte substrate) initially passing through the four pre-treatment stages before coating in the electroless nickel solution takes place.

Figure 16 illustrates various steps of the ECD process. In general acidic EN solutions plate at a faster rate than their alkaline counter parts. Additionally, they are also known to yield thicker deposits.

3.2 Factors influencing the ECD process

Several factors determine the nature and properties of coatings obtained by ECD. To successfully employ the coating technique, a good understanding of the effect of the variables is required.

3.2.1 Bath additives

EN solutions, which can be either acidic or alkaline as previously mentioned, are aqueous solutions consisting of various components that serve different purposes. The primary material in an EN solution is the source of the metal which in most cases is nickel sulphate for acidic solutions or nickel chloride for alkaline solutions. To ensure longevity and suitable performance of the solution, various additives are further introduced into the bath. Their role it must be noted, is not negligible and must be considered for efficient performance during the coating process.

Stabilising agents are compounds that are generally added to an EN bath to prevent bath decomposition. Though one of the main components of the bath, exceeding certain concentrations may result in complete inhibition of the deposition process.

Complexing agents, also known as chelators are a set of additives which bind to the nickel ion, temporarily inactivating and preventing the metal ion from reacting with other bath components. A careful choice of compounds to perform this role is necessary since in addition to performing its role, it also affects the pH of the solution.

Reducing agents supply electrons which reduce the metal, nickel, from its ionic state, Ni^{2+}, to a zero-valent state, Ni^{0}, before its subsequent adhesion to the substrate. The concentration of the reducing agent in the solution is of great importance as it has a direct influence on not only the structure and composition of coatings obtained, but also on the rate of co-deposition. With bath parameters held constant, an increase in the concentration of the reducing agent such as the popular sodium hypophosphite, is known to result in an increase of the rate of deposition of the process. Due to the nature of the reaction, a constituent element of the reducing agent (phosphorus, boron or nitrogen – depending on the reducing agent is used), also generally forms an alloy with nickel in the deposit.

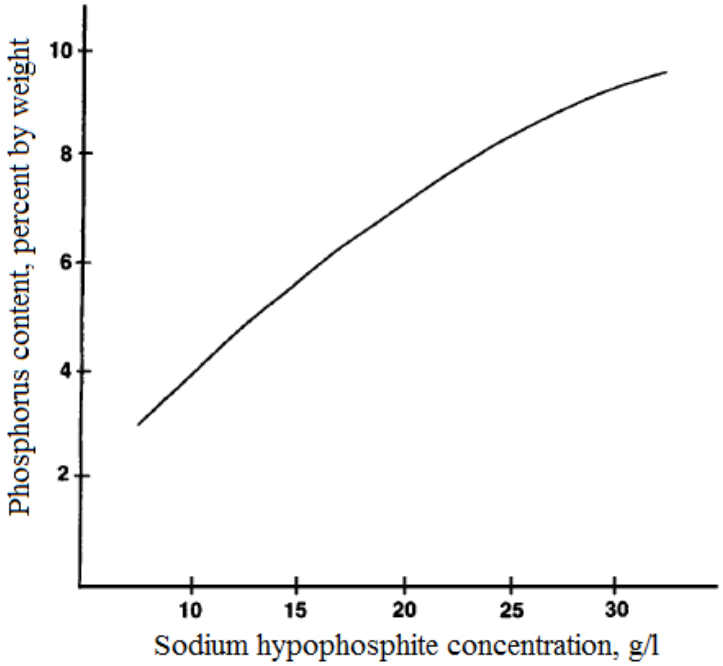

Figure 17. Effect of hypophosphite reducing agent concentration on Ni-P alloy composition

With respect to the structure of the coatings, as the concentration of the reducing agent increases, the microcrystalline structure of plain electroless nickel deposits transform into an amorphous structure due to the increased entrapment of elements such as phosphorus or boron that forcibly distort the ordered face-centred-cubic crystal structure of nickel. This

occurrence has many implications as the magnetic feature of the co-deposits tends to change from magnetic to non-magnetic with increasing phosphorus or boron content. The corrosion resistance of the co-deposits amongst other features, also vary with the amount of reducing agent in the EN solution due to its effect on the coating's level of porosity.

3.2.2 Potential Hydrogen (pH)

The nature of ECD is such that the concentration of hydrogen ions in the solution strongly influences the efficiency of the bath. It is known that for every mole of nickel deposited, 3 moles of hydrogen are generated (Mallory, 1990) [a]. If this occurs in an acidic solution, the pH

$$Ni^{+2} + 4H_2PO_2^{-} + H_2O \longrightarrow Ni^0 + P + HPO_3^{-2} + H2PO_3^{-} + 3H + 3/2H_2 \qquad (3.5)$$

of the solution may lower and consequently pose a challenge to the co-deposition process. In an alkaline EN solution, the required addition of basic compounds such as ammonium hydroxide (NH_4OH) or sodium hydroxide (NaOH), to raise the pH of the solution to greater than 7 often results in excess OH^- ions in the solution. When the OH^- ions are consumed during plating, excess hydrogen is left in the alkaline EN solution and in a similar manner to the acidic solution, consequently lowers its pH. A few problems that may arise as a result of pH variation during ECD are as follows;

(i) If the pH of an alkaline EN solution is allowed to drop to between 8.0 to 8.5, basic nickel salts or complexes will precipitate and result in the solution becoming turbid.

(ii) Phosphite ions which arise as a result of the oxidation of hypophosphite ions used as a reducing agent continuously result in the generation of the compound nickel phosphite. At certain pH values, nickel phosphite is more insoluble and as such will precipitate. If this is allowed to occur, the bath becomes unusable

and must be subsequently discarded. The transformation to nickel phosphite is delayed more at certain pH values e.g. 4.6 as against 5.0 for an acidic EN solution, and as such aiming to maintain the pH at given values is essential.

With the pH of an EN solution of great importance during the co-deposition process, it thus becomes essential that it be controlled with suitable stabilising agents or alternative additives.

3.3.3 Plating temperature

The liberation of chelated nickel ions in an EN solution is required before metallic deposition can occur. As such, an activation energy must be attained before any reaction can commence during the ECD process. Whilst the minimum plating temperature for different EN plating solutions varies, an awareness of the maximum allowable plating temperature for every solution is required. This is because excessive energy input (very high temperatures) has its drawbacks. Deposits produced at high temperatures are often rougher and the risk of plate-out (quick bath decomposition) is high. In fact, according to Mallory, 1990,[b] amine borane reducing agent baths are more temperature sensitive and will hydrolyze excessively at high temperatures causing wasteful side reactions.

3.3 Pre and post co-deposition characterisation techniques

3.3.1 Pre co-deposition

3.3.1.1 Ultra violet visible spectrophotometry

Ultraviolet visible spectroscopy (UV-Vis) offers ample opportunity for the finger printing of an EN solution. This is particularly important if the fact that EN solutions often yield different results when their compositions have been altered. Additionally, since the manufacture of SOFC electrodes involves the co-deposition of nickel and second phase

ceramic particles onto the electrolyte (substrate), the UV-Vis technique will allow for the much required particle dispersion in an EN solution to be assessed.

The technique relies on absorption spectrophotometry, which operates on the principle of electronic transition of molecules under the influence of electromagnetic radiation in the visible (400 ~ 800 nm) and ultra violet (200 ~ 400 nm) wavelength ranges of the electromagnetic spectrum. Incident light is related to emergent light by the Beer-lambert law of;

$$-\log\left(\frac{I1}{Io}\right) = A = \varepsilon bc \qquad (3.6)$$

where A is absorption – a unitless quantity, I_o the incident radiation given in $W.cm^{-2}$, I_I the emergent radiation through the solution also quantified in $W.cm^{-2}$, ε the molar absorptivity given in $L.mol^{-1}.cm^{-1}$, b the cell path length in cm and c the concentration of the solute in the solution in $mol.cm^{-3}$. By varying the parameters in the equation, the relationship very importantly allows for the identification of prevalent species in a solution.

The process can be carried out using a double or single beam process. In the former process, a light intensity of both a reference sample and the test sample are determined at the same time while in the latter process, the reference sample is tried first of all before the test sample

A typical acidic EN solution, such as Slotonip 1850 used in this research is green to the naked eye (Figure 18). UV-Vis evaluation of the solution – which shows distinctive hyperchromicity around the 400nm range, due to the green octahedral hexaquonickel ions $[Ni(H_2O)_6]^{+2}$ (Figure 19) that originate from $NiSO_4.6H_2O$ salts used during makeup of the solution, generally yields a spectrum of the nature showed in Figure 20.

Figure 18. Acidic Slotonip 1850 electroless nickel solution. Green colour synonymous with the presence of green octahedral hexaquonickel ions $[Ni(H_2O)_6]^{+2}$

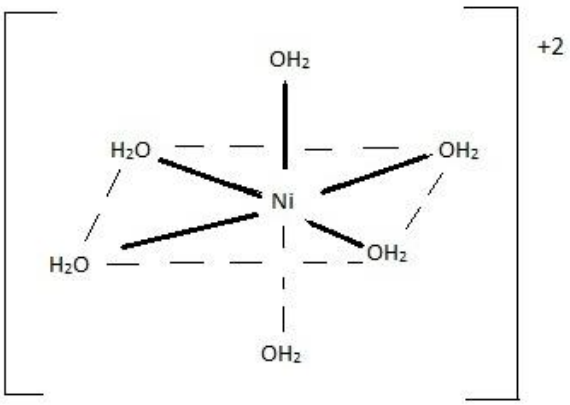

Figure 19. Schematic representation of the green octahedral hexaquonickel ion ($[Ni(H_2O)_6]^{+2}$). (Mallory,1990)

Having the knowledge of such a spectrum is of great importance as it enables for example, the evaluation of particle precipitation ratio (i.e. ratio of dispersed particles to those settled under the effect of gravity) within the solution.

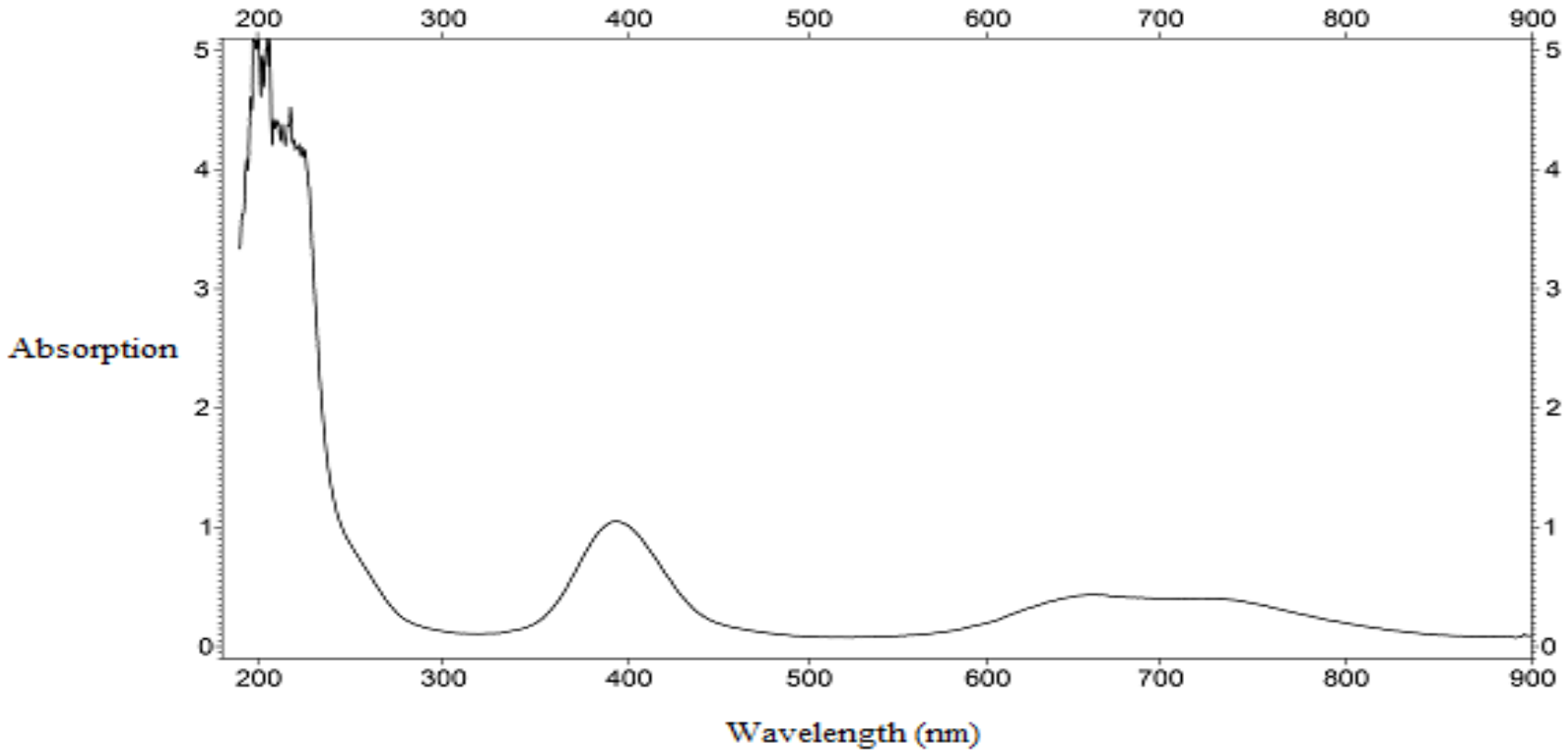

Figure 20. UV-Vis spectra of slotonip 1850 electroless nickel plating solution distinctively showing corresponding high elevations which agree with the green colour of the solution

3.3.1.2 Zeta potentiometry

The importance of zeta potential assessment (ζ) as a pre-coating tool for SOFC electrode manufacture is reflected in its use across almost all (traditional & emerging) SOFC manufacturing techniques. As the achievement of adequate particle dispersion is critical for optimum particle incorporation during ECD or during the makeup of inks for some other SOFC electrode manufacturing techniques, zeta potential measurements allows for good understanding of particle behaviour/dispersion in a given solution.

When a particle is introduced into an aqueous medium (of which an EN solution is one), its behaviour is governed by colloidal principles. Adsorption of anions or cations existing in the solution onto the surface of the particle occurs with the resultant formation of a strong layer of surface charge known as the stern layer. The sea of counter ions still attracted to the particle along with a proportion of co-ions present in the region, tend to form another layer around the particle known as the guoy layer or more popularly the diffuse layer. The build up of these charges ultimately results in an electric potential which, under the influence of a uniformly applied electric field, creates particle mobility relative to the surrounding fluid. The corresponding particle mobility or behaviour, relative to the applied electric field, forms the foundation of what is known as the zeta potential theory (ζ) (electrokinetic effect) (Hunter, 1981).

While a particle possessing a high zeta potential i.e. above +/– 30mV has enough charge to repel a neighbouring particle and thus be dispersed, there is the tendency for particles possessing charges in the band width of –30mV through to +30mV to agglomerate and either be more localised in the coating or settle to the bottom of the bath under gravitational pull (see Table 2). Zeta potential measurements thus very importantly allows for the determination of the tendency of the particles to be dispersed during ECD.

Table 2. Stability of particles in relation to zeta potential (Riddick, 1968)

Stability Characteristics	Avg. Zeta potential (mV)
Maximum agglomeration and precipitation	0 to +3
Range of strong agglomeration and precipitation	+5 to -5
Threshold of agglomeration	-10 to -15
Threshold of delicate dispersion	-16 to -30
Moderate stability	-31 to -40
Fairly good stability	-41 to -60
Very good stability	-61 to -80
Extremely good stability	-81 to -100

3.3.2 Post co-deposition

3.3.2.1 Optical and scanning electron microscopy

Coatings applied for use as SOFC electrodes require inspection at microscopic level. It not only allows for the evaluation of coating thicknesses and uniformities – which are obtainable at micron scales, but enables the visualisation of the nature of pores obtained which include their shapes, size (micro, meso or macro) and distribution.

Using objective lens that magnify a beam of light focused through a condenser lens from an object to a projector lens, images of specimens can be magnified by an optical (light) microscope by as much as a thousand times.

Scanning electron microscopy (SEM) however operates on the principle of bombardment of a beam of high energy electrons on the surface of a specimen. As the electrons decelerate after bouncing off the surface of the specimen, the energy lost in the process dissipates in the form

signals. Amongst the signals given off are very importantly, secondary and back scattered electrons, responsible for visualisation of the morphology and topography of a sample.

3.3.2.2 Energy Dispersive X-ray Analysis

Often an in-situ SEM analytical tool, an energy dispersive x-ray analysis (EDXA) crystal and associated software allows for the compositional analysis of a sample by detecting and processing x-rays emitted during the bombardment of electrons on the sample.

EDXA operates on the principle that the electrons on the shells of a sample can be ejected when struck by a beam of electrons emitted from an electron gun. Because electrons are initially elevated to an excited state which leave vacancies that are subsequently filled by electrons from higher energy states, the energy difference between both energy states, given off in the form of x-rays enables the evaluation of the nature of elements present in the sample.

EDXA is a very useful tool for SOFC electrode characterisation and is extensively used in various other fields such as metallurgy, composites and ceramics.

3.3.2.3 Mercury intrusion porosimetry (MIP)

As mentioned earlier, the nature of pores obtained during SOFC electrode manufacture is critical for efficient gas transportation to the TPB. Open pores are desired as against closed pores that lead nowhere and pore sizes generally sought after for adequate gas transportation are often in the region of 50nm. To ensure that the electronic conductivity function of the electrode is not compromised via a reduction of the electrodes surface area, it is normally ensured that the total void fraction of the electrode is not above 30%.

Considering that if the alignment of pores in an electrode is not right, the fuel cell will still suffer from gas starvation and little or no power will be produced. In line with this,

determining the nature of pores present in a manufactured electrode thus becomes of utmost importance. While instruments like the SEM may help identify pores, more in-depth analysis of the electrode is often required.

Mercury intrusion porosimetry (MIP) is a process by which an element such as mercury – based on its surface tension related non-wetting effects, is forced into existent pores in a bid to determine the percentage number of pores present, shape of such pores (whether closed or open), their size and distribution across the substrate. The process involves submerging the sample in a chamber filled with a known volume of mercury. Mercury will not flow into the pores due to surface tension effects. However, as the applied pressure is increased, different pores are identified by comparing the volume fraction of pores intruded (%) against the intruding pressure (MPa). The total % of intruded volume against the pore diameter in µm is also determined. Macroscopic pores (pores greater 50nm) can often be detected at pressures of below 40KPa while meso (2 – 50nm) and microscopic pores (<2nm) are investigated in autoclaves at pressures as high as 0.2MPa. The relationship,

$$p = \frac{2y\cos\emptyset}{r} \tag{3.7}$$

where p represents applied pressure (MPa), y, mercury's surface tension in $N.m^{-1}$, Ø the contact angle of mercury with the material (degrees) and r the pore radius (m) which is expected to be infiltrated by mercury, is subsequently used to calculate the size of the pores.

3.3.2.4 Atomic Force Microscopy

The structure of an electrode is such that it should have a large surface area in order to increase its rate of reaction by as much as possible. In addition to possessing adequate porosity, rougher electrode surfaces immensely contribute to increment of the reaction kinetics in an SOFC.

To adequately assess the nature of electrodes co-deposited, atomic force microscopy (AFM) is often relied upon for authentic surface topography profiling. Also known as scanning force microscopy (SFM) and though variations exist, its mechanism of operation involves electric potentials being given off by piezoelectric elements travelling along the surface of a specimen. An image of the surface is correspondingly obtained during the mechanical movement of a cantilever-like probe. The process may be carried out in contact or non-contact modes. Maximum image able heights are of the order of 10 – 20µm with maximum scanable ranges in the region of 150 x 150µm.

Of the results produced, the rugosity i.e. the identified average surface roughness value of the coating (Ra) which is the combined average of the difference between the peaks and valleys on the specimen, is of greatest importance. Ra values are also popularly referred to as centre line average (CLA) or arithmetic average (AA) values.

Chapter 4

Potential plating aids:
Surfactants and magnets

This chapter focuses on external factors, introduced in an attempt to enhance the ceramic content of SOFC electrodes manufactured by the electroless nickel ceramic co-deposition process. In addition to an outline of the underlying principles behind the selection of electromagnets and surfactants as key co-deposition external agents, other variables outwith the solution that could also alter the rate of co-deposition during the plating process are further highlighted and discussed.

4.0 Introduction

Seldom considered to be of much importance during the co-deposition process, the dispersion stability of particles during the ECD process, is a critical condition that must be considered and optimised if maximum incorporation of ceramic particles into the nickel matrix is desired. According to Balaraju et al. (2003), unless the particle density is low, if the rate of agitation is too slow (laminar flow), the particles may not disperse completely in the solution. Conversely, if the rate of agitation is high (turbulent), the particles may not have sufficient time to get attached to the surface of the substrate and consequently result in poor particle incorporation into the nickel matrix.

Various methods of encouraging particle dispersion in a medium have continued to evolve over the years and many have found use in several industries. While some are primarily relied upon, others are often used as complements. It was envisaged that the application of certain traditional and evolving particle dispersion techniques during the co-deposition process may present ample opportunities for enhanced second phase particle dispersion during ECD.

4.1 Surface active agents (Surfactants)

4.1.1 Rudiments of surfactants

With molecules consisting of lyophilic – hydrophilic moieties (i.e. amphiphilic), surfactants are surface active agents. Their classification is based on the manner in which they dissociate in a medium and underlying principles exist for their selection in any process

A surfactant's molecule consists of a hydrophobic hydrocarbon or fluorocarbon tail of 8 − 18 carbon atoms and a hydrophilic part having an affinity for water i.e. amphiphilic (Figure 21).

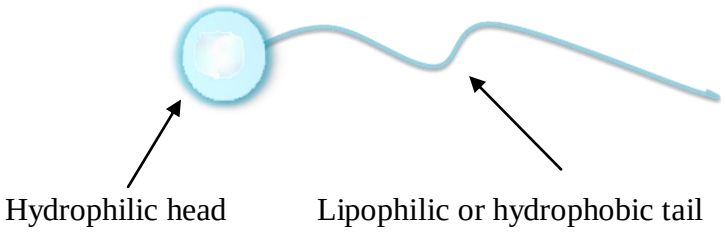

Figure 21. Simplified schematic representation of a single surfactant molecule

Surfactants that dissociate in a medium to yield negatively charged amphiphilic ions are classed as anionic surfactants. Those that produce positively charge amphiphilic ions are referred to as cationic surfactants while those that do not dissociate at all and thus bear no charge are known as non-ionic surfactants.

4.1.2 Essential criteria for surfactant selection

The criteria for selecting a surfactant often revolves around having a good appreciation of a compound's hydrophile – lipophile balance (HLB). Other factors such as the temperature at which the surfactant is being used, its stability and reactivity with the solution (Nwosu et al., 2012), also have major bearings on the type of surfactant suitable for use in any given medium.

Calculated on a molecular weight basis, high HLB number surfactants (>10) are generally soluble in water while those that are less than 10, are soluble in oil. A balance between the hydrophobic and hydrophilic portions of a surfactant is generally required because if the molecules of a surfactant are too soluble in medium – water or oil, they cannot suitably perform and may dissolve completely into that phase.

In very low concentrations in a bath, surfactants tend to exist as single molecules (Figure 22). As the concentration increases, the molecules begin to transform into aggregates known as

micelles. Amongst the numerous effects of this transition includes a reduction of the solution's surface tension (Figure 21).

The concentration above which the micelles are first detected is known as the critical micelle concentration (CMC). The CMC which directly affects the performance of a surfactant is unique to every surfactant and is affected by many factors.

4.1.3 Surfactant selection

In this research, a series of factors were considered during the surfactant selection process. As one of the aims of the project was to reduce the manufacturing costs of SOFC's, relatively affordable, effective and commonly available materials were sought after to serve as surfactants.

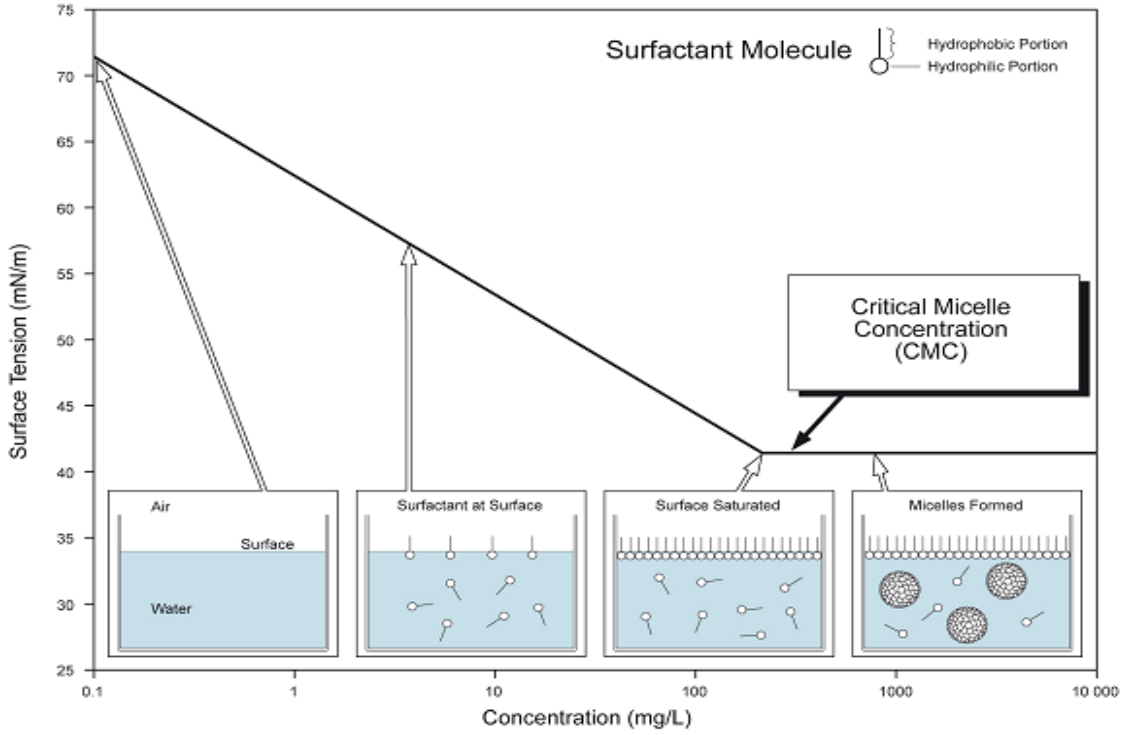

Figure 22. Surface tension vs surface concentration. The critical micelle concentration is highlighted. (www.kruss.de)

With an HLB of 40 indicating excellent water solubility characteristics, sodium dodecyl sulphate (SDS) (Figure 23), an anionic surfactant with good dispersing, wetting, emulsifying and solubilising characteristics was selected as first choice for the experiments. Additionally,

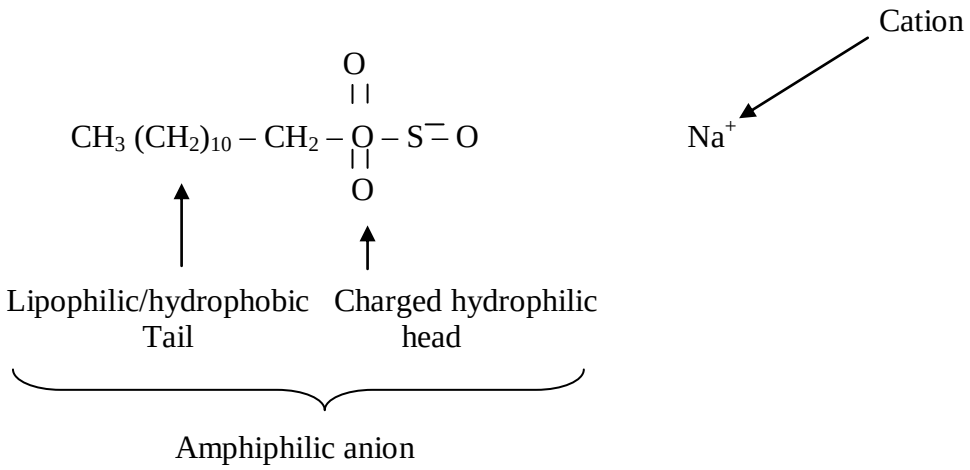

Figure 23. Chemical structure of a dissociated sodium dodecyl sulphate molecule

since SDS possesses a krafft temperature (the temperature below which a soluble surfactant becomes insoluble in a medium and cannot achieve the critical micelle concentration) of between 8 – 16^{o}C (Watanabe et al., 2005) and is stable at high EN deposition temperatures, the compound appeared to be the most appropriate for use during the co-deposition process.

To investigate the possibility of another type of surfactant having a different effect on the dispersion stability of the ceramic particles, a non-ionic surfactant was further selected. Non-ionic surfactants in a similar manner to inert fluoro surfactants notably exhibit stability in aqueous solutions due to non existence of charges

Polyethylene, a cheap and commonly available material was the first port of call. However because polyethylene consists of two methylene groups (CH_2) (Figure 24) – which are completely insoluble in water (non-polarity arising from fully opened bonds between carbon and hydrogen atom – CH bond) the polymer was unsuitable for the intended purpose.

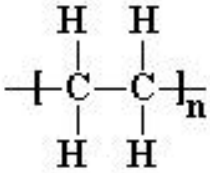

Figure 24. Molecular structure of polyethylene

From literature, Gabrielson & Edirisinghe, (1996) and Rao et al., (2003) have suggested that good ceramic particle dispersions can be obtained by using high molecular weight polymers such as co-polymers rather than homopolymers. In line with their works, the possibility of combining some averagely low to medium costing materials was considered. The polymers polystyrene (PS) and polymethyl methacrylate (PMMA) were chosen based on their structure.

As PS contains phenyl (C_6H_5) and CH_2 groups (Figure 25(a)) while PMMA contains a soluble ester group with double and single carbon-hydrogen bonds (Figure 25(b)), it was expected that both materials would have varying degrees of solubility in an aqueous medium – PS completely hydrophobic and PMMA relatively hydrophilic.

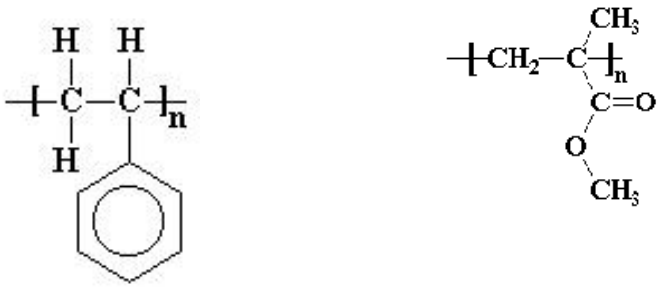

(a) (b)

Figure 25. Molecular structure of (a) polystyrene and (b) polymethyl methacrylate

As both polymers seemingly met the conditions for use as a non-ionic surfactant whereby a non-ionic surfactant's molecule must contain at least one hydrophilic portion while the other part contained a hydrophobic segment, it was considered that a block co-polymer consisting of both polymers could be used as a surfactant

For successful co-polymerisation of PMMA and PS, reactivity ratios of polymers which determines the affinity of a monomer for itself or another monomer was consulted (Table 3)

Table 3. Extract of polymer reactivity ratios (Rudin, 1999)

Monomers	Reactivity ratios	
Styrene	0.5	r_1
Methyl methacrylate	0.5	r_2

With r_1 referring to the rate of reaction of the first monomer and r_2 referring to the rate of reaction of the second monomer, it is known that when $r_1 * r_2$ is less than 1, both monomers will polymerise. From Table 3, it is clear that both styrene and methyl methacrylate monomers have encouraging reactivity ratios towards each other ($r_1 * r_2 = 0.3$) and thus can be synthesised and used for experimentation.

4.1.3.1 Synthesis of block co-polymer surfactant, PMMA/ PS

The respective monomers, methyl methacrylate for PMMA and styrene for PS – which unlike their solid polymerised forms exist as liquids at room temperature, were used in the manufacture of a copolymer surfactant. Both were obtained from Sigma Aldrich, U.K.

Emulsion polymerisation, a form of free radical polymerisation, was chosen as the method of manufacturing the co-polymer surfactants. The ability for excellent heat control during

polymerisation, opportuned by the presence of a continuous phase of water that provides a heat sink, allowed for a high level of safety during the operation.

A 5-neck condenser vessel (Figure 26) was used and the recipe was adopted from the work of Lautrey, 2009. Essentially, the vessel contained 128.2 ml of de-ionised (D.I.) water to act as the dispersing medium, 100 ml of the surfactant SDS to act as an emulsifier and 31.4 ml of the water soluble oxidant and polymerisation initiator, potassium per-sulphate (PPS) to trigger the process by opening up the reactive sites of respective monomers (Rudin, 1999).

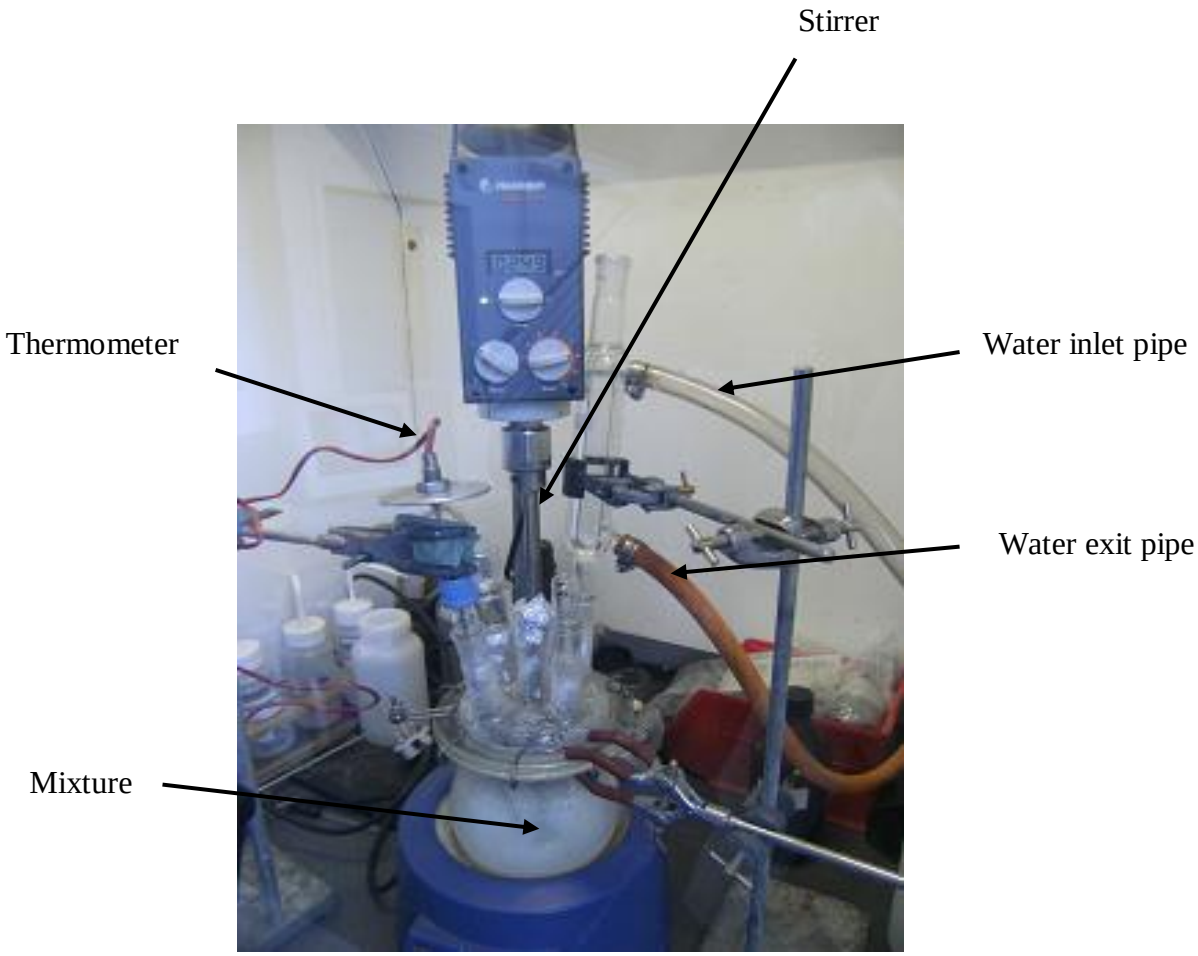

Figure 26. Five neck condenser vessel showing the experiment setup for emulsion of polymerisation of co-polymer surfactants and precursor constituents

The reactants were added at room temperature i.e. 20^{o}C in the order of D.I. water first, SDS then PPS. Thereafter equal quantities (35.6g) of the monomers styrene and MMA were added. The temperature of the mixture was raised to 80^{o}C and stirring was maintained at the rate of 250rpm. The process was allowed to proceed for 6 hours although a length of 3 hours would have sufficed if there was nitrogen to remove oxygen from the reaction which normally retards it.

A solid white material (Figure 27) was formed after the polymerised PMMA/PS was left in air for about 15 hours – a result suggestive of polymerisation.

Figure 27. Image of dried polymethyl methacrylate/ poly styrene after being left in air about 15 hours

To confirm the extent to which the monomers co-polymerised, if at all, subsequent experiments involved applying the same procedure detailed above to polymerise monomers of methyl methacrylate and styrene separately. Figure 28 obtained with the aid of a Perkin Elmer 881 infrared spectrophotometer, agrees with the standard obtainable infrared spectrum of the polymer poly methyl methacrylate (carbonyl C=O, ~1725 cm^{-1}, ether C–O–C, ~1230 – 1170 cm^{-1}) while Figure 29 distinctively confirms poly styrene with strong peaks between

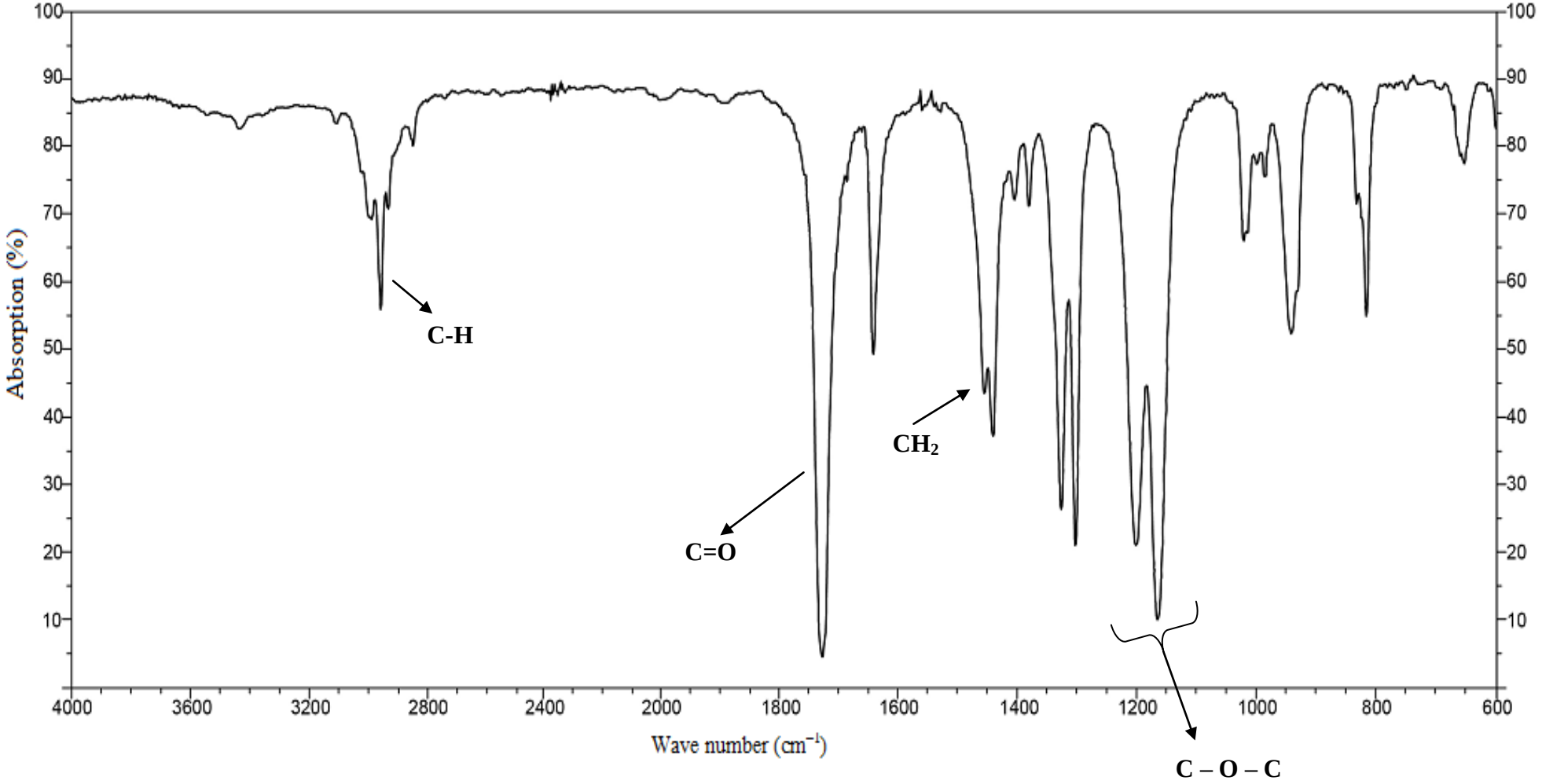

Figure 28. Infrared spectrum of polymethyl methacrylate as confirmed by the carbonyl (1735 cm^{-1}) and ether (1230 – 1170 cm^{-1}) peaks.

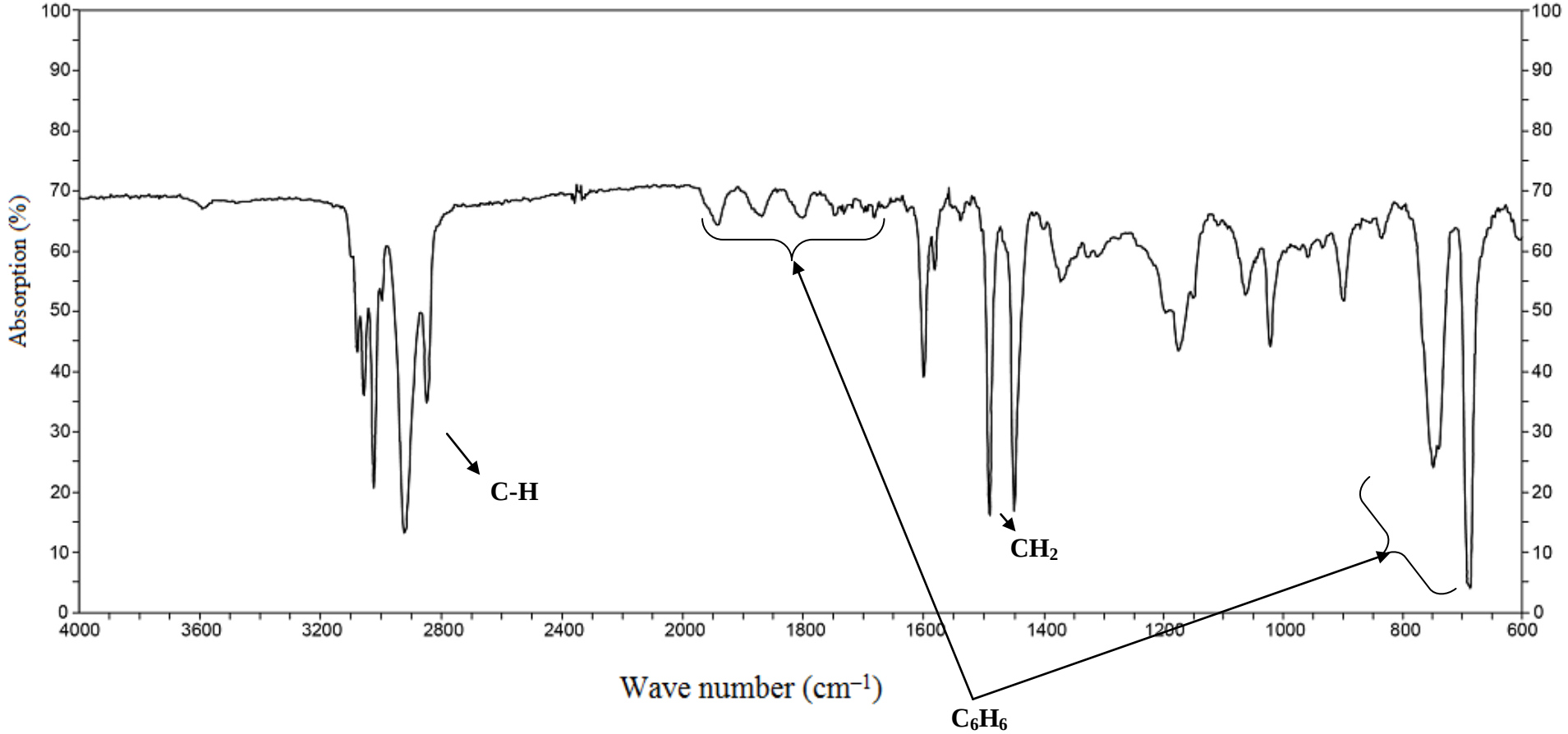

Figure 29. Infrared spectrum of poly styrene confirmed by the presence of carbon hydrogen bonds (~3000 cm^{-1}) and a phenyl unit (800 – 700 cm^{-1})

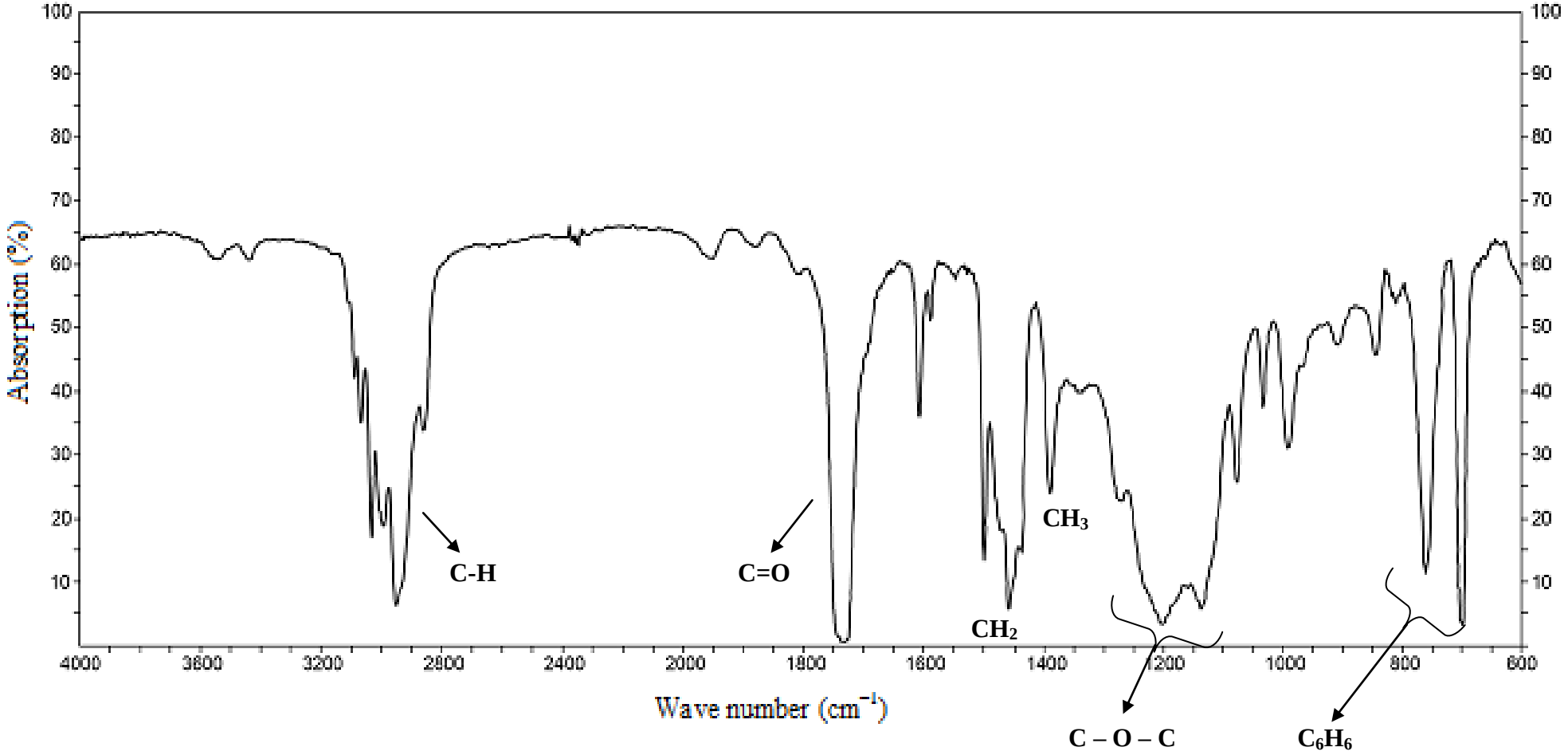

Figure 30. Infrared spectrum of polymethyl methacrylate/ poly styrene copolymer. Distinctive peaks confirm presence of both methyl methacrylate and styrene units.

800 – 700 cm^{-1} & 2000 – 1600 cm^{-1} verifying the presence of the phenyl ring. When compared to Figure 30, the presence of all the peaks in one spectrum can be clearly seen – a finding suggestive of successful copolymerisation of styrene and methyl methacrylate monomers.

4.2 Magnetic field

On the back of the fact that ions exist in an EN solution, the possibility of exploiting the consequent effects of ionic motions within the solution arises. Since the movement of charged particles is known to generate magnetic fields, imposing an external field may in-line with theories such as that of mass spectrometry, control the direction of flow of the ions within the solution. It is believed that if ions or particles within the solution can be channelled in the direction of the substrate, then the opportunity to improve the nature of deposits obtained by ECD arises.

Since the ECD process involves the introduction of second phase particles and some form of attraction must exist for the influence of the magnet to be felt, a caveat may then exist that any particle/ powder to be used in the ECD process must at the barest minimum also be magnetic. Figure 31 illustrates the theory and as can be seen, for it to be effective, any powder to be co-deposited with nickel may be required to have a strong magnetic orientation.

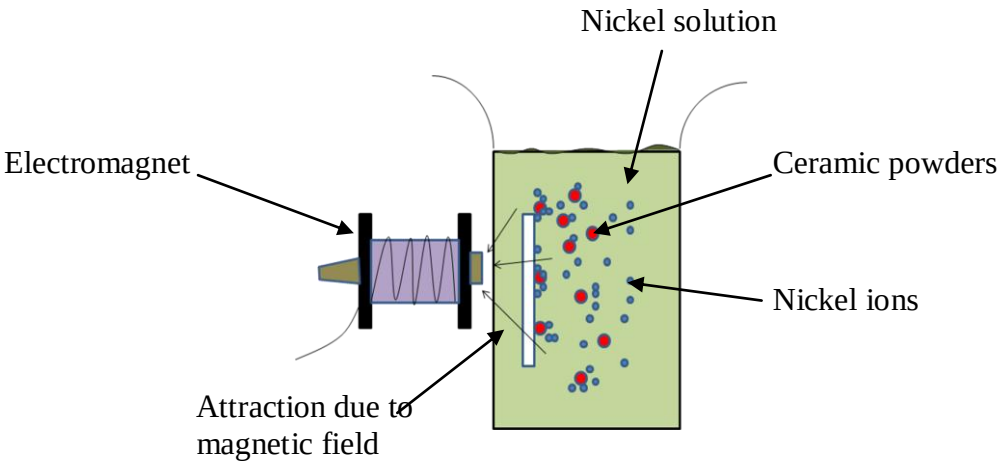

Figure 31. Illustration of particle attraction to the substrate

4.2.1 Magnetic properties of LSM particles

Arising from the doping of strontium at the A- site of the $A_mB_nX_p$ perovskite crystal structure anti-ferromagnetic ceramic material (Figure 32) lanthanum manganate ($LaMnO_3$), the SOFC cathode material, LSM, is well known to possess a magnetic orientation. Though an attribute

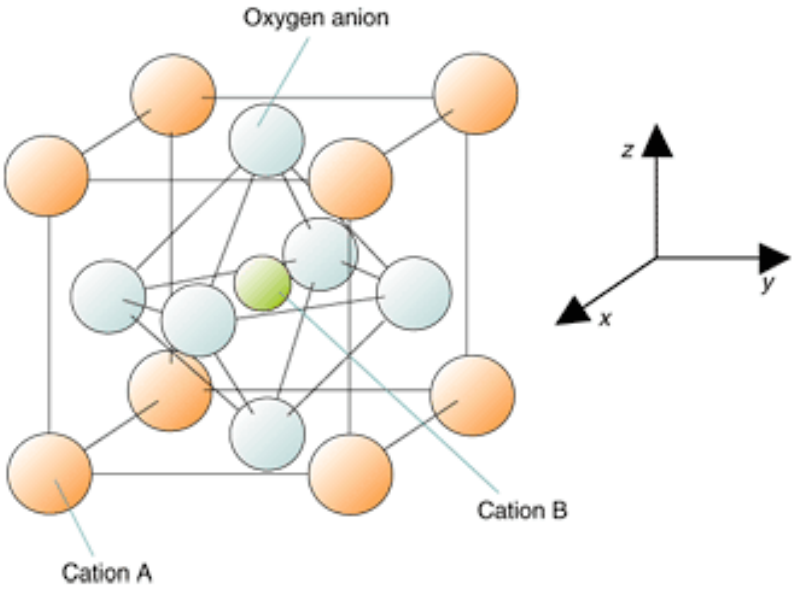

Figure 32. Crystallographic structure of Lanthanum Strontium Manganate showing A- , B- and X sites (Imai et al. 2007)

that may seemingly suggest its suitability for co-deposition by ECD under the influence of a magnetic field, the level of strontium doping in LSM strongly alters the physical properties of the material and thus prompts careful consideration prior to the material's selection for use in in the ECD process and furthermore, SOFC technology. This is because as strontium is a lower valent metal than lanthanum, lanthanum transforms from its La^{3+} ionic state to La^{2+} as former is introduced into the matrix. As a spin off effect, a change occurs in the manganese – oxygen (Mn – O) interactions whereby Mn^{3+} ions transform to Mn^{4+} to compensate for charge loss at the A- site (Figure 33). In order for manganese and oxygen to exchange electrons with

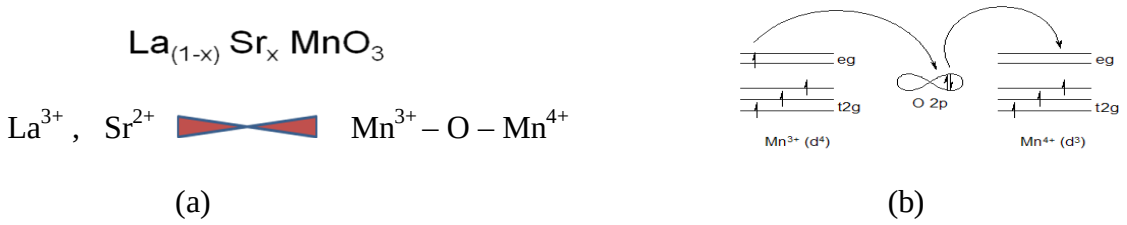

(a) (b)

Figure 33. Illustration of (a) La, Sr, Mn and O ionic interaction and (b) Mn-O electron orbital exchange typical of the double exchange mechanism (illustration (b) taken from Zener, 1951)

the lowest possible amount of energy, the interchange alters and the electrons begin to spin in the same direction – a theory referred to as the double exchange mechanism and first proposed by Clarence Zener in 1951 (Zener, 1951; Jonker & Van santen, 1950; Watanabe, 1961). Once uniform directional alignment is achieved, the material becomes ferromagnetic (McCarrol et al., 1999).

As the level of strontium doping increases, the electronic conductivity of LSM (generally about 107 $S.cm^{-1}$) also correspondingly increases as well. However, while this condition which steadily makes LSM more metallic should be favoured in SOFC applications, it has a downside. The increasing metallic nature of the material generally translates to it possessing a higher coefficient of thermal expansion. Higher coefficients of thermal expansion generally nurture a coefficient of thermal expansion mismatch between the electrode and other components of the cell. If this event is allowed to happen, a compromise of the cell's integrity during operation will most likely occur (Ullmann et al., 2000).

Since the degree of magnetic susceptibility of the particles has an effect on some physical properties of the cathode electrode, the composition of the powder becomes of paramount importance in the manufacture of SOFC electrodes and the co-deposition process.

4.2.1.1 Magnetic susceptibility of selected LSM powders.

To test the magnetic characteristics of LSM, a simple test was set up. An electromagnet was placed near a beaker filled with 100 ml D.I. water and 1g of LSM powder. When a source of electricity was switched on, the particles in the solution were strongly attracted to the pole pieces inserted into the middle of coil. Conversely, when the power source was switched off, the particles dispersed and settled to the bottom of the beaker.

At this juncture, the effect of the strength of the magnetic field could not be investigated as any increase of magnetic intensity above a magnetic field strength of 20mT produced the same results of all the particles being strongly attracted to the pole pieces.

4.3 Other variables considered

4.3.1 Bath loading

Sheela & Pushpavanam (2002) highlighted the effect of bath loading on the nature of cermets manufactured by electroless nickel co-deposition technique. They varied the powder concentration in the bath from 0 to 10g/l and observed that the % incorporation by volume of second phase particles into the nickel matrix varied from as low as 10.90 vol. % at 2g/l to as high as 27.70 vol. %. Waugh (2009) observed the same relationship even when different ceramic particles were used (YSZ as compared to diamond used by the former). However both researchers obtained their highest ceramic content at different powder loadings.

Initial experiments in this study were focused on determining the optimum loading of ceramic powders prior to the use of any external agent. Along with the effect on the composition of coatings deposited, the associated consequence on dynamics such as rate of deposition and coherence of the coating were also examined with a view to establishing the best coating parameters.

4.3.2 Particle size

Electroless nickel plating operates on the principle of metal nucleation at catalytically sensitive areas on the surface of a substrate. Subsequent growth occurs in an isotropic manner. If it is envisaged that particle entrapment will require the growth of the nickel layer around the particles (Figure 34), then the particle size should be expected to have a contributory effect on the rate at which the nickel layer grows and subsequently envelopes the particles. This theory is experimented in this research to observe if the particle size plays any part in determining the rate of particle incorporation or growth of the nickel layer.

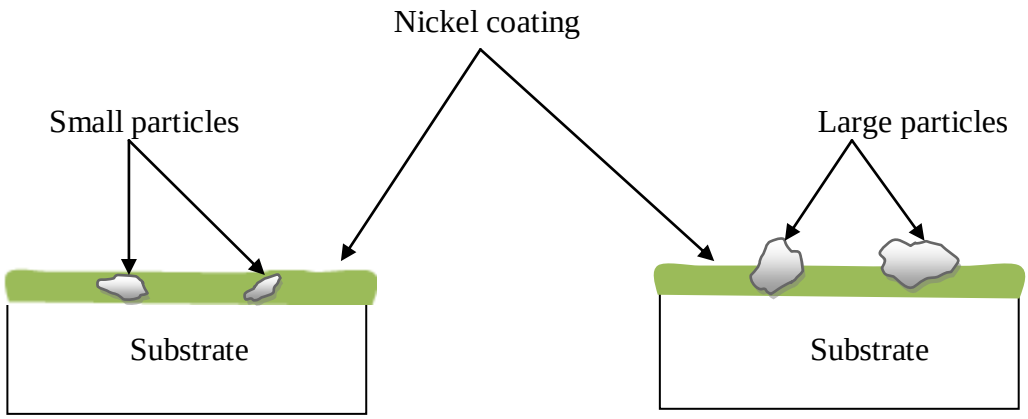

Figure 34. Schematic representation of the possible effect of particle size on particle incorporation during electroless nickel ceramic co-deposition

4.3.3 Rate of agitation

The work of Baba in 2010 showed that the method of particle agitation during ECD had a strong influence on the degree of particle incorporation into the nickel matrix. Sisti and laplante (2001) also proffered that the rate of agitation if not controlled and regulated, may have serious detrimental effects to the nature of deposits obtained by electroless nickel plating. To ensure that the best results were obtained during the ECD process, careful consideration for the effect of agitation on the nature deposits achieved was given in this research through a thorough selection process.

Chapter 5

Experimental work – Part I:

Preliminary assessments

The findings from preliminary investigations carried out to evaluate the effect of the selected external agents on ceramic particle behaviour in an electroless nickel (EN) solution, are detailed in this chapter. As well as focusing on the specific influence of the EN solution on the particles' dispersion stability, other key factors that may have considerable effects on the nature of coatings obtained from the co-deposition process are also discussed. The framework for different designs of experiment matrix used during the co-deposition stage is subsequently built on the information presented in this chapter.

5.0 Introduction

Initial practical work focused on the establishment of parameters required to possibly obtain the best experimental results. The type and quantity of surfactants required to achieve adequate particle dispersion stability, response of the particles to magnetic attraction and the possible interaction between the solution and particles were all assessed and pre-determined.

5.1 Electroless nickel solution – ceramic particle interaction

5.1.1 Assessment by ultraviolet visible spectrophotometry

5.1.1.1 Sample preparation

Prior to plating with external agents, tests were carried out to determine the influence of the EN solution on the particles' dispersion stability. An acidic electroless nickel solution which as mentioned in section 3.1 offers a faster rate of deposition and is generally more stable than its alkaline counterpart, was used. The rate at which the particles sediment (if at all) known as the particle precipitation ratio (PPR) was assessed by the ultra-violet visible spectrophotometry (UV-Vis) technique. The instrument used was a Perkin Elmer Lambda 7 Ultraviolet–Visible spectrophotometer and all assessments were carried out at room temperature.

A high PPR would indicate large particle instability while a low PPR would suggest good particle stability and in turn reduce the magnitude of negative forces acting against the external agents when used. To verify the UV-Vis results and also determine the charges of the particles which may aid attraction to the charged surface of the substrate, the zeta potential of the particles was also assessed. A Malvern instruments zetasizer nano ZS was used to obtain the necessary data.

Determining a suitable datum for the UV-Vis assessments initially involved a complete ultraviolet – visible spectrum (190 – 900nm) scan of the electroless nickel solution. As previously shown in Figure 20, the spectrum revealed a peak and a slight elevation around the 400nm and 700nm wavelengths. Since the hyperchromicity around the 400nm wavelength was responsible for the green colour of the solution, it was selected for the PPR assessments.

At the summit of the absorption peak – around the 400nm wavelength, a maximum absorption of 1.072 was noted against a wavelength of 392.8nm. An extract of this peak from Figure 20 can be seen in Figure 35 below.

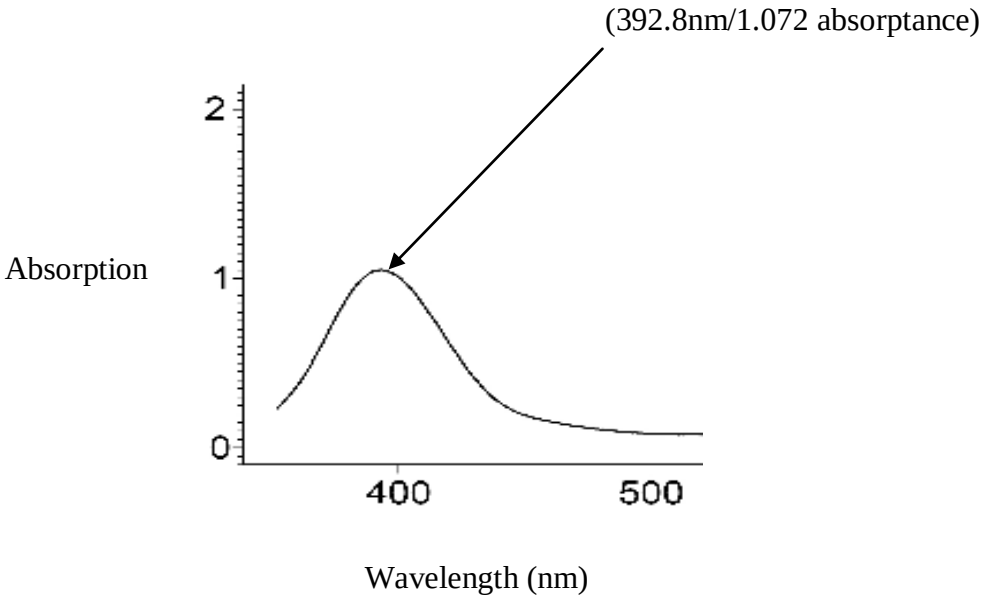

Figure 35. Dominant peak of acidic UV–VIS spectra of acidic electroless nickel solution

An absorption-time scan was thereafter carried out at the 392.8nm wavelength in order to establish the stability of the solution and determine a datum for the PPR assessments. This yielded a constant absorption of 1.072 – an observation that not only confirmed that the solution on its own was stable but also showed that all the materials used in its make-up had dissolved in it (Figure 36).

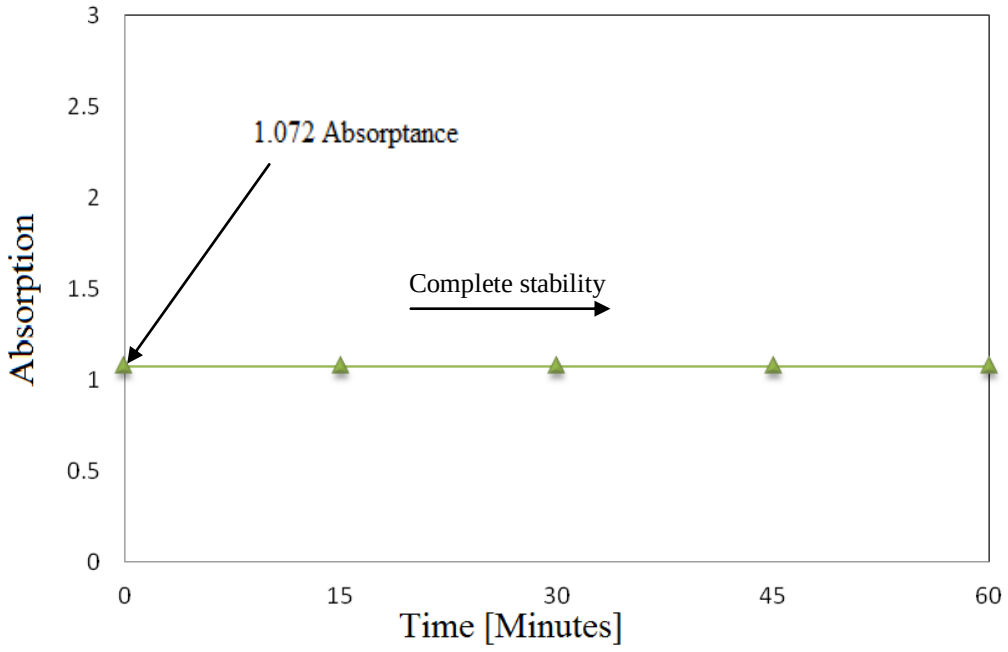

Figure 36. Absorption of electroless nickel solution at 392.8nm. The unchanged absorption over a 60 minute period indicates complete stability of the solution.

With the datum established, the particles were then introduced. Prior to their introduction though, samples were prepared by initially dispersing 1.25g of powder (YSZ or LSM) in 25ml of EN solution – equivalent to 50 g/l. A Heidolph MR 3001 magnetic stirrer-heater with a stirring speed of 700rpm was used to achieve this purpose

Upon mixing the ceramic powder with the EN solution, the solution became white when YSZ particles were introduced and black, when LSM powder was added (Figure 37). An accompanying feature of both solutions as seen in Figure 37 (b) & (c) was the opaqueness of the solutions which made the UV-Vis test less difficult. This was because based on the principle of the Beer-Lambert law given in equation 3.6 (page 40), I_o (the incident radiation) would remain constant, while the absorption A, which depends on the amount of particles in suspension will substantially increase due to the obstruction light passing through the solution. As sedimentation occurs (if at all) and clear nickel solution begins to separate above, a corresponding change in I_1 (the emergent radiation) which would concomitantly be reflected in the degree of light absorption (A) by the EN solution would be observed (Figure 38).

(a) (b) (c)

Figure 37. Images of the electroless nickel solution (a) before and after the introduction of (b) YSZ and (c) LSM powders

5.1.1.2 Analysis

With the theory established and the analytical samples prepared, aliquots of the dispersed solutions were poured into a 5 ml quartz cuvette positioned in the spectrophotometer's cradle. As a reference for the scan, another cuvette filled with de-ionised water was place in an adjacent cradle in the equipment. The cell path length used for the scan was 1 cm and the scan

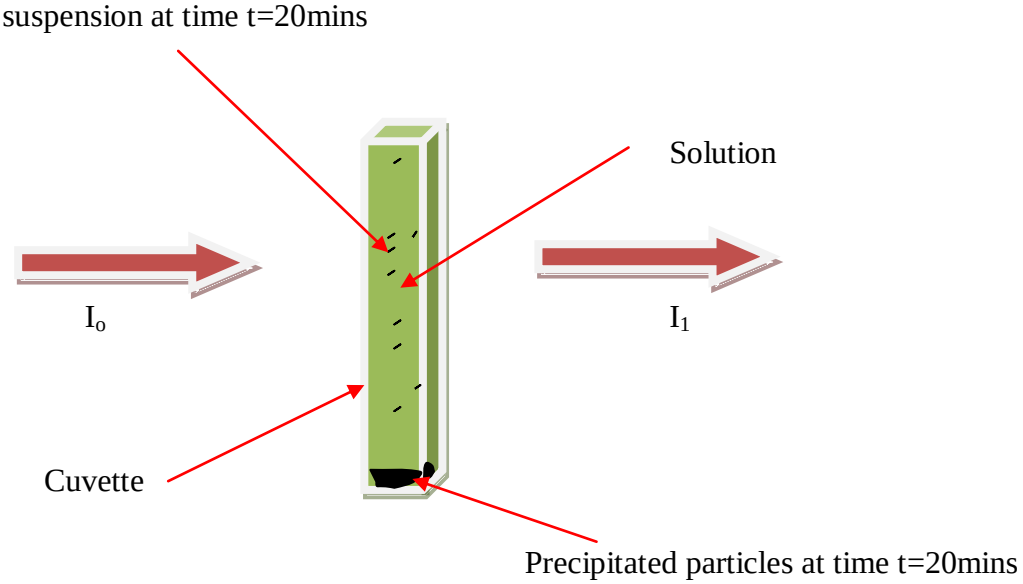

Figure 38. Schematic representation of Beer Lambert law showing incident light beam, precipitated particles and particles in suspension.

rate was 480nm.min^{-1}. Since nucleation and deposition during electroless nickel plating mainly occurs within the first hour, the sedimentation patterns were observed over a 60 minute period.

5.1.1.3 Result of EN solution – ceramic particles PPR experiment

Figure 39 shows the sedimentation patterns of YSZ and LSM particles in an acidic EN solution. As can be seen, the particles displayed high levels of instability in the solution. With initial absorption values of 5.549 and 6.071 at time t = 0 and 2.084 for YSZ and 1.216 for LSM respectively at time t = 15 minutes, it was clear that 77% of YSZ particles (very high PPR) and 97% LSM particles (indicative of even faster settlement) had settled to the bottom of the cuvette within the first 15 minutes.

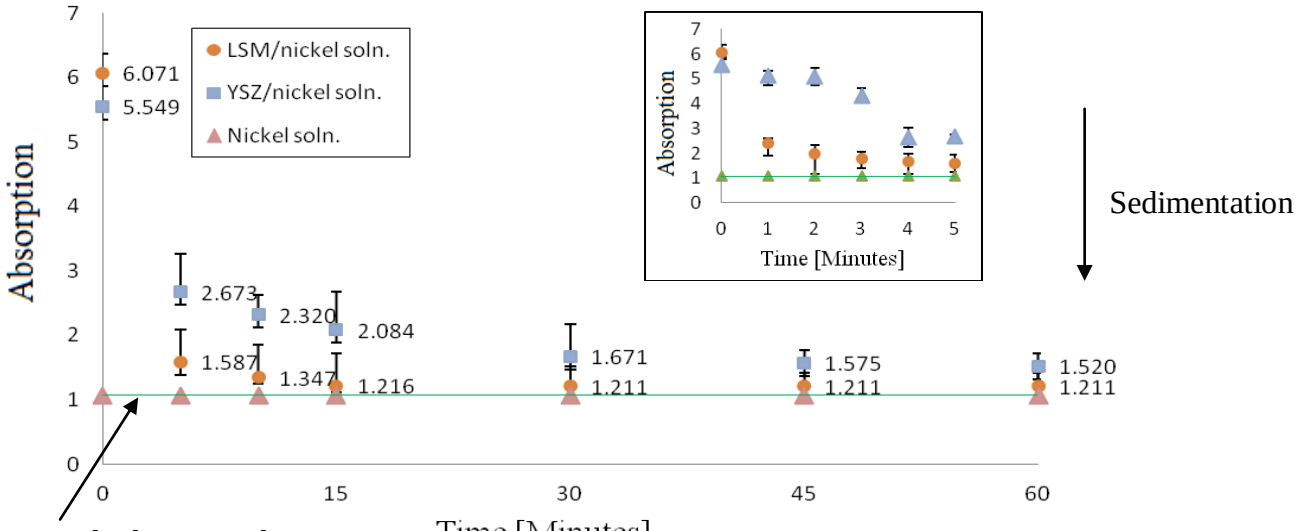

Figure 39. Sedimentation patterns of both LSM and YSZ particles in an acidic EN solution. Insert shows sedimentation pattern of particles within the first 5 minutes

When PPR tests were conducted in plain de-ionised (which was used in the make-up of the EN solution), the YSZ particles showed large stability (low PPR) with little particle

sedimentation occurring on the contrary (Figure 40). Though better than that displayed in the electroless nickel solution, LSM again showed poor stability.

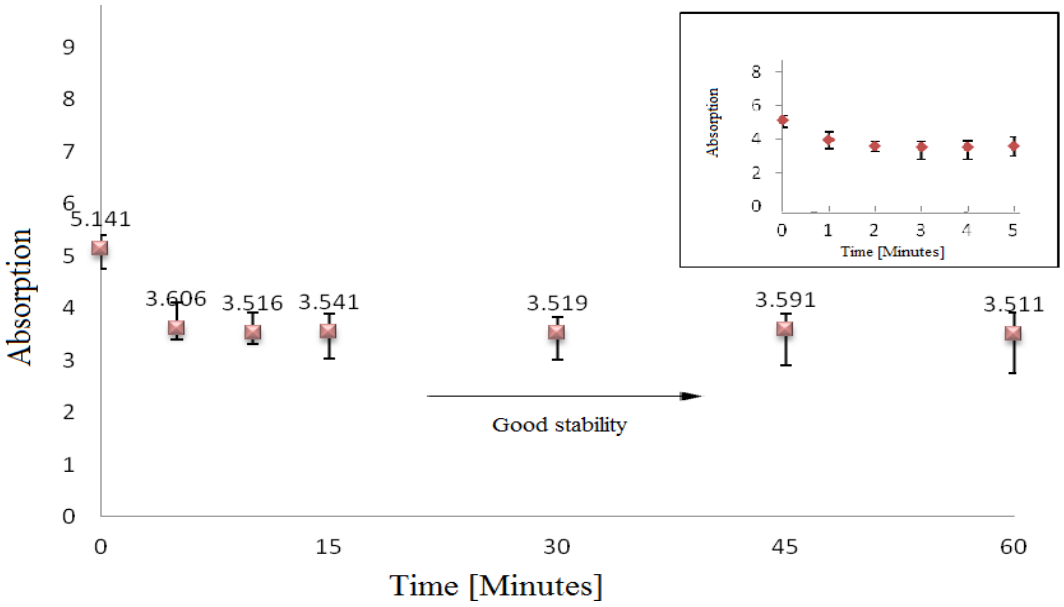

Figure 40. Absorption vs. time plot of YSZ particles in deionised water (Error bars indicate spread of values).

5.1.2 Zeta potential assessment of YSZ & LSM particles in an EN solution

Zeta potentiometry technique was used to verify the dispersion stability (PPR) UV-Vis spectrophotometry results. It was additionally hoped that the results obtained from the assessment would provide more information with regards to the overriding dynamics between the particles and the EN solution.

Before the prepared samples were assessed, 1.5 ml disposable folded capillary cells used for the test were flushed with 50% ethanol to eliminate and prevent the build up of wall charges inside the container. 5 measurements were taken for every set of 14 runs and 3 rounds of tests were conducted for every solution analysed.

Table 4 shows the zeta potential of both YSZ and LSM particles in deionised water and EN solution (tests carried out separately). The low zeta potentials exhibited by the particles in the

EN solution as compared to the high zeta potentials recorded in water – which suggested better repulsion between the particles, highlighted a negative effect of the EN solution on particle stability. A comparison of both solutions' conductivities it is believed provided an explanation to the observed phenomenon.

Table 4. Zeta potential of LSM and YSZ particles in deionised water and EN solutions

Medium	YSZ	LSM
Deionised water	29 mV	7 mV
EN solution	– 12mV	– 3 mV

While the electroless nickel solution had a conductivity of 39.79 $S.cm^{-1}$ – indicative of a high ionic strength originating from ions such as NH_4^+, Na^+, Cl^-, H_2PO^- and Ni^{2+} in the solution, the conductivity of D.I. water was found to be as low as 3.6×10^{-6} $S.cm^{-1}$. As it is known from literature, a high ionic strength will tend to compress (Jakob et al., 2000) or in some cases collapse (Dukhin & Goetz, 2002) the double layer surrounding the particles in the solution. If compression or collapse of the double layer occurs, particle agglomeration will result (Derjaguin et al., 1941). As a consequent effect and due to density, particle sedimentation will tentatively occur.

On analysis of the particle size with the zetasizer, it was apparent that particle agglomeration was occurring in the EN solution – thus confirming the theories cited above. Evidence for it could be seen from the fact that submicron YSZ particles used for the test accurately had an average size of 692.4 nm when analysed in D.I. water. When assessed in the electroless nickel solution, the agglomerate sizes had grown to an average 2,672 nm within 60 seconds of introduction in the solution (Figure 41). LSM exhibited instability in both water and

electroless nickel solution. The solubility of the particles (discussed in chapter 6), it is believed, was responsible for the occurrence.

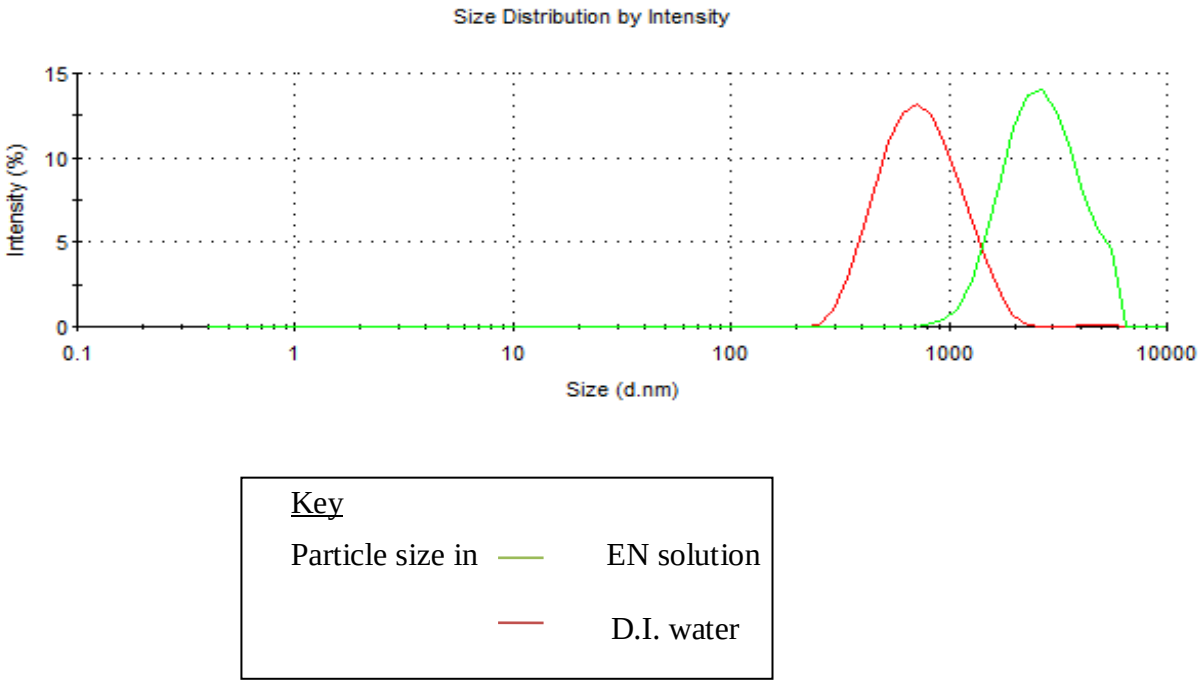

Figure 41. Size distribution of YSZ particles in water and EN solution

5.2 Electroless nickel solution – ceramic particles – surfactants

The effect of the selected surfactants, PMMA/PS and SDS on the dispersion stability of both YSZ and LSM particles was evaluated by initially assessing the effect of a carefully randomly selected amount (0.3g/l) of the additive on the dispersion stability of the particles.

The ratio was 0.3g/l of surfactant to 5g of ceramic powder to 100 ml of EN solution.

Initial dispersions were made with the aid of a Heidolph MR 3001 heater - magnetic stirrer and the mixtures were stirred for 30 minutes at 700 rpm before assessment.

From Figure 42 it can be seen that the PMMA/PS copolymer is less effective than SDS in stabilising the ceramic particles. As such, it was suspected that the mixture was probably not

hydrophilic enough and as such tended to separate to the top of the solution within minutes – leaving the particles to quickly settle to the bottom of the beaker.

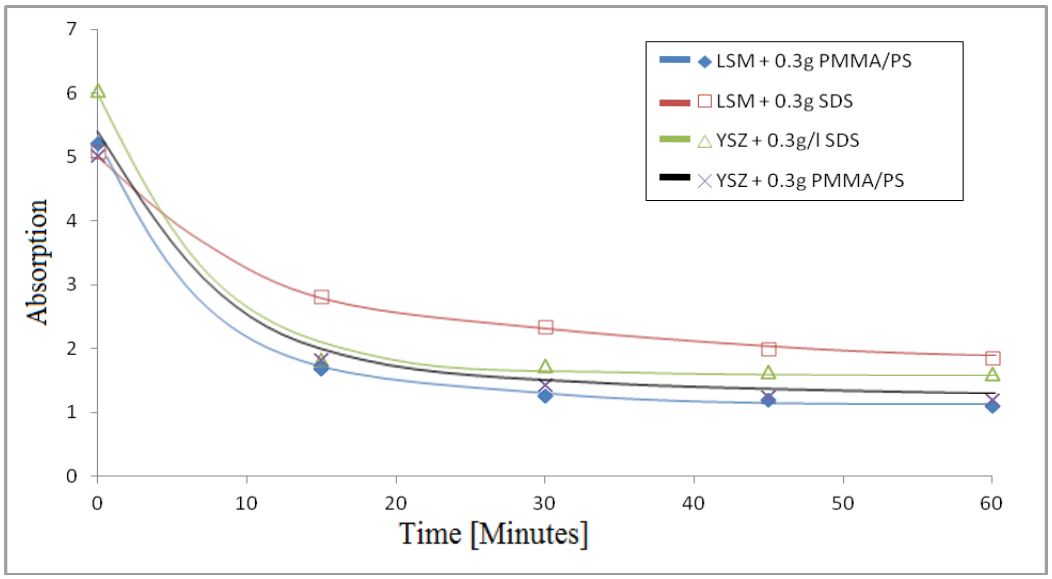

Figure 42. Effect of PMMA/PS and SDS on YSZ and LSM dispersion stability

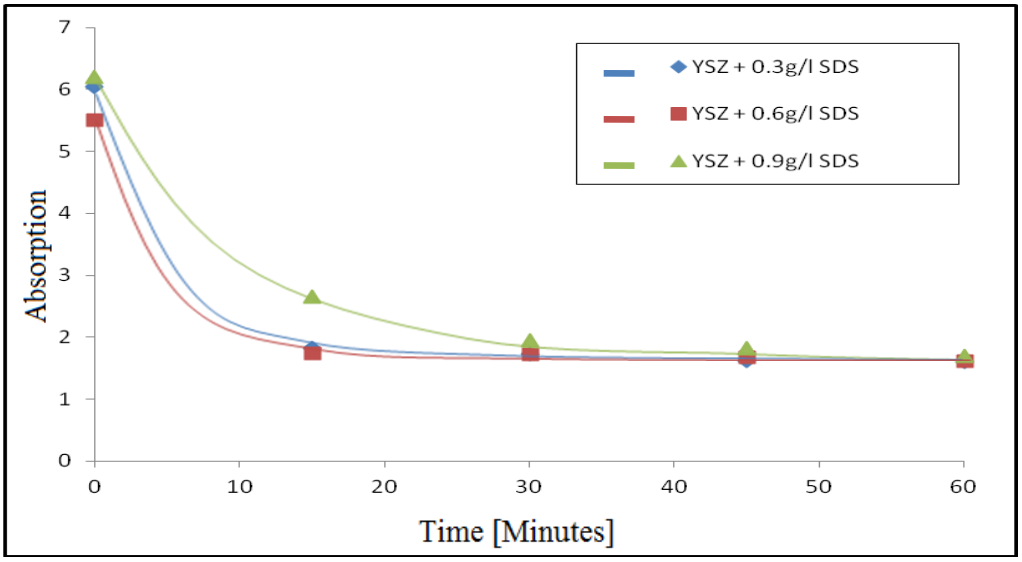

Figure 43. Absorption as a function of time for an EN solution containing YSZ particles and various concentrations of SDS surfactant.

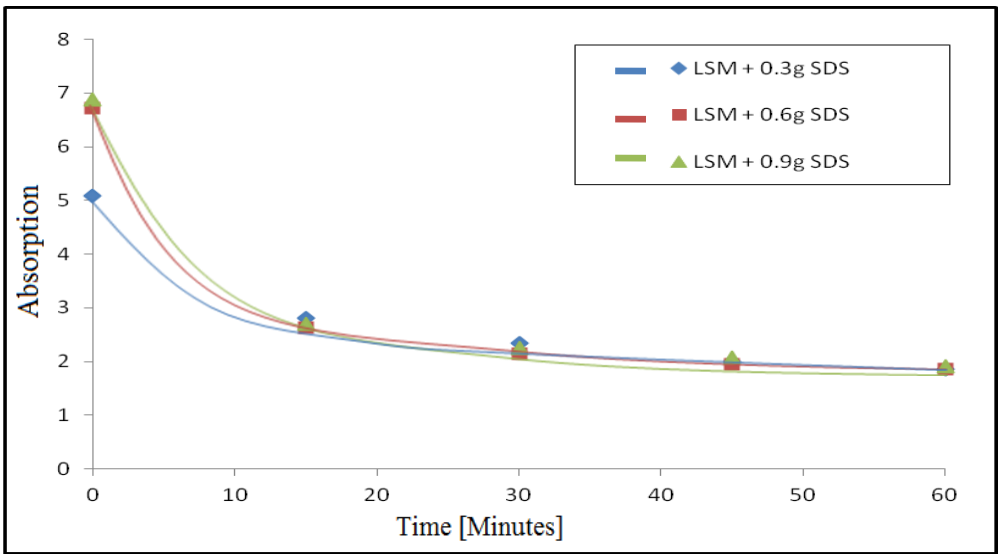

Figure 44. Absorption as a function of time for an electroless nickel solution containing LSM particles and various concentrations of SDS surfactant

The effect of increasing the SDS concentration (0.6 & 0.9 g/l) in the EN solution was thereafter observed. From Figures 43 & 44, it can be seen that the stability of the particles varied directly with the concentration of SDS in the solution.

5.2.1 Zeta potential assessments: Influence of surfactants

A slight increase of the zeta potential of YSZ particles as seen in Figure 45 was in agreement with the results of the UV-Vis tests, thus confirming that the SDS surfactant did have an effect on the dispersion stability of particles in the EN solution. The maximum –17 mV zeta potential though observed however indicated that the surfactant, at the concentrations used, would be unable to independently stabilise the particles. Thus it was believed that with a suitable complementary dispersion technique such as a method of agitation, SDS could still be an effective surfactant for use during the co-deposition process.

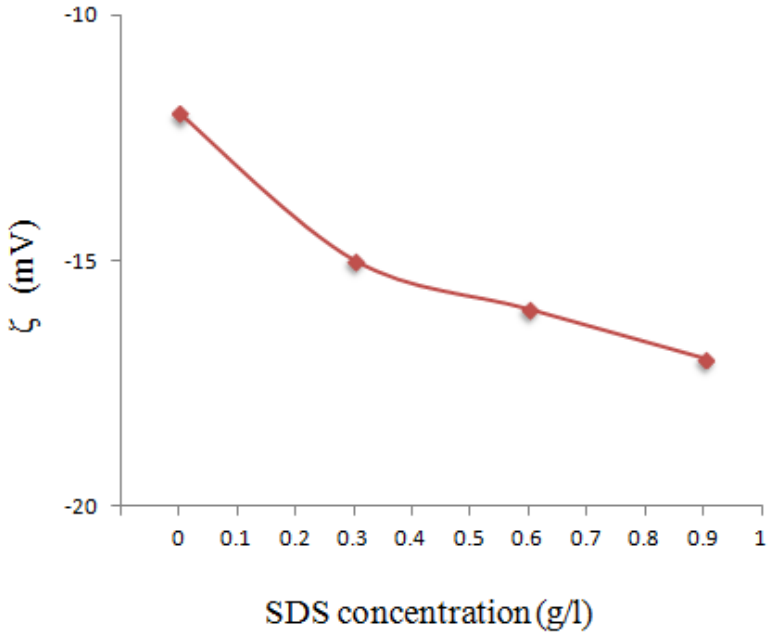

Figure 45. Zeta potential of YSZ particles in an EN solution containing various concentrations of SDS surfactant

5.3 Conclusions

Following the experiments conducted in section 5.2, the results achieved with the co-polymer surfactants discouraged their further use. Added to the fact that the use of polystyrene in fuel cell technology is not strongly recommended due to its reputation to yield carbon deposits/ residue during decomposition, the use of PMMA/PS copolymers was completely discontinued and not adopted during the plating process.

It was decided that the quantity of SDS to be used during experimentation would be varied from 0.3g/l to 0.9g/l. Results obtained from such studies would subsequently decide what parameters would be changed.

As the LSM particles were attracted to the magnet, it was decided that an electromagnet be used in order to enable the degree of influence of the magnet on the particles, and their subsequent incorporation into the nickel matrix to be studied. A magnetic field strength of 65

mT was arbitrarily initially selected with the intention of either increasing or decreasing it depending on results obtained.

Chapter 6

Experimental work – Part II:

Co-depositon

This chapter focuses on the findings from work carried out to electroless co-deposit nickel and ceramic particles, YSZ and LSM with and without external agents.

6.0 Introduction

The co-deposition of nickel and YSZ or LSM was carried out according to experimental matrices, setup with the aim of observing the effect of varying one parameter at a time.

Where the manufacturers' notes were not explicit, experiments were conducted to determine the optimum conditions for any experimental material used in the co-deposition process (from pre-treatment to post-plating).

All product material safety data sheets (MSDS) were reviewed for detailed information about the nature of materials used in the co-deposition process. From these documents, the control of substances hazardous to health (COSHH) report was prepared (Appendix B).

A risk acceptance criteria highlighting the associated risk of using any equipment, apparatus or chemical substance was also prepared and is detailed in Appendix C.

6.1 Experimental materials

6.1.1 Substrate

For cost effectiveness, white planar alumina tiles (Al_2O_3) marketed under the trade name AD 96 by Coorstek Ltd. were used as substrates for most of the experiments (Figure 46). Supplied in 5 x 5 cm dimensions of which various sizes were cut according to the number of variables (e.g. plating thickness, composition, surface roughness e.t.c) being investigated with respect to a particular coating, the substrates had a nominal composition of 96% Al_2O_3 and a reported average roughness of 0.89 Ra.

Cost-wise, the tiles were almost 20 times less expensive than traditional YSZ substrates (alumina £19.5/kg and YSZ £363/kg) used as electrolytes in SOFC technology.

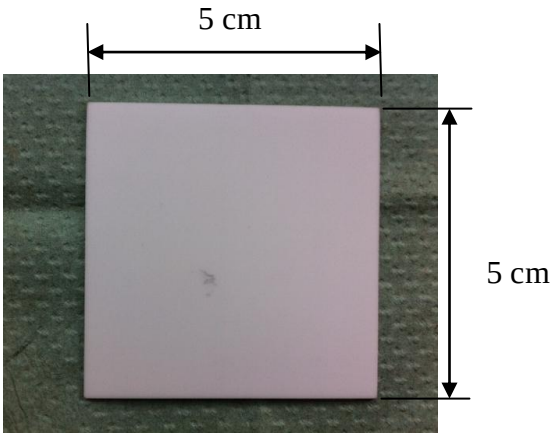

Figure 46. Image of an alumina tile used for the co-deposition process

6.1.2 Ceramic powders

Powders of the most established/ reliable SOFC electrode constituent materials were employed in the experimental part of this work.

Co-deposition of yttria stabilised zirconia (YSZ) with nickel would result in the manufacture of an anode while the introduction of the pervoskite ceramic, lanthanum strontium manganate (LSM) would yield a cathode. In fact, in order to improve the performance of SOFC cathodes (such as its catalytic activity (Wang et.al.,1998)), the manufacture of mixed ionic – electronic conducting cathodes, achieved by co-depositing both YSZ and LSM at the same time, is well recommended.

White, 13% Yttria Stabilized Zirconia powder ($(Y_2O_3)_{13}(ZrO_2)_{87}$) manufactured by Unitec ceramics limited was employed for work related to the use of YSZ while two different types of LSM powders were used in this research. These were $(La_{0.8}Sr_{0.2})_{0.98}$ MnO_3 marketed by Inframat U.S.A, with a maximum of 20% strontium doping and denoted as LSM_{20} for the purpose of this work and $La_{0.82}Sr_{0.18}MnO_x$ supplied by Merck, Germany and noted as LSM_{18}.

Both powder compositions provided an opportunity to not only investigate the correlation between the powder composition and the chemical composition of the coatings, but also allowed for data acquisition that would enable the extraction of any relationship between the field strength of the magnet and the composition of both the powder and coating to be achieved. Whilst Figure 47 is scanning electron micrograph of the ceramic particles, Figure 48 is an EDAX spectrum of LSM_{20} powder.

6.1.3 Pre-treatment chemicals

6.1.3.1 Cuprolite

Cuprolite is the first of 4 pre-treatment chemicals used during the preparation of substrates for the co-deposition process. Supplied by Alfachimici, Italy, it is an alkaline cleaning solution.

To make up the solution, Cuprolite X-96 DP A, Cuprolite X-96 DP B and de-ionised (D.I.) water are used as precursor solutions.

A typical 1 litre volume would require mixing 50ml of Cuprolite X-96 DP A, 5 ml of Cuprolite X-96 DP B and 945ml of D.I. water in any order.
Cuprolite is generally a syrupy and colourless liquid. Though it does not expire with time, its viscosity by and large increases with usage and as such requires changing after a couple of experiments.

As a guide, its pH after make-up is normally around 11.65.

6.1.3.2 Pre-catalyst

Being a ceramic with naturally passivating characteristics, the pre-catalyst step serves to sensitise the surface of the substrate as a prelude to its activation. Natividad et al. (2004) suggests that a probable occurrence during the pre-catalyst step is the oxidation of Sn^{2+}

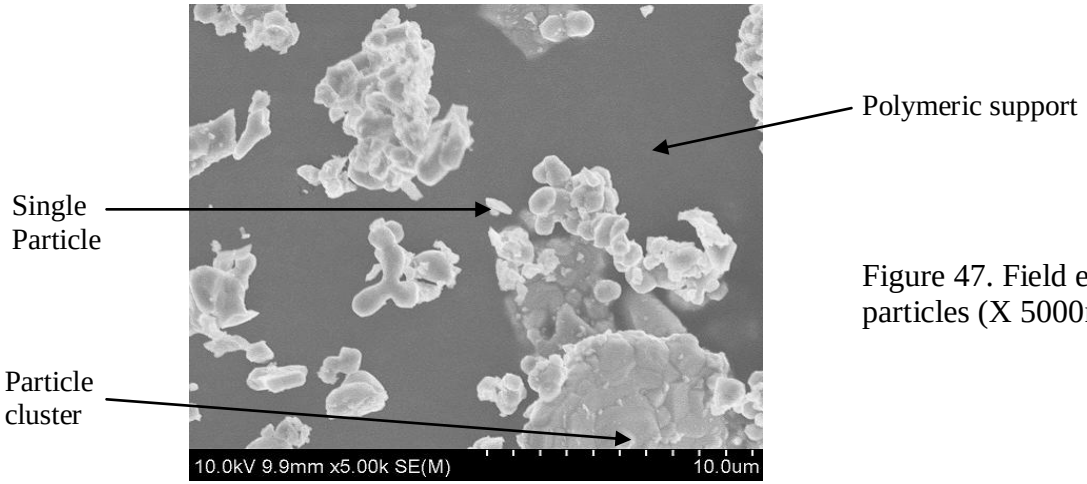

Figure 47. Field emission scanning electron micrograph of ceramic particles (X 5000mag.)

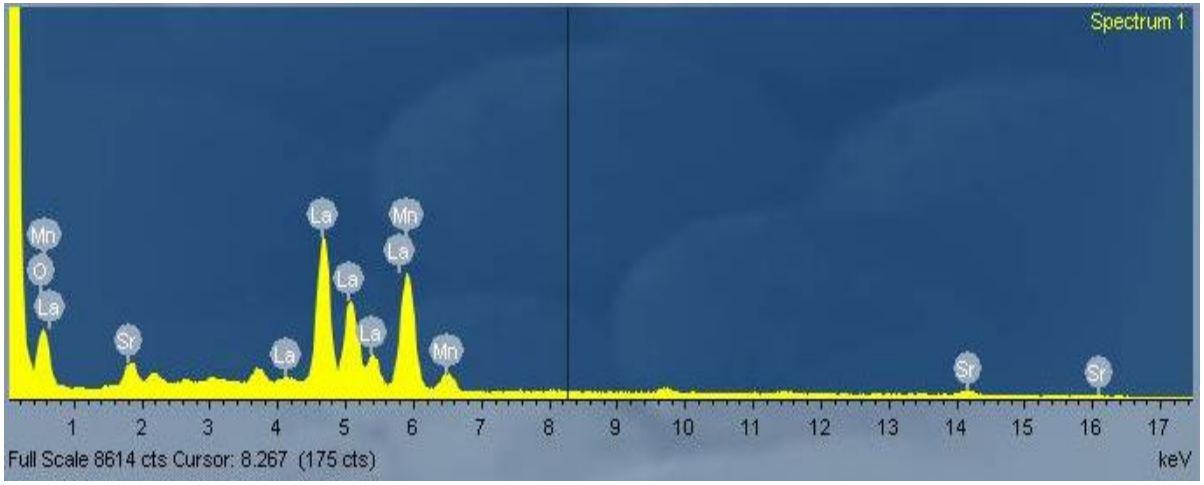

Figure 48. Energy dispersive x-ray spectrum of LSM_{20} powder. Peaks of lanthanum, manganese, strontium and oxygen are clearly visible.

species in the water to yield Sn^{4+} ions which subsequently adsorb on the surface of the substrate (equation 6.1).

$$O_2 \text{ (in water)} + 4H^{+}\ 2Sn^{2+} \quad \longleftrightarrow \quad 2Sn^{4+} + 2H2O \qquad (6.1)$$

Mainly composed of tin chloride and marketed under the trade name Uniphase PHP, the pre-catalyst solution used in this research was made up of Uniphase PHP A salt (200g/l) i.e. tin chloride salt, 37% hydrochloric acid RP (20ml/l) and D.I. water (balance). The order of make-up of a litre of pre-catalyst solution involves introducing 750 ml of D.I. water in a beaker before adding all the uniphase PHP A salt. The HCl solution is then added after which D.I. water is again introduced to bring the mixture up to volume. Unsettled particles are sieved at the end of the process.

The pH of the pre-catalyst is generally about 0.88.

In the same manner as the cuprolite solution, the pre-catalyst does not expire but is changed after a number of experiments.

6.1.3.3 Catalyst

Immersing the substrate in a catalyst, which activates the surface of the substrate by providing a surface that is strongly reducing in nature, is the penultimate pre-treatment step. The reduction of Pd^{2+} ions by Sn^{2+} to zero-valent palladium (Pd^{0}), before its oxidation to PdO and subsequent deposition on the surface of the substrate to act as an activator has again been proposed by Natividad et al. (2004) as the underlying reaction process (equations 6.2 & 6.3).

$$Sn^{2+} + Pd^{2+} \quad \longleftrightarrow \quad Sn^{4+} + Pd^{0} \qquad (6.2)$$

$$O_2 \text{ (in water)} + 2Pd^{0} \quad \longleftrightarrow \quad 2PdO \qquad (6.3)$$

To make up a litre of the catalyst solution, 20 ml of the chemical Uniphase PHP B (mainly comprised of palladium chloride), is essentially added to the composition of the pre-catalyst detailed above. Precisely, Uniphase PHP B is introduced just after the HCl is added to the solution. The mixture formed is a colloidal catalyst with a pH often of the order of 0.34.

6.1.3.3.1 Stability of the catalyst

Unlike cuprolite and the pre-catalyst solution, the Uniphase catalyst is generally unstable in air. If exposed to air over a period of time (as short as 120 hours), it oxidises in a similar manner to equation 6.3 and can no longer effectively activate the surface of substrates.

To ensure that the catalyst solution used during the research was maintained in optimum conditions, an analysis of the sensitivity of the solution to air was carried out to determine its pattern of degradation. A UV-Vis spectrophotometer was used to carry out the assessment.

Visibly, the solution was observed to gradually change colour from black to almost colourless over a period of 120 hours (Figure 49). Figure 50a shows the spectrum of a freshly made-up

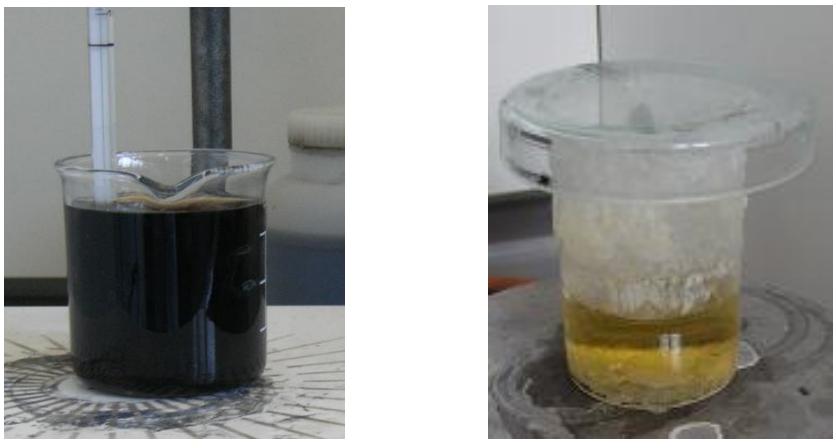

(a) (b)

Figure 49. Image of catalyst solution (a) freshly made up and (b) after 120hours of exposure to air.

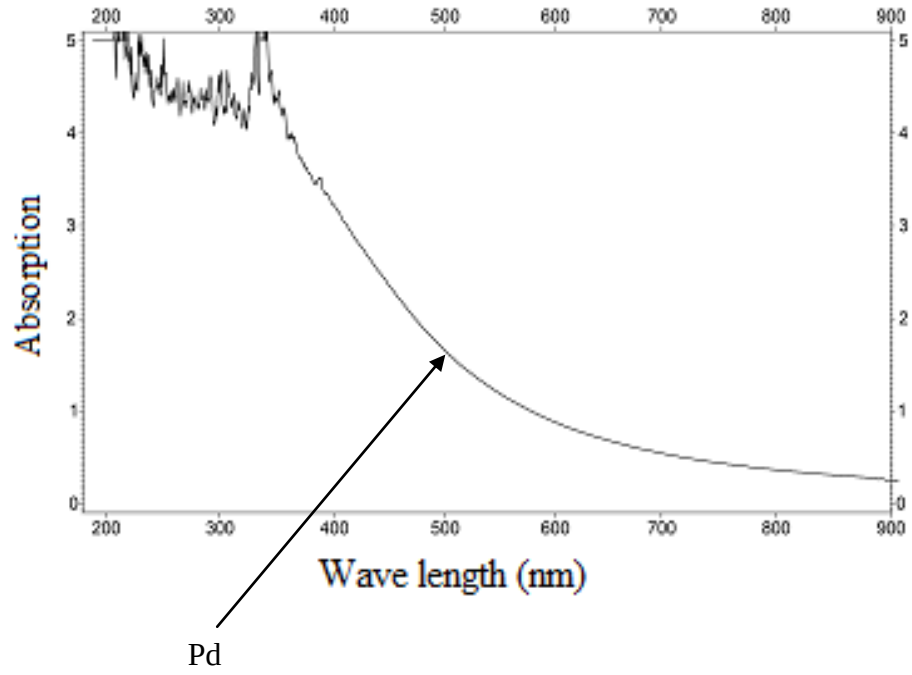

(a)

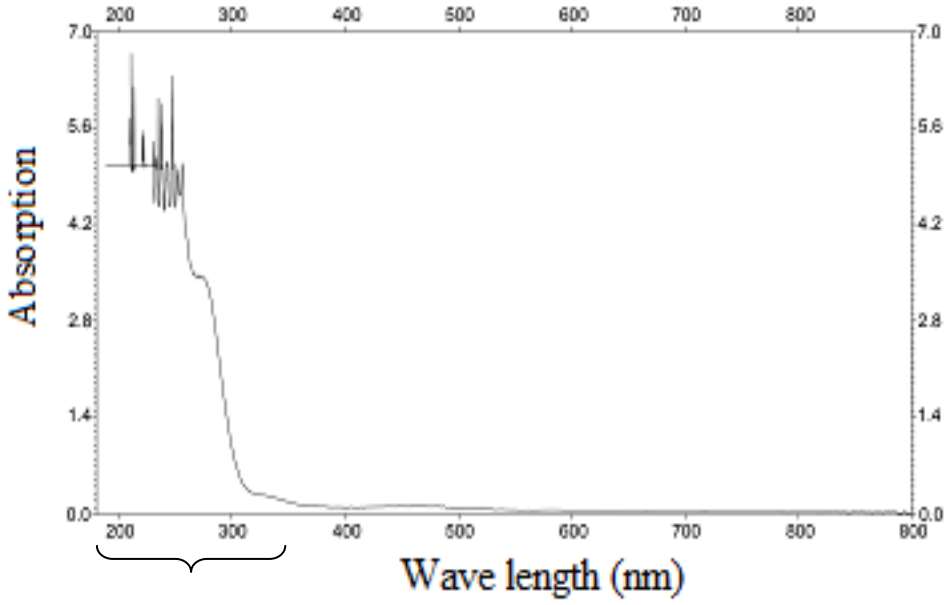

(b)

Figure 50. UV-Vis spectra of catalyst solution (a) freshly made up and (b) expired. Spectrum of the freshly made up solution clearly shows absorption across the whole visible wavelength range which is responsible for the black colour of the solution. As can be seen in the expired solution, there is no absorption across the whole visible wavelength range.

catalyst solution. As can be seen and in complete agreement with the visible dark colour of the solution, light was absorbed across the whole spectrum. On the contrary, Figure 50b presents a spectrum showing little or no light absorption across the visible range. Since palladium is known not to reflect any light and is visibly dark in colour, the latter spectrum appeared to suggest the complete oxidation of Pd to PdO. Another solution was thereafter made up and kept in a sealed container for a period of two weeks. It was observed that no transformation took place – a result which confirmed the solution's intolerance of air for long periods of time.

Following the finding, in order for the catalyst to remain very effective, it was ensured that it was stored in a completely sealed container when not in use.

6.1.3.4 Niplast at 78

Generally simply referred to as just Niplast, Niplast at 78 is a pre-treatment solution that serves to prevent loose catalyst drag-in during plating. Although essentially hydrochloric acid (HCl), it is supplied under the trade name niplast at 78 by Alfachimici, Italy and is made up by simply adding 1 part of the solution to 9 parts of D.I. water (i.e 1 litre = 100 ml Niplast at 78 + 900 ml of D.I. water).

Niplast at 78 is a colourless liquid and does not expire.

6.1.4 Plating solutions

Proprietary acidic electroless nickel plating solution supplied by Schloetter plating technology was the main plating solution used in the experimental part of this work. An alkaline solution was however made up at the latter stages in a bid to facilitate a better understanding of certain results obtained. For ease of identification, each bath made up, was uniquely denoted with a solution composition (SC) number.

6.1.4.1 Acidic electroless nickel solution

Marketed under the trade name Slotonip 1850 by Schloetter plating technology, the proprietary acidic electroless nickel solution was made up from slotonip 1851 starter and 1853 replenisher solutions. The medium phosphorus (around 8%) cadmium and lead free solution, capable of coating ferrous and non-ferrous substrates such as ceramics and plastics, was comprised of amongst others, ammonia, sodium malate, sodium hypophosphite and nickel sulphate salts.

Preparation of 5litres of the solution generally requires the use of 0.75 litres of slotonip 1851, 0.3 litres of slotonip 1853 and 3.95 litres of D.I. water.

2.5 litres of D.I. water is introduced prior to the addition of both slotonip 1851 and 1853 (in that order). The remaining 1.45 litres is then filled to volume with D.I. water. The required pH of the solution is 4.9, thus if the pH is too low, ammonium hydroxide is used to increase it and if it's too high, sulphuric acid is used to reduce it.

6.1.4.2 Alkaline electroless nickel solution

Whilst not proprietary, the alkaline electroless nickel solution was made up with an intention to replicate the phosphorus content of the proprietary acidic solution i.e. medium phosphorus, also used in this experiment.

The source of nickel ions was nickel chloride ($NiCl_2$) manufactured by BDH chemicals Ltd. Poole, England, and the complexing agent was ammonium chloride (NH_4Cl) supplied by Scientific and chemicals supplies Ltd. Sodium citrate ($Na_3C_6H_5O_7$) produced by Fisher Chemicals was employed as a stabiliser while sodium hypophosphite (NaH_2O_2P) supplied by Acros Organics was utilised as a reducing agent. Table 5 lists the composition of the solution. The solution was made up by first adding ammonium chloride to 1 litre of D.I. water before

Table 5. Composition of alkaline plating bath

Compound	Quantity (g/l)	Supplied as
Nickel chloride	30	Nickel (II) chloride hexahydrate ($NiCl_2.6H_20$)
Sodium hypophosphite	25	Sodium hypophosphite monohydrate ($Na_2H_2PO_2.H2O$)
Sodium citrate	25	Tri sodium citrate ($Na_3C_6H_5O_7.2H_2O$)
Ammonium chloride	50	Ammonium chloride (NH_4Cl)

introducing sodium citrate. Nickel chloride followed next before the reducing agent, sodium hypophosphite.

Typical pH after make-up of the solution is usually about 6.5. About 55 ml of Ammonium hydroxide (NH_4OH), Sigma Aldrich U.K., is normally used to increase the pH to 9.5.

Addition of ammonium hydroxide does change the dynamics of the solution compared to the acidic solution. It was observed that the excess ammonia present, not only made the pH of the solution basic, but completely transformed the nature of nickel complexion. From Figure 51 it can be seen that the solution turned blue from green, clearly indicating the increasing transformation of the green octahedral hexaquonickel ions $[Ni(H_2O)_6]^{+2}$ reported in section 3.3.1.1 to the blue nickel-ammonia complex, $[Ni(NH_3)_6]^{+2}$.

As regards stability of the solution, it was observed that the alkaline EN solution was very unstable when exposed to air and as such had to be stored in tightly sealed containers when not in use. This was because the vapour pressure of ammonia hydroxide, used to shift the pH of the solution to the alkaline region, 9.5, was approximately equal to the atmospheric pressure. The implication of this was that once exposed, ammonia in the solution starts to escape into the air and the pH of the solution generally drops from 9.5 to as low as 7.33.

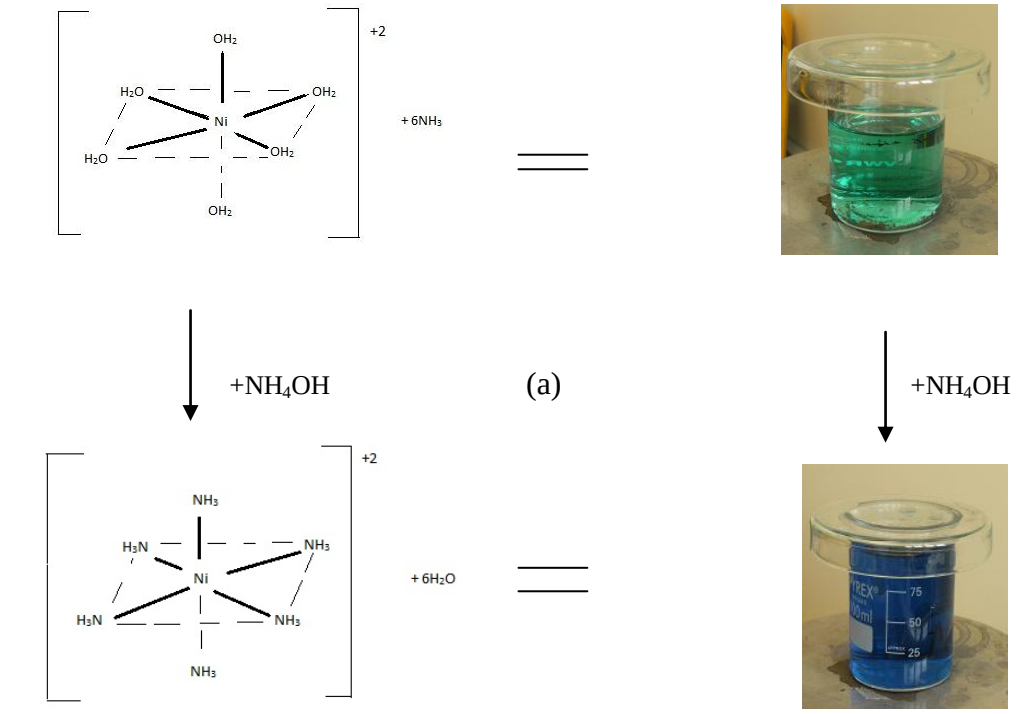

(b)

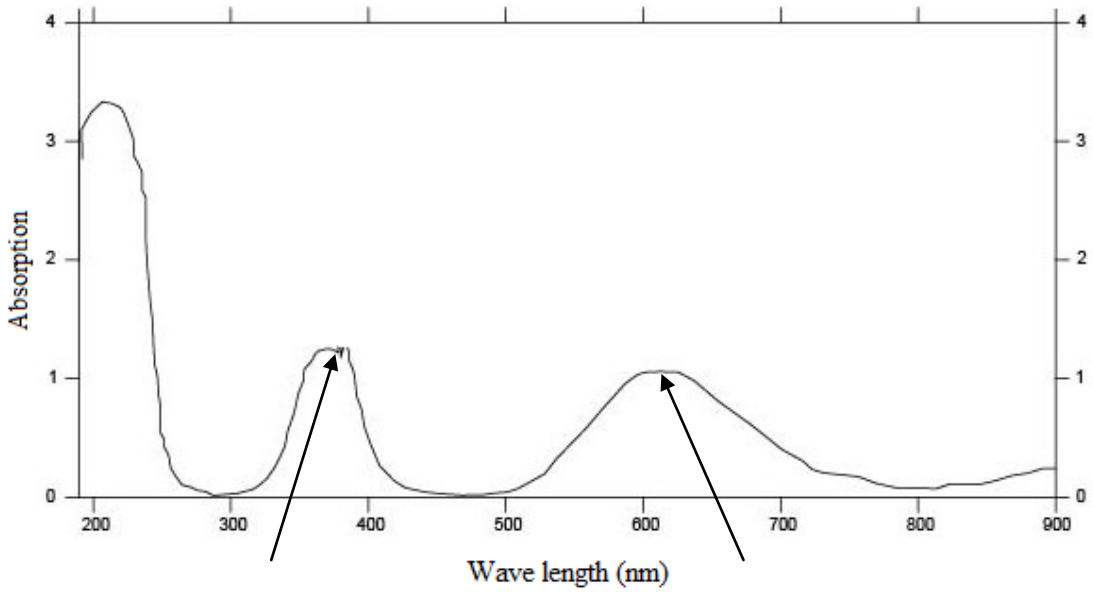

Decreasing green peak Increasing blue peak

(c)

Figure 51. Transformation of (a) green octahedral hexaquonickel ions to (b) blue nickel-ammonia complex with increasing ammonium hydroxide concentration. Image (c) is a UV-Vis spectrum of an alkaline electroless nickel solution showing a decreasing green peak in comparison to a growing blue peak.

6.2 Post co-deposition sample preparation and characterisation equipment

Sample preparation after plating generally involved as a first step, rinsing the substrate with D.I. water in order to rid its surface of loose particles. Thereafter, for surface morphology examinations, a Cambridge S90 B scanning electron microscope was employed. In-situ Oxford Instruments Inca energy dispersive x-ray analysis (EDXA) software, incorporated into the SEM was used for elemental composition analysis of the coatings. For assessment of the coatings' thicknesses, a Leitz Aristomet Hi-power light microscope was utilised.

Coated samples were on most occasions cut into required dimensions with a Struers Accutom-5 precision cutter. Generally a feed rate of 0.02 mm/s was used to avoid damage to the alumina substrates. Samples were thereafter mounted in 40mm diameter epoxy resin and subsequent grinding and polishing was carried out with the aid of the TegraForce-5/ TegraPol-21. Contact force for both operations was normally set to 50N with an anti-clockwise rotation of 150rpm.

6.3 Co-deposition

ENP, the platform on which ECD operates is such that a change in one variable can positively or adversely affect the nature of deposits obtained. To this end and in order to achieve the best results with the use of surfactants and magnets, ideal plating parameters were initially sought after and pre-determined.

6.3.1 Determination of suitable ceramic bath loading for the coating process

In Sheela and Pushpavanam's study (Sheela & Pushpavanam, 2002) of diamond dispersed electroless nickel coatings, although their results showed that the orientation of a substrate affected the amount of second phase particles incorporated into the nickel matrix, the researchers found that a steady increase in the concentration of the ceramic powder in the

bath, correspondingly resulted in an increase of the quantity of particulate matter co-deposited in the coating (Sheela & Pushpavanam, 2002).

Determining the value of ceramic bath loading which will yield the highest amount of second phase particles in the nickel matrix, unarguably in this research, increased the prospect of further enhancing the ceramic content of coatings manufactured with the aid of the external agents at a later stage.

6.3.1.1 Control run

As a standard, plating of the substrate (alumina tile) was carried out in an EN solution devoid of any ceramic (YSZ or LSM). This was done in order to not only establish the operability of the bath, but to also determine the characteristics of deposits produced from it without ceramics (YSZ and LSM) in it.

The plating(s) was carried out in acidic EN solutions and as a basis for the research; all experiments were carried out with the substrates suspended in the vertical position. Section 3.1 – depicted in Figure 16, provides details of the plating steps used.

6.3.1.1.1 Result I: Plain coatings

Figure 52 is an image and cross sectional micrograph of a coating achieved after 1 hour of plain nickel deposition. On analysis, it was found that the thickness achieved was as high as 36 µm and as can be seen from the photo micrograph – as evidenced by clearly visible excellent interlocking between the metallic coating and ceramic substrate (Figure 52.a) – good adhesion also appeared to have been achieved. Due to the solution containing only nickel and no ceramic, the coating was shinny – as typical of excellent light reflecting materials.

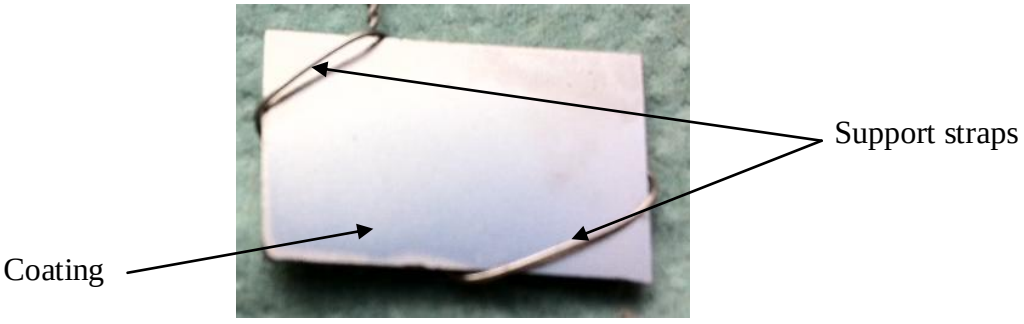

(a)

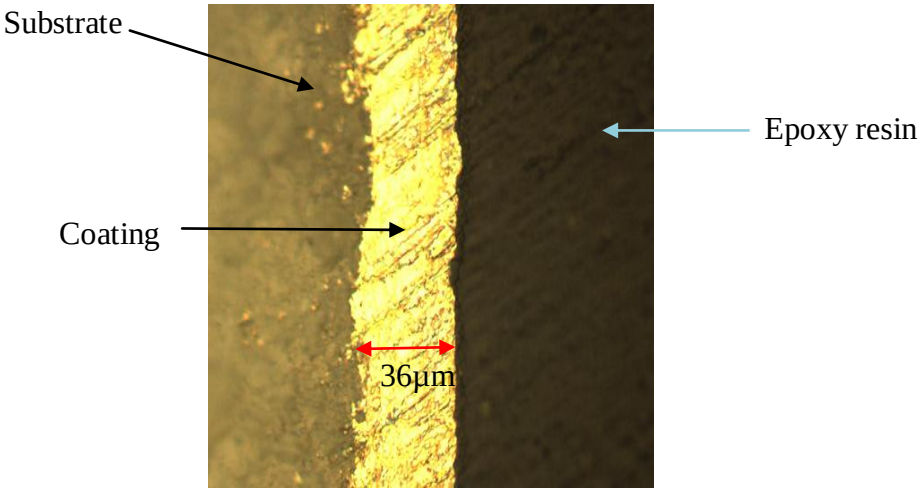

(b)

Figure 52. (a) Image of an EN coating produced from a solution devoid of any ceramic in the bath and (b) photo micrograph of the coating showing its cross sectional view (x500 mag.)

6.3.1.2 Nickel/YSZ co-deposition

With the functionality of the bath confirmed, the experimental matrix detailed in Table 6 below was designed to firstly investigate the effect of ceramic bath loading on the composition of coatings. Representative of an SOFC anode, YSZ powder was the initially used. The concentration of YSZ powder was varied from 10 to 100 g/l. Particle size was 5µm

Table 6. Setup I: Experimental matrix for the study of the effect of bath loading on the composition of electroless nickel – YSZ coatings

Bath	YSZ loading (g/l)
SC 1	10
SC 2	50
SC 3	100

and the required particle dispersion was achieved with an overhead stirrer. The rotating speed was 400 rpm.

6.3.1.2.1 Result II : Co-deposition of nickel/YSZ in free-from external agents EN solutions

Initial platings carried out yielded relatively poor results with little or no deposit observed for baths SC1, 2 and 3. As a precautionary measure, it was decided that the final pre-treatment step (Niplast) be dropped and retrials carried out to observe the effect of the step on coatings obtained from the bath. This is because although Niplast is supposed to prevent loose particles from getting dragged in during co-deposition, being a liquid that is relied upon to etch the surface of substrate during plain electroless nickel plating, it was suspected that is was actually displacing the catalyst particles successfully deposited on the substrate `during the previous stage.

Subsequent coatings manufactured were successful and reproducible and the results are discussed below.

Visibly, the coatings progressively changed colour from the traditionally smooth and shiny metallic silver EN coating appearance seen in Figure 52.a, to dark black (Figure 53.c). Plausibly, it was believed that the change was due to the continuously reducing metal exposure (increasing ceramic content) which resulted in lower light reflection from the surface of the coating.

Elemental composition of the coatings obtained from all three different solutions plus the control sample (plain nickel plating), is detailed in Table 7. A sharp increase followed by an immense drop was observed for the metallic content of the coatings. From the table, it is evident that the nickel content of all the coatings was at its lowest level when the YSZ content in the EN solution was 50g/l (SC 2).

(a)

(b) (c)

Figure 53. Image of electroless nickel coatings produced from (a) bath SC 1 (b) bath SC 2 (c) bath SC 3.

The results detailed in table 7 not only confirmed that the ceramic content in ECD coatings tended to vary with the powder concentration in the bath, but that about 50g/l (SC 2) would

Table 7. Composition of electroless nickel – YSZ coatings

	Composition (Volume %)					
Sample produced from baths	Ni	Y	Zr	O	P	Si
free from any ceramic	91.29	-	-	-	7.92	0.79
SC 1	68.23	1.85	9.44	18.83	1.65	-
SC 2	58.71	2.85	11.45	25.75	1.24	-
SC 3	69.02	1.96	9.85	18.85	0.75	-

produce ECD coatings with the lowest nickel content. After the co-deposition process was repeated thrice from baths SC 1, 2 and 3, and similar results again obtained without an external aid, it was concluded that no further particle inclusion was possible beyond the 50g/l loading as some form of saturation was possibly occurring beyond that loading.

To ensure that 50 g/l YSZ loading was the optimum concentration for the manufacture of SOFC electrodes by ECD, other key properties of SOFC electrodes such as the thickness and surface roughness of the coatings, were examined. An optical microscope was used for this purpose.

Figure 54. shows optical micrographs of the cross sectional view of coatings produced from baths SC 1 , 2 and 3. It can be seen that the coatings become progressively rougher and thinner as the YSZ loading in the bath increases. Though roughness is a desired property of SOFC electrodes since it helps channel gas flow into the electrodes' pores – increasing their catalytic activity in the process, an inverse relationship was found to exist between the coatings' thickness and YSZ bath loading (Table 8).

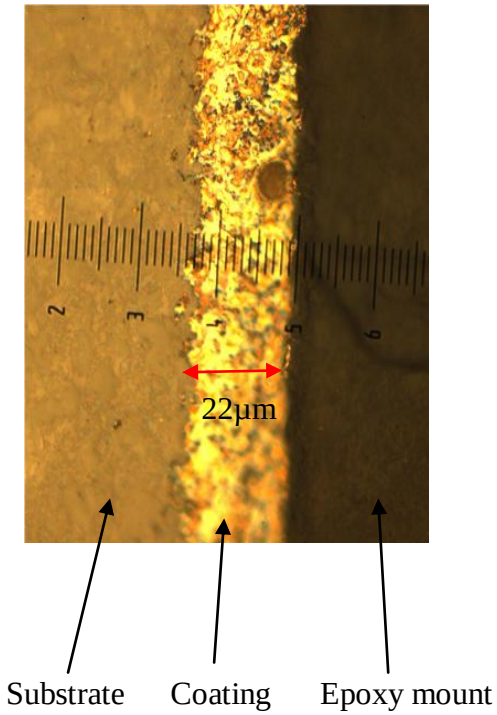

(a)

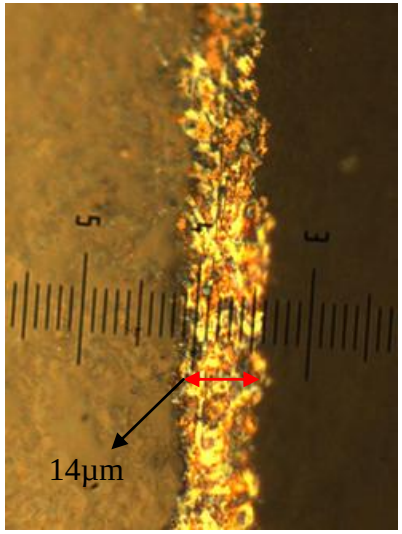

(b)

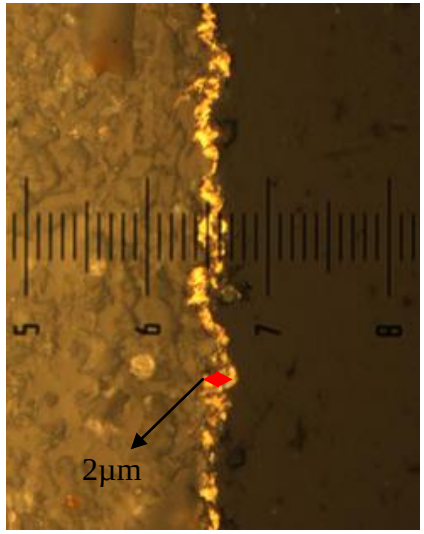

(c)

Figure 54. Photo micrographs of the cross section of electroless nickel – YSZ coatings produced from baths (a) SC 1 (b) SC 2 (c) SC 3. (x500 magnification) Coating can be seen to reduce in thickness with increasing ceramic bath loading. Roughness is also a feature seen to be affected by the level of ceramic bath loading.

Table 8. Thickness of electroless nickel – YSZ coatings as a function of YSZ bath concentration

Sample produced from bath	Thickness (µm)
with no ceramic loading	36
SC 1	22
SC 2	14
SC 3	2

6.3.1.2.2 Inference

As un-activated co-deposited YSZ particles provide less reactive insulating facets that do not encourage the autocatalytic deposition of nickel metal continuously reduced from its ions, increase in YSZ loading may have resulted in growth retardation of the deposit layer. In fact, examination of coatings carried out with 100 g/l YSZ bath loading, which showed a thickness of only about 2 µm (Figure 54.c), is evidence that the YSZ powder formed an almost complete barrier to nickel adsorption on the surface of the substrate. Baraju et al. (2003) and

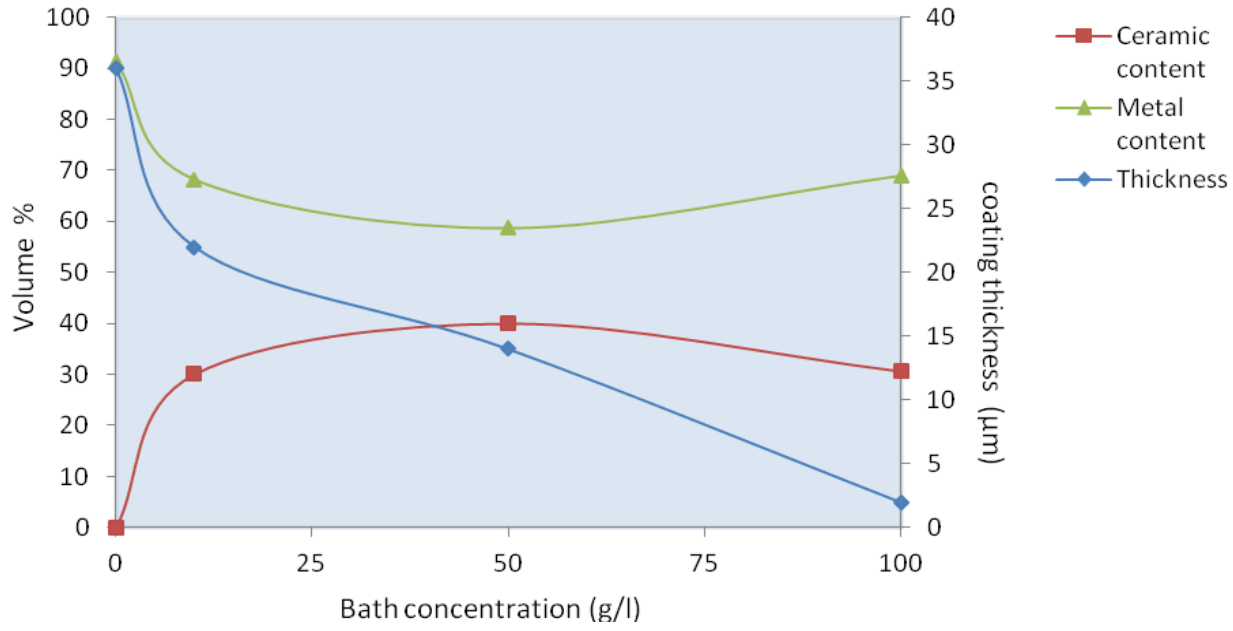

Figure 55. Relationship of YSZ bath concentration, coating thickness and ceramic content in an electroless Ni-LSM coating.

Sheela and Pushpavanam (2002) are amongst a group of researchers who have also observed a similar trend. The former though alternatively proffers that the emergent pattern may be ascribed to the possibility of grouping or agglomeration of second phase particles which result from a decrease in the mean distance between them.

Combining the results of the effect of ceramic powder loading i.e. the amount of YSZ particles incorporated into the coating and the coatings' thickness, the value of 50 g/l was selected as the optimal value (Figure 55).

6.3.1.3 Nickel/ LSM co-deposition

Table 9 outlines the experimental matrix designed to investigate the optimum ceramic loading required for the co-deposition of nickel and LSM.

Table 9. Setup II: Experimental matrix for the study of the effect of bath loading on the composition of electroless nickel – LSM coatings

Bath	Concentration (g/l)	LSM powder type
SC 4	10	LSM_{20}
SC 5	50	LSM_{20}
SC 6	100	LSM_{20}
SC 7	10	LSM_{18}
SC 8	50	LSM_{18}
SC 9	100	LSM_{18}

6.3.1.3.1 Result III : Co-deposition of nickel/LSM in free-from external agents EN solutions

The coatings were very erratic with successful deposition recorded on only a few occasions. In fact, only baths SC 5 & 8 barely yielded any form of coating at all. Figure 56 is a high magnification (x 1000) SEM micrograph of the surface of a coating produced from SC 5, while Figure 57 shows its corresponding EDXA spectrum.

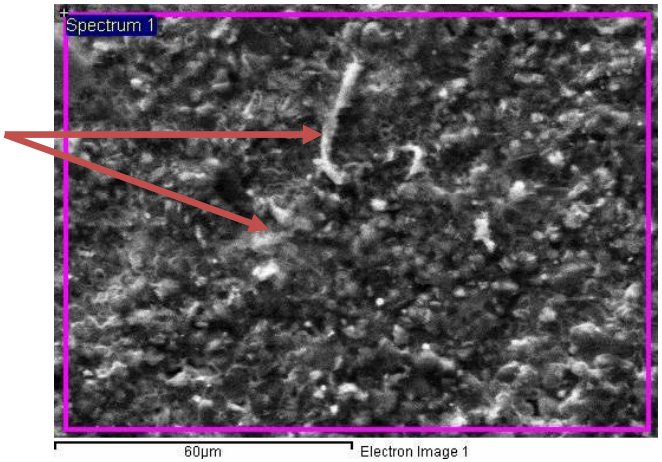

Figure 56. SEM micrograph of electroless Ni - LSM_{20} coating produced from bath SC 5 (x 1000 magnification).

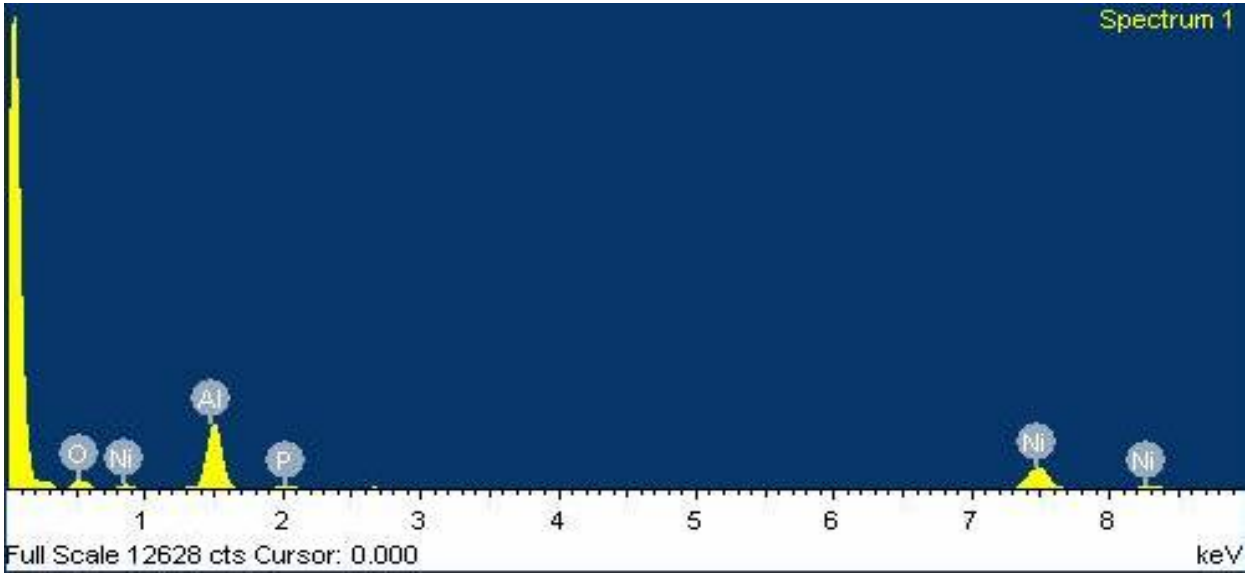

Figure 57. EDXA spectrum of electroless Ni - LSM_{20} coating from bath SC 5.

From the white bands and patches visible in Figure 56, and the dominant aluminium peak observed in Figure 57, it was evident that poor surface coverage had occurred. In a bid to understand the possible underlying phenomenon that gave rise to the selective coating on the surface, EDAX analysis was carried out. No lanthanum, strontium or manganese peaks observed. When the sample was viewed under the light microscope, no visible coating thickness could be seen at even a thousand (x 1000) magnification confirming in the process that the coating was also very thin and barely deposited.

To determine at what point, plating initiation commenced or discontinued, a 15 minute plating was alternatively carried out.

Figure 58 and 59 present an SEM micrograph and EDXA spectrum of a 15 minute plating sample obtained from bath SC 5. Though the images confirmed that some degree of initiation had occurred within the first 15 minutes, it was evident that some form of resistance, repulsion or unfavourable condition to further nickel nucleation on the surface was prevalent. In fact, with most solutions failing to co-deposit, the observation also seemed to suggest that the length of time allowed for the process was irrelevant as the LSM was probably obstructing nickel from nucleating on the surface of the alumina tile.

Failure of both types of LSM powders to appropriately co-deposit in the nickel matrix meant that an optimum ceramic concentration couldn't be determined without trouble shooting.

6.3.1.4 Effect of LSM on the pH of acidic EN solution

The hypothesis here was that either the magnetic property of LSM created a repulsion that hindered the ECD process or that the chemistry of LSM created an unfavourable plating condition in the bath. While the former could possibly be rectified with the aid of a magnet to reverse the effect, it was necessary to understand if the latter had a contribution.

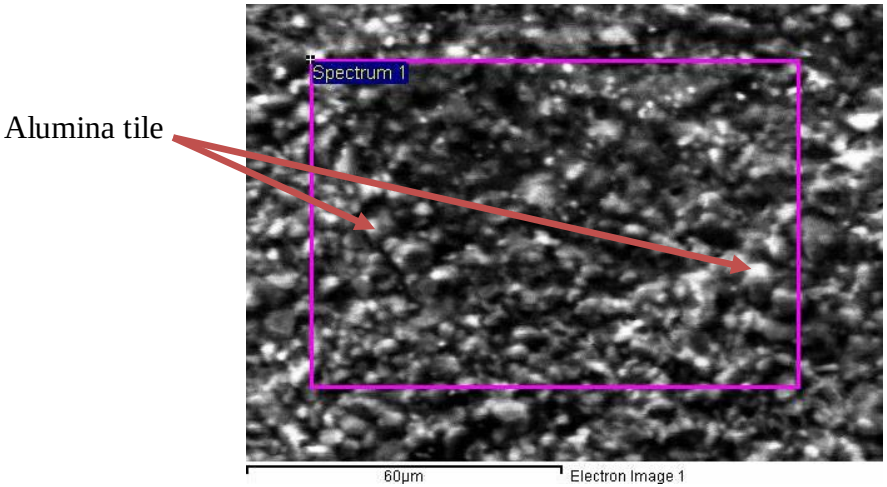

Figure 58. SEM micrograph of electroless Ni - LSM_{20} after 15 minutes. Coatings were produced from bath SC 5 (x 1000 magnification)

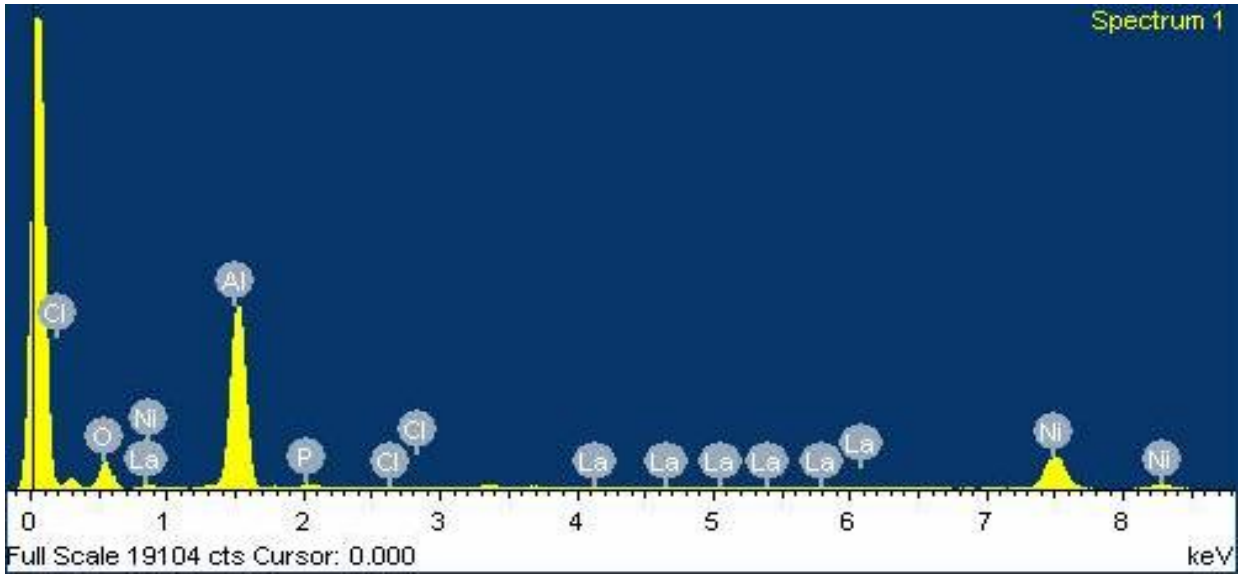

Figure 59. EDXA spectrum of electroless Ni - LSM_{20} after 15 minutes. Coatings were produced from bath SC 5

It is known that the pH of the plating solution amongst several variables strongly influences the efficiency of the bath (section 3.2.1). Mallory stated that if the pH of an acidic bath is allowed to drop too far (< 4.0 for commercial plating baths), a very low plating rate will be observed (Mallory, 1990) [a]. To this end, the effect of LSM on the pH of the solution was studied.

6.3.1.4.1 EN/LSM pH study 1

Co-deposition of Ni and LSM was again attempted from baths SC 5 and 8 (refer to Table 9) and the pH of both solutions was checked before and after the after the co-deposition process As control samples, a plain nickel plating without any LSM powder and another plating from bath SC 2 (50 g/l YSZ) were also assessed.

It can be seen from Table 10 that while the pH of the plain electroless nickel solution negligibly altered;, both YSZ and LSM powders induced significant shifts on the pH of their plating solutions. However, whilst the pH of bath SC 2 was still within an acceptable range

Table 10. pH of EN solution as a function of bath composition

Bath used	pH of EN solution before plating	pH of EN solution after plating
Plain nickel	4.94	4.62
SC 2	4.94	3.94
SC 5	4.94	7.05
SC 8	4.94	7.13

for acidic electroless nickel plating to occur, the pH of baths SC 5 and SC 8 had completely shifted to the alkaline range and thus must have impeded the plating.

A 2-step test was thus further set up to investigate the alkalinity of LSM.

6.3.1.4.2 EN/LSM pH study 2

Firstly, 0.1ml of sulphuric acid (H_2SO_4) was dropped into a 100 ml beaker filled with D.I. water. The pH was found to shift from 7.0 to 3.0. At this juncture, 1g of LSM was added to the beaker. After stirring the mixture continuously for an hour, the pH was found to have shifted to 6.84.

6.3.1.4.3 EN/LSM pH study 3

The second set of experiments carried out to completely ascertain the effect of LSM on the pH of EN solutions, was the addition of 1g of LSM into a 50ml beaker containing 25ml of EN solution. The solution was stirred and heated up to 89^{o}C. The pH was tracked at defined intervals and the observation is detailed in Table 11.

Table 11. Influence of LSM on the pH of an acidic electroless nickel solution

Time (minutes)	pH of electroless nickel solution
0	4.94
15	5.81
30	6.8
45	7.08
60	7.14

As can deciphered from Table 11, the pH change of the EN solution was so rapid with the introduction of LSM that within 15 minutes of addition of LSM, the pH of the solution had moved from 4.9 – the normal plating range, to 5.81.

Based on the results, it was theorised that while YSZ could be co-deposited in an acidic bath, LSM would probably be more suited to an alkaline bath due to its ephemeral co-deposition nature when in an acidic bath. Support for this theory was found when the chemistry of LSM was analysed.

6.3.1.4.4 Chemistry of LSM

LSM is a product of a solid state reaction between the ceramic powders, lanthanum oxide (La_2O_3), strontium oxide (SrO) and manganese oxide (Mn_3O_4). While La_2O_3 and Mn_3O_4 are insoluble in water, SrO is a soluble, strongly basic oxide which reacts with water to yield strontium hydroxide (equation 6.4).

$$SrO\ (s) + H_2O\ (l) \longrightarrow Sr(OH)_2\ (aq) \qquad (6.4)$$

The strontium hydroxide may further dissociate to exist as strontium and hydroxyl ions (OH^-) (equation 6.5).

$$Sr(OH)_2 \rightarrow Sr^{2+} + 2OH^- \qquad (6.5)$$

From equation 6.5, which shows the emergence of the hydroxyl group when strontium oxide is allowed to come into contact with a solution containing water, it is believed that the excess OH^- group, inadvertently consequently existent in the solution, will ultimately result in a shift of the pH of the plating solution to an alkaline region without any limitations.

6.3.1.5 Alkaline LSM plating

Using only LSM_{20} powder, the plating solution was switched from acidic EN solution to alkaline EN solution. In the belief that LSM possibly had a lower saturation loading than that

Table 12. Setup III: Experimental matrix for the study of the effect of bath loading on the composition of alkaline electroless nickel – LSM coatings

Bath	LSM powder concentration (g/l)
SC 10	0
SC 11	10
SC 12	20
SC 13	30
SC 14	40
SC 15	50

of YSZ, observed in section 6.3.1.2, initial powder concentration was varied from 10 g/l to 50 g/l as detailed in Table 12. As can be seen from Table 13 below, although all the substrates immersed in all six different baths successfully plated, it is evident that besides nickel and phosphorus deposits in a majority of them, LSM only appreciably co-deposited with nickel in the coating obtained from bath SC 15. Figure 60 shows an SEM micrograph of the surface of a coating produced from bath SC 10.

Table 13. Composition of alkaline electroless nickel – LSM coatings

	Composition (Volume %)					
Samples produced from bath	Ni	La	Sr	O	Mn	P
SC 11	89.88	-	-	-	-	10.22
SC 12	94.05	-	-	-	-	5.95
SC 13	83.71	-	-	8.87	-	7.42
SC 14	85.01	-	-	7.85	-	7.86
SC 15	82.11	0.51	-	7.76	0.39	9.23

(i.e plain nickel plating with no LSM powder). By comparing Figure 60 with SEM images of the surface of the coatings produced from bath SC 15 (Figures 61 & 62), the successful co-deposition of LSM into the nickel matrix can be visibly seen. In fact, a further comparison of

Typical 5-fold cauliflower-like amorphous nickel deposit

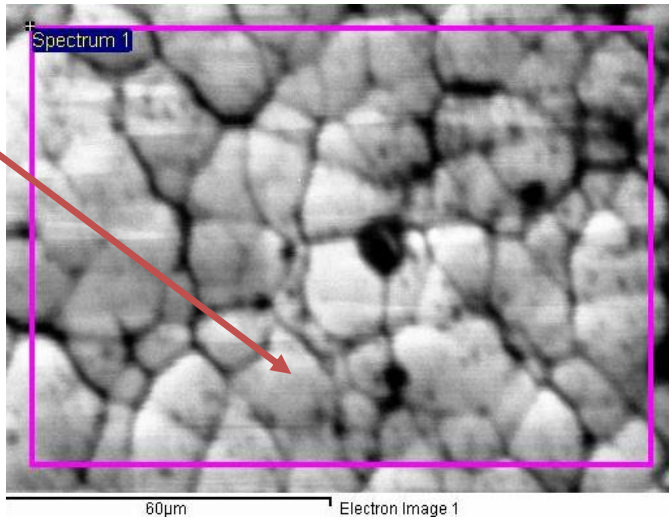

Figure 60. SEM micrograph of a plain electroless nickel plating produced from bath SC 10 (x1000 magnification).

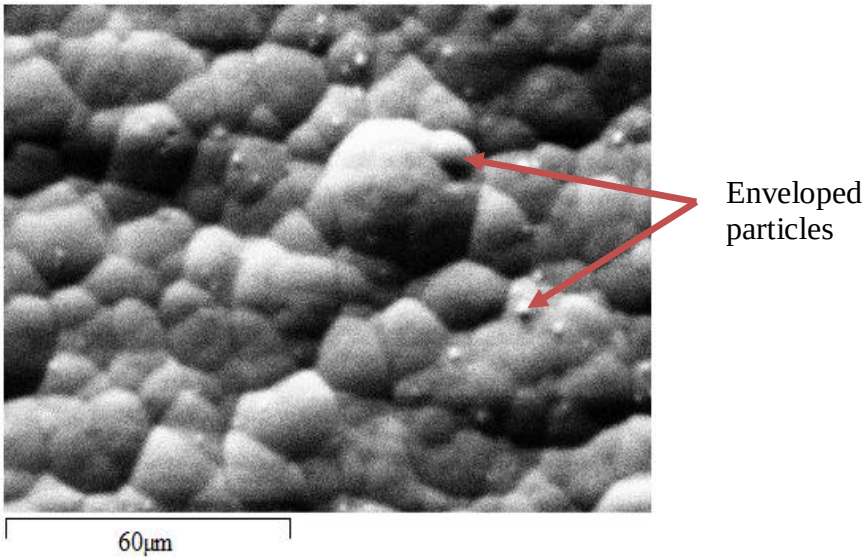

Figure 61. SEM micrograph of a electroless nickel - LSM plating produced from bath SC 15.(x1000 magnification).

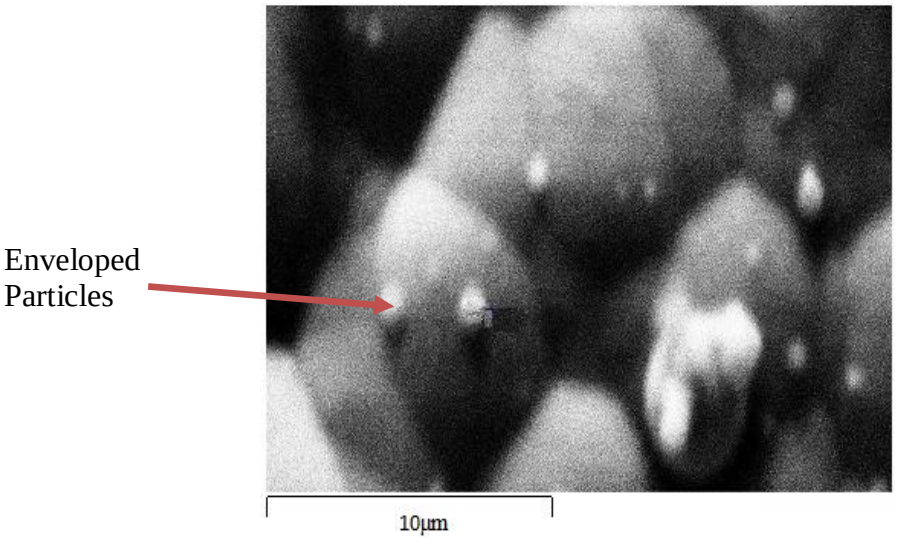

Figure 62. SEM micrograph of an electroless nickel - LSM plating produced from bath SC 15 (x5220 magnification).

the EDXA spectra of coatings produced from bath SC 5 (Figure 57 (page 99)) and SC 15 (Figure 63 below), along with the findings reported in Table 13 clearly showed that, although the LSM content in the coating produced from bath SC 15 was still quite negligible, the complete disappearance of an aluminum peak in the coating unarguably confirmed the achievement of a good surface coverage.

Figure 63. EDXA spectrum of electroless Ni - LSM_{20} coating from bath SC 15

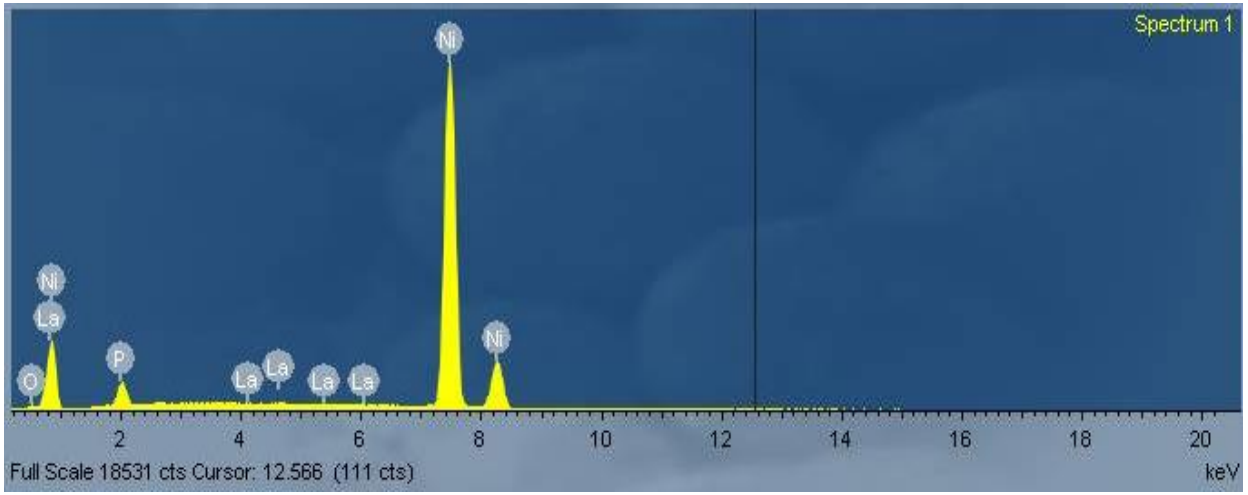

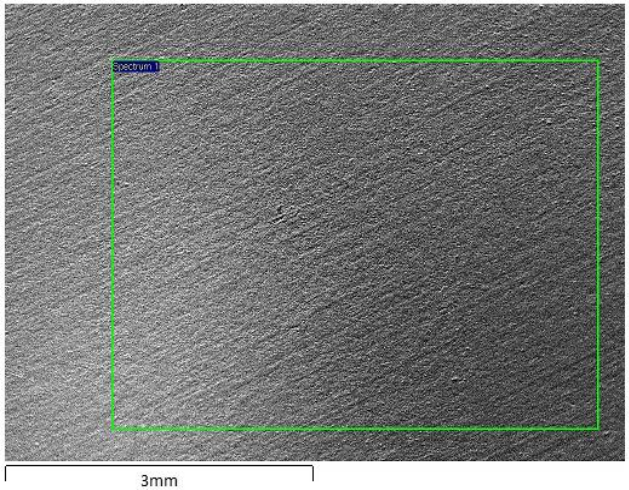

Figure 64. SEM micrograph of an electroless nickel – LSM plating produced from bath SC 15 (x18 magnification).

In line with the findings above, a powder concentration of 50 g/l LSM was selected for further experimental work.

6.3.2 Influence of surfactants

Surface active agents (surfactants) perform different roles when introduced in any medium. If the powder added to an EN solution is of a hydrophobic nature such as carbon black, the surfactant may in addition to other roles and depending on its concentration, act as an emulsifier. As a result of the tendency of the molecules of an ionic surfactant to generate electrostatic repulsion between them or those of a non-ionic surfactant to sterically stabilise particles in a medium, the dispersion stability of particles is also often achieved with the addition of surfactants.

In SOFC electrode manufacture, both influences of surfactants are desired because they will not only ensure adequate particle dispersion in the coating which will discourage areas with less second phase particles having poor mechanical and chemical properties, but possibly also enhance the coating thickness and rate of particle incorporation into the nickel matrix.

For any of these roles to be achieved though, a set of variables must be established.

6.3.2.1 Design of experiment

From preliminary tests conducted and detailed in Chapter 5, 0.3 to 0.9 g/l had been confirmed to have an effect on the dispersion stability of ceramic particles in the bath. In accordance with tests carried out in section 6.3.1 above on the influence of bath loading on the composition of ECD coatings, a powder loading of 50 g/l was employed.

As YSZ ‘readily’ co-deposits with nickel, the surfactant experiment was conducted with the powder.

Two average YSZ powder particle sizes of 1 µm & 5 µm were selected for the study in a bid to also determine if any relationship existed between the surfactants and the particle size.

Whilst stirring, the experimental procedure involved adding the surfactant – sodium dodecyl sulphate (SDS) to the heated EN solution (89^{o}C) before the powder was poured in. This was carried out so as to ensure adequate dispersion of the surfactant within the solution prior to any other activity. After adding the surfactant to the EN solution, the substrate was introduced.

The experimental matrix adopted to investigate the potential influence of SDS on the composition of ECD coatings is detailed below in Table 14.

Table 14. DoE I: Experimental setup for surfactant (SDS) incorporated coatings

Bath	SDS loading (g/l)	YSZ particle size (µm)
SC 16	0.3	1
SC 17	0.6	1
SC 18	0.9	1
SC 19	0.3	5
SC 20	0.6	5
SC 21	0.9	5

6.3.2.2 Result IV: Effect of SDS on the composition of electroless nickel-YSZ coating

Utmost care had to be taken during the experiments as substantial foaming of the solution occurred on every occasion, after the surfactant SDS, was added to the bath. It is believed that the occurrence was associated with the tendency of surfactants to reduce the surface tension of a liquid which allowed it to expand appreciably. With hydrogen gas trapped beneath the surface of the EN solution, bubbles resultantly form and subsequently swell up in the form of foam.

Figures 61, 62 and 63 are EDXA spectra of coatings obtained from baths SC 16, 17 and 18 respectively. As can be seen from the rising peaks of yttrium and zirconium, and the decreasing peaks of nickel with increasing surfactant concentration, the ceramic content of coatings carried out with 1 µm YSZ particles, was found to have a positive relationship with the surfactant concentration in the baths. The exact content of the coatings is detailed in Table 15.

Table 15. Composition of electroless nickel - 1µm YSZ - SDS coatings

	Composition (Volume %)			
Sample produced from bath	Ni	Y	Zr	O
SC 16	66.25	1.63	8.82	13.77
SC 17	54.66	2.42	18.92	23.99
SC 18	39.23	4.05	21.88	34.29

The achievement of a 60:40 ceramic to metal ratio from bath SC 18 highlighted the potential effect of surfactant use during SOFC electrode manufacture.

In line with the design of experiment detailed in Table 14, the YSZ powder size was then changed to 5µm in order to allow for the study of the effect of particle size on ceramic particle incorporation.

Table 16 details the composition of coatings obtained from baths SC 19, 20 and 21.

Table 16. Composition of electroless nickel - 5µm YSZ - SDS coatings

	Composition (Volume %)			
Sample produced from bath	Ni	Y	Zr	O
SC 19	64.5	2.88	15.01	17.60
SC 20	58.34	2.72	16.21	22.36
SC 21	52.36	3.08	18.01	25.59

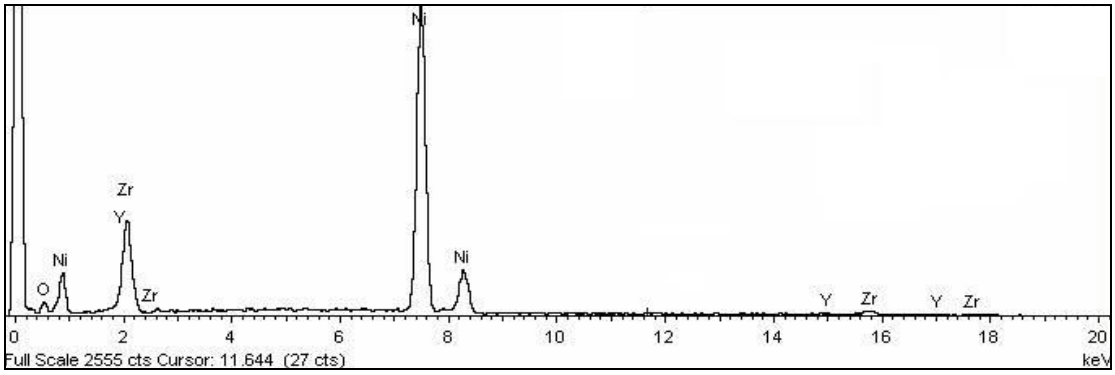

Figure 65. EDXA spectrum of electroless Ni - µm YSZ - 0.3 g/l SDS coating from bath SC 16

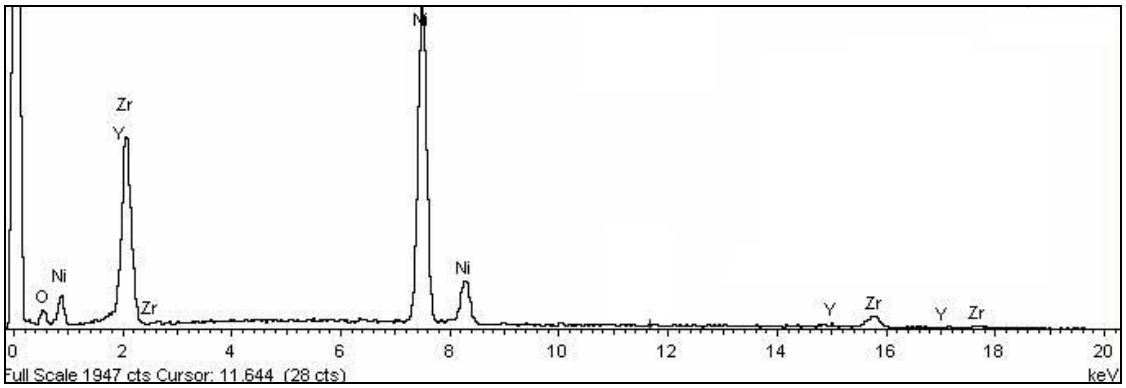

Figure 66. EDXA spectrum of electroless Ni - µm YSZ - 0.6 g/l SDS coating from bath SC 17

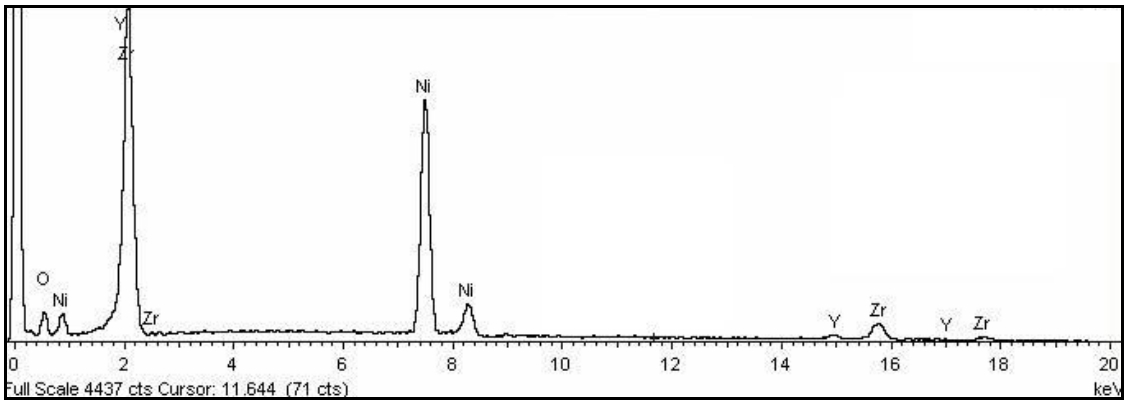

Figure 67. EDXA spectrum of electroless Ni- 1µm YSZ- 0.9 g/l SDS coating from bath SC 18

In comparison to the coatings carried out with 1µm average particle sizes, the maximum achievable ceramic content was about 47.24 volume % (net difference between the nickel content and 100% material composition). However although it seemed that the 1µm particle size coatings would be more suitable for SOFC coatings, the use of surfactants during the plating process was found to alter several physical conditions of the coatings. As these were either favourable or unfavourable to SOFC electrode manufacture, they had to be considered.

6.3.2.3 Favourable effect(s) of SDS incorporation on SOFC electrodes manufactured by ECD

6.3.2.3.1 Composition

Results obtained from surfactant incorporated experiments appeared to suggest that the surfactant – SDS can act as a barrier to excess nickel co-deposition. In order to better appreciate this effect, a 50 g/l - 1µm YSZ coating without any surfactant (bath SC 22) was carried out. A similar experiment with 5µm average sized YSZ particles had already been carried out, earlier (bath SC 2, Table 7).

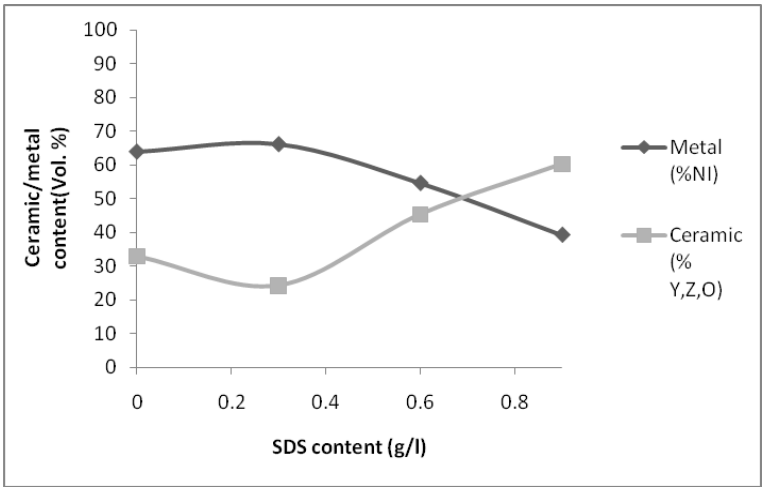

Figure 68. Composition of Ni -1µm YSZ coatings with various concentrations of SDS

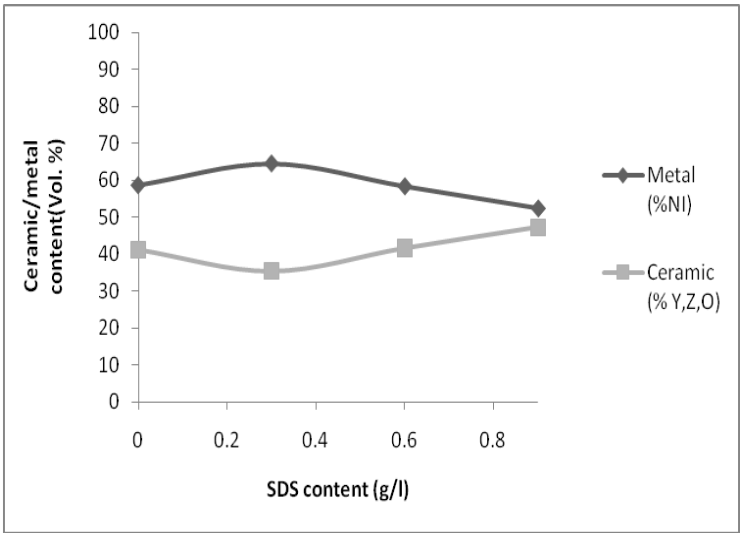

Figure 69. Composition of Ni- 5µm YSZ coatings with various concentrations of SDS

Without the surfactant, the average metal to ceramic ratio of coatings produced from bath SC 22 was 64.025 : 32.84. By plotting Tables 14 and 15 – combined with the composition of coatings obtained from baths SC 22 and 2, it was observed that with increasing surfactant concentration, the metal content of the coatings progressively decreased (Figures 68 & 69).

Although Figures 68 and 69 depict an overall positive effect of SDS on the reduction of the metal content of electroless nickel YSZ coatings, an anomaly was found to exist. At surfactant concentrations – below 0.6 g/l, the metal content of the coatings was found to be on the increase before stabilising at that value and subsequently decreasing. This behaviour as can be seen in Figure 68 was replicated in both particle size coatings and is believed to be closely linked to the CMC of SDS. According to Newberry (1979), the CMC of SDS in divalent metal solutions is far less than its usual $8x10^{-3}$ M in pure water – being $4x10^{-3}$ M for nickel and $2x10^{-3}$ M for copper. As $4x10^{-3}$ M corresponds to 0.6 g/l SDS content, it can be inferred that the attained CMC enhanced YSZ particle dispersion stability which correspondingly yielded an increased level of ceramic incorporation into the coating from the SDS loading of 0.6 g/l and above (Figure 70).

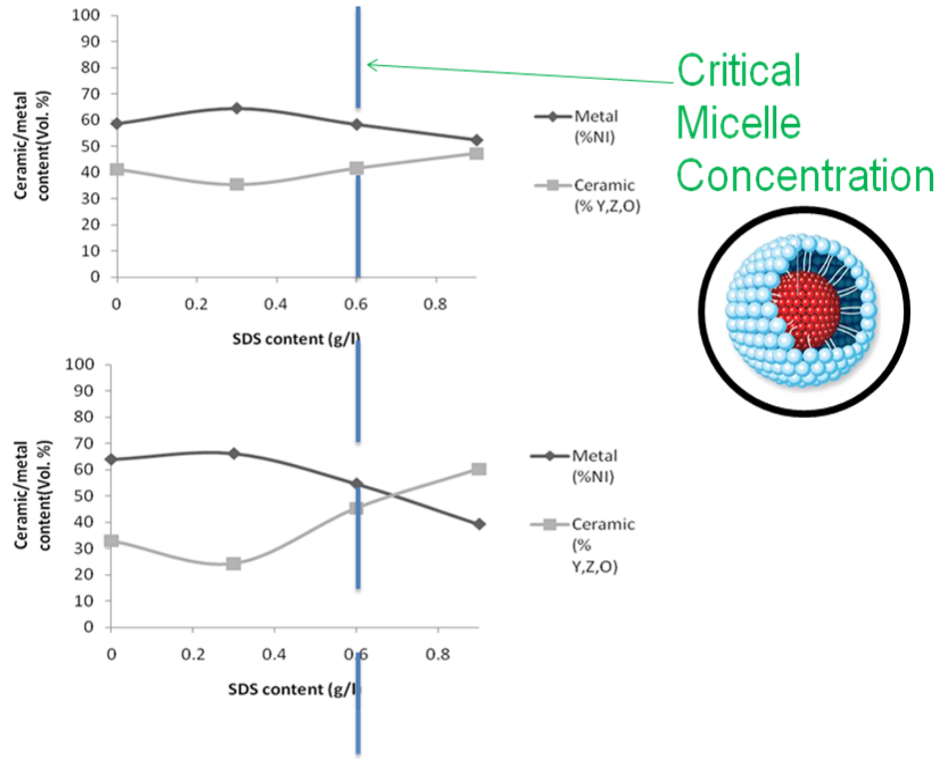

Figure 70. Illustration of the effect of critical micelle concentration (CMC) on coating composition

On the basis of experimental evidence, it was clear that surfactants could shield excess metal from co-depositing in the coating as long as the surfactant concentration was above its CMC.

6.3.2.3.2 Surface morphology

Figures 71, 72 and 73 show the surface morphology of coatings manufactured from baths SC 16, 17 and 18. From the SEM micrographs, it is clearly evident that the surface roughness of the coatings directly increases with the bath surfactant concentration. For SOFC electrode manufacture, this is desired since a rough surface texture will significantly provide a large surface area which will in turn increase the rate of reaction in the region. Alsari et al. (2001)

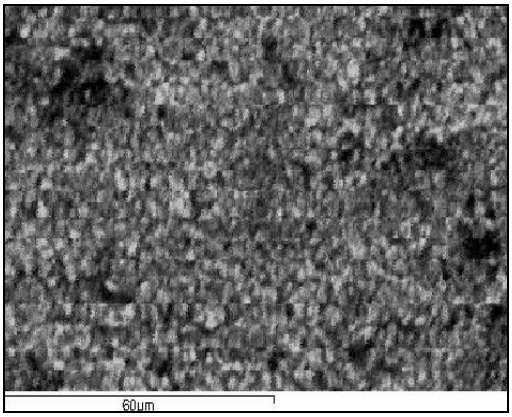

Figure 71. SEM micrograph of Ni - 1 µm YSZ - 0.3 g/l SDS coating from bath SC 16 (x 1,000 magnification)

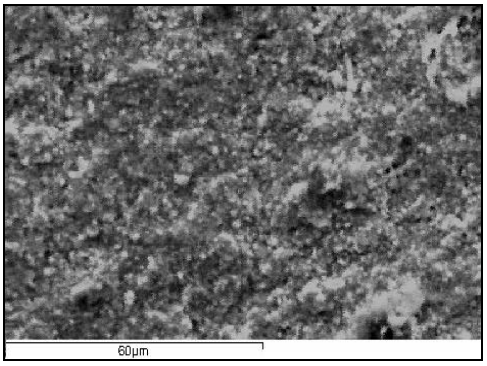

Figure 72. SEM micrograph of Ni - 1 µm YSZ - 0.6 g/l SDS coating from bath SC 17 (x 1,000 magnification)

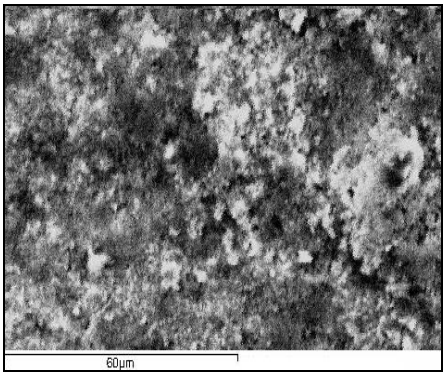

Figure 73. SEM micrograph of Ni - 1 µm YSZ - 0.9 g/l SDS coating from bath SC 18 (x 1,000 magnification)

who studied the effect of SDS solutions as gelation media on the formation of polyethersulfone membranes noted similar observations in their work and ascribed the occurrence to a consequential increase in pore size upon SDS attaining its CMC.

6.3.2.4 Unfavourable effect(s) of SDS incorporation on SOFC electrodes manufactured by ECD

6.3.2.4.1 Coating thickness

While the use of SDS significantly increased the ceramic content of the coatings and improved their surface roughness, an undesired inverse relationship was found to exist between the coating thickness and the concentration of SDS in the bath. In resemblance to the effect of the surfactant on the composition of the coatings, the effect of SDS was found to be more pronounced on coatings carried out with 1µm YSZ particles.

Figures 74 and 75 show the thickness of the coatings as a factor of SDS bath loading. It can be seen that while the decrement is negligible with 5 µm coatings, the 1 µm coatings decreased from about 15 µm without surfactant addition in the bath, to about 2 µm at 0.9 g/l SDS concentration.

The finding above (Figures 74 & 75) however appeared to contradict the findings of Chen et al. (2002). The authors reported that when used during EN plating, surfactants tended to attach themselves to evolved hydrogen bubbles. Owing to this attachment, the surfactants were found to prevent the hydrogen bubbles from masking the surface of the substrate and as a result promoted faster deposition rates (i.e. coating thickness) (Figure 76).

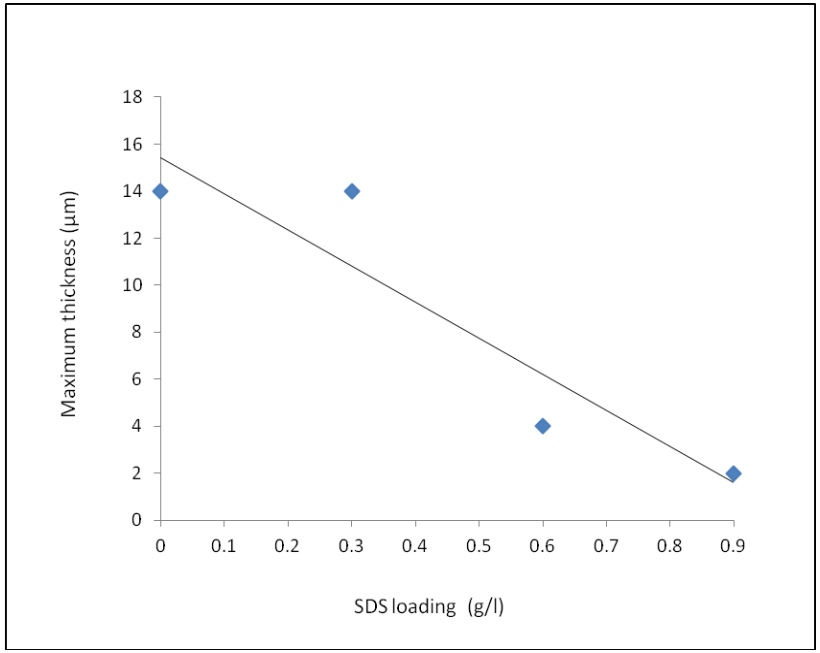

Figure 74. Influence of SDS on the coating thickness of Ni - 1µm YSZ coatings

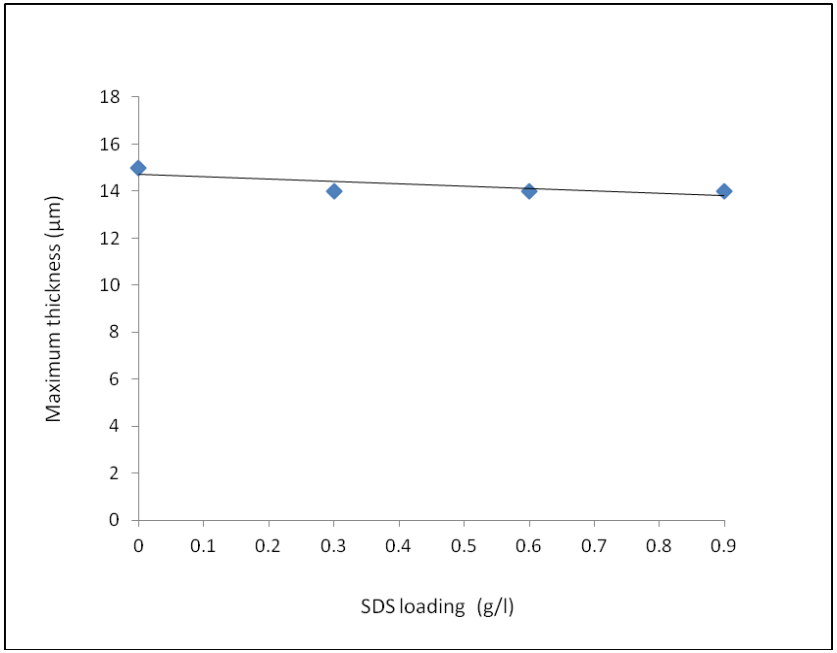

Figure 75. Influence of SDS on the coating thickness of Ni- 5µm YSZ coatings

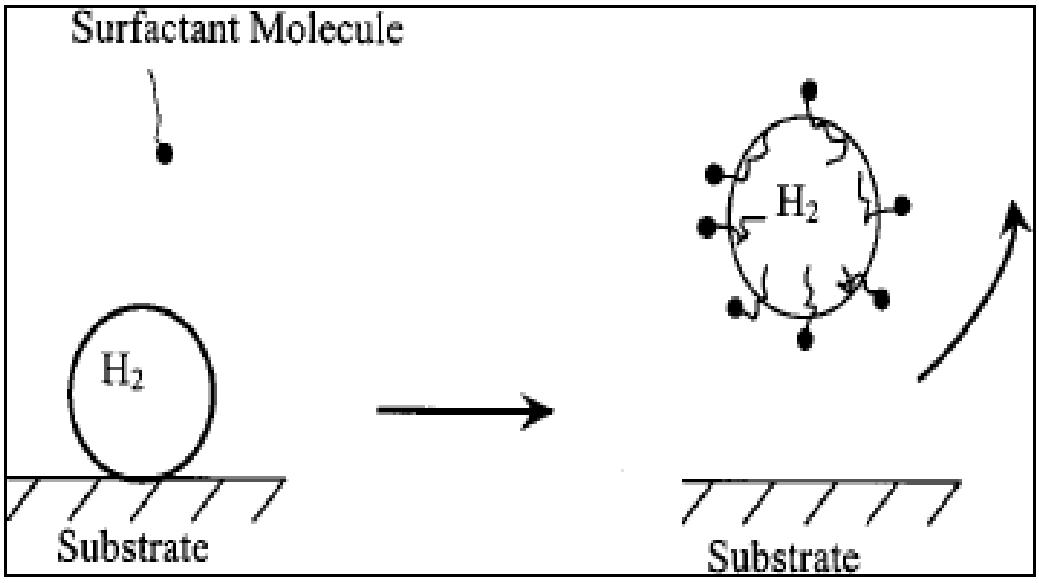

Figure 76. Schematic diagram of surfactant aided hydrogen evolution (Chen et al., 2002)

On comparing the ratio of surfactants used in the work of chen et al. to that used in this work, and in line with the findings by Janczuk et al. (1994), a plausible cause of the occurrence was found. The tendency for surfactants to accumulate at surfaces and interfaces often leads to the formation of a monolayer. As the concentration of the surfactant increases in the solution, the monolayer gradually becomes stable (Janczuk, 1994) and consequently impedes nucleation and growth of the co-deposit. Needing to only ensure that hydrogen bubbles did not mask the surface of the substrate, Chen et al. used only small quantities (3ppm (~0.003g/l) – 7ppm (~0.007g/l)) of various types of surfactants. This was in direct contrast to this work where particle dispersion was desired.

From preliminary experiments carried out and detailed in Chapter 3, surfactant concentrations in the range used by Chen et al. would not have effectively acted as dispersants.

6.3.2.4.2 Coating coherence

From further investigation of coatings obtained from the surfactant experiments, it was found that the coatings also became increasing incoherent with increasing surfactant concentration. Figure 77 shows a photo micrograph of an Ni/ 1µm YSZ / 0.6g/l SDS coating. Clearly it can

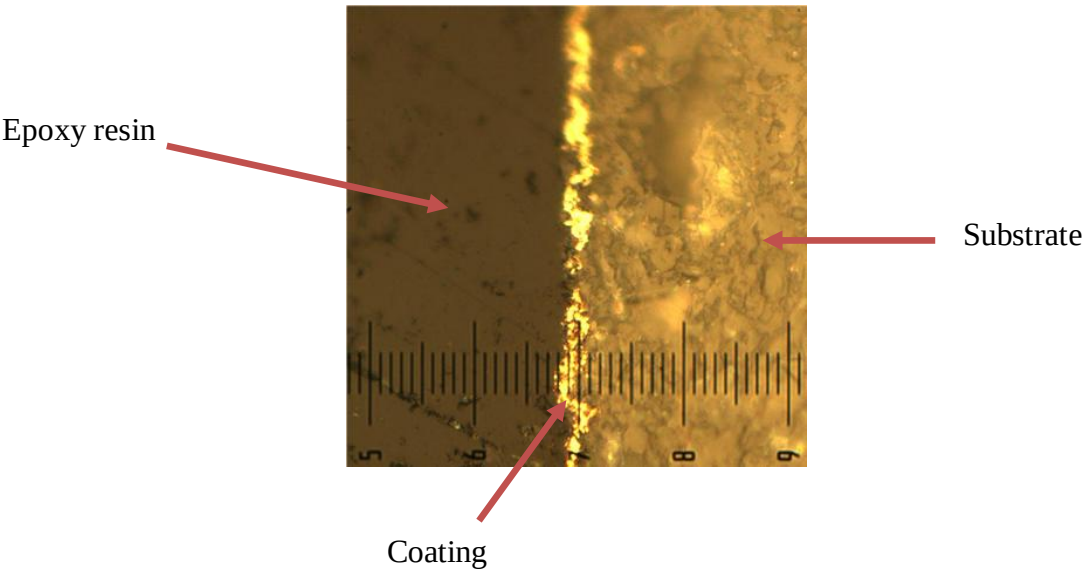

Figure 77. Photo micrograph of an Ni - 1µm YSZ - 0.6g/l SDS coating (x1000 magnification)

be seen that the growth of the nickel layer was anisotropic (i.e. some areas tended to grow faster than others). For wear resistance purposes, Ger and Hwang attempted to co-deposit soft polytetraflouroetylene particles into a nickel matrix in the presence of a cationic surfactant, fluorinated alkyl quaternary ammonium iodides (FC) and found a similar occurrence (Ger and Hwang, 2002). Presented in the form of an adsorption isotherm (Figure 78), the authors who also employed the surfactant in similar concentrations to those used in this study found that, with increasing surfactant concentration, the amount of surfactant adsorbed onto the surface of the substrate correspondingly increased. In the light of this, they concluded that at high

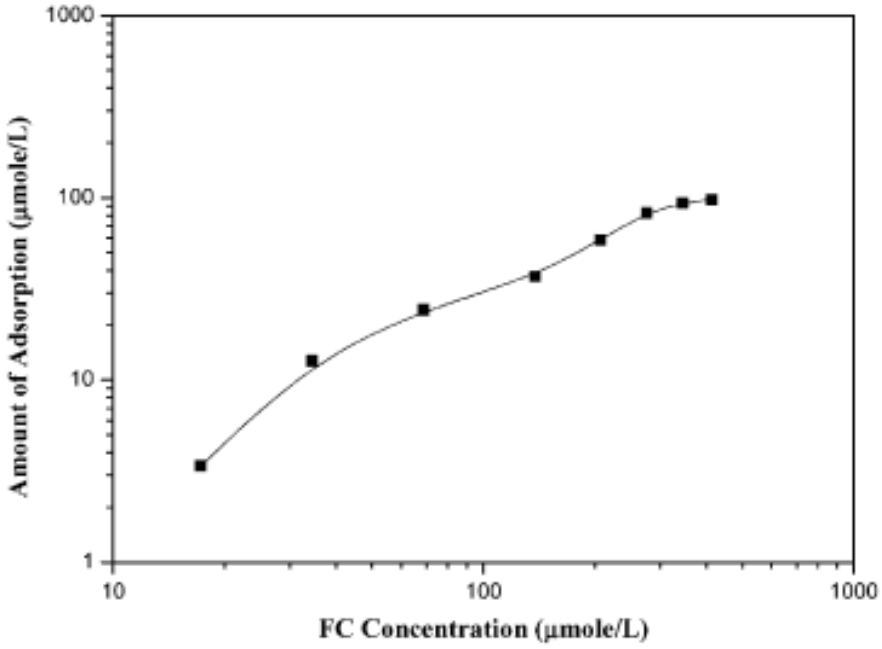

Figure 78. Adsorption isotherm of FC surfactant. (Ger & Hwang, 2002)

concentrations, surfactants presented a considerable barrier to not just the desired reduced nickel deposition as seen in Figures 68 & 69, but also to the growth of the deposit layer (unwanted).

As a possible solution to some observed unfavourable effect(s) of using surfactants in the manufacture of SOFC electrodes by ECD, it is believed that multiple coatings, applied from several baths in a step wise manner, will resolve the problem. As this line of investigation was beyond the scope of this research, proving this theory was not pursued.

6.3.3 Influence of a magnetic field

6.3.3.1 Magnetic orientation of YSZ

YSZ is a mixture of Yttria (Yttrium oxide – Y_2O_3) and Zirconia (Zirconium (IV) oxide – ZrO_2) which have different magnetic inclinations. While the former is paramagnetic with a

magnetic susceptibility of $+44.4/10^{-6}$ $cm^3.mol^{-1}$, the latter is diamagnetic with a susceptibility of $-13.8/10^{-6}$ $cm^3.mol^{-1}$. (Landolt-Bornstein, 1986; Tables de Constantes et Donnees Numerique, 1957).

With the combined ceramic – YSZ, being paramagnetic (Burova et.al., 2012), it was of no surprise that when poured into an EN solution and the beaker placed in front of an electromagnet of 100 mT magnetic field strength, the YSZ ceramic particles showed no attraction to the magnet.

As such and in line with the observation, it was concluded that YSZ was not suitable for use with the magnets unless coated with ferromagnetic materials such nickel, cobalt or iron.

6.3.3.2 Co-deposition of lanthanum strontium manganite particles under the influence of a magnetic field

Based on the fact that for an external force to be able to effectively create a positive effect (or overcome a negative one) on particle dispersion or mobility in an EN solution, an imposed magnetic field must be able to adequately attract or repel the particles in the solution, the co-deposition of ceramic powder and nickel under the influence of a magnet becomes a potentially effective technique for ferromagnetic materials such as LSM.

6.3.3.2.1 Experimental setup

In order to enable the variation of the magnetic field strength, an electromagnet was used instead of a permanent magnet.

A 90Ω coil was connected to a power pack with a maximum power supply of 100 V. The resultant current out flow of up to 1.1A translated to a magnetic flux density of as high as 200 mT at the utilised iron pole pieces which were 37.17mm in diameter and placed at both sides of the beaker (Figure 79).

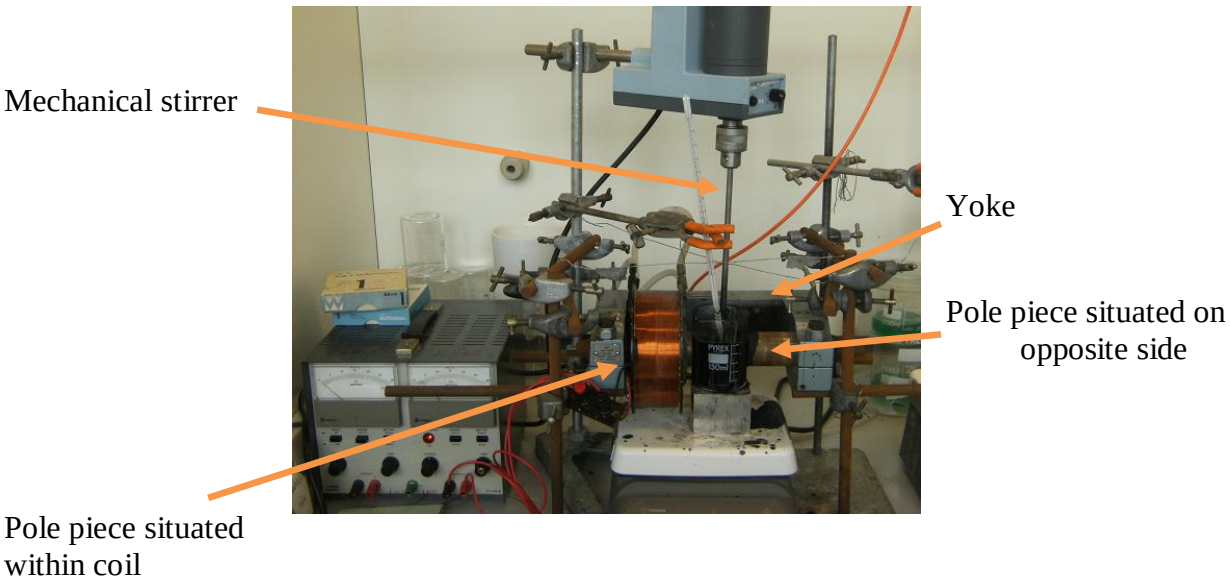

Figure 79. Experimental setup for magnetic Ni – LSM co-deposition process

It was observed that although a yoke was used as a means of achieving a uniform flux around the plating beaker, the pole piece directly located within the coil generated a magnetic flux density of at least 4 times the amount generated at the pole piece not inserted into the coil (opposite side). To compensate for any flux difference, it was decided that if needed another coil would be placed over the second pole piece to nullify the disparity.

6.3.3.2.2 Experimental procedure and rationale

The experimental procedure involved heating the nickel solution to 89^{o}C before introducing the LSM powder. Prior to switching on the coil's power supply, the substrate (alumina tile) was inserted into the solution as close as possible to the pole piece (Figure 80). This was carried out in order to ensure that the magnetic attraction on the particles would keep both the substrate and the particles in the same area. Ferro chromium alloy ($FeCrO_y$) wires were

furthermore, specifically used to suspend the substrate in order to ensure that it was drawn as close as possible to the pole pieces during deposition.

For the first set of experiments, an acidic plating bath was used. Though previous assessments in a similar bath where a magnetic field was not used, had yielded erratic results (section 6.3.1.3), it was decided that the effect of the magnetic field on the tendency of LSM to shift the pH to the alkaline region be initially studied and verified. It was hoped that the experiments would also reveal if nickel's magnetic nature was responsible for the erratic deposition earlier observed, Table 17 details the experiment matrix adopted and LSM_{20} powder was used for the study. The loading was 50g/l and the stirring rate was 400 rpm during the plating process.

Table 17. Setup IV: Experimental setup for acidic electroless Ni-LSM coating under the influence of a magnet.

Bath	Magnetic field strength (mT)
SC 23	30
SC 24	65
SC 25	150
SC 26	200

6.3.3.3 Findings

In a similar manner to the non-magnetic experiments, all the acidic EN baths produced very erratic co-deposits even under the influence of a magnetic field. In fact, most substrates did not coat. The most stable coating though was produced from bath SC 24. Table 18 shows the elemental composition of the few coatings that successfully coated (poor surface coverage though) while Figure 81 shows the respective EDXA spectrum of the coating produced from bath SC 24.

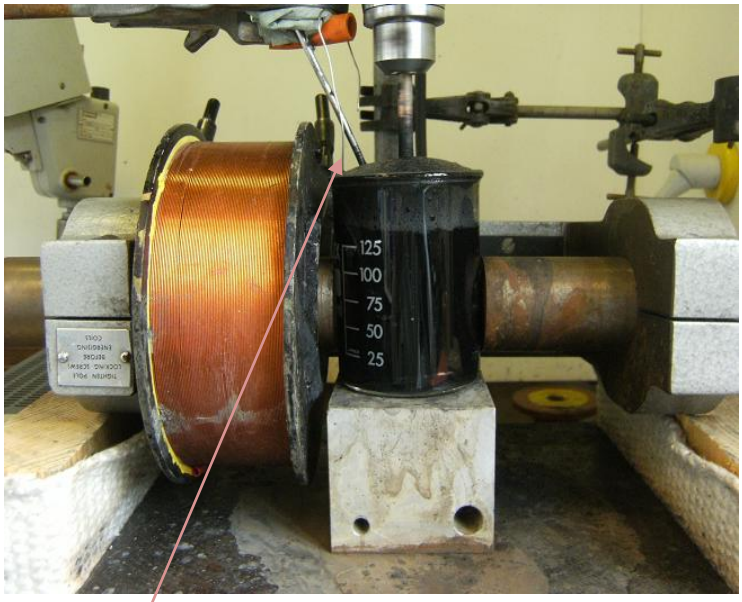

FeCroy wire used to suspend substrate

(a)

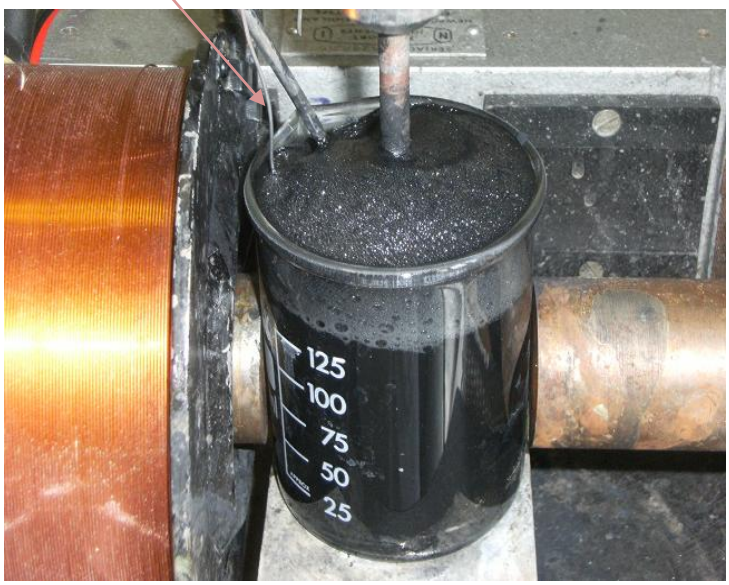

(b)

Figure 80. Side (a) and aerial (b) views of a substrate immersed in an electroless Ni – LSM coating.

Table 18. Composition of acidic electroless nickel – LSM coatings under the influence of a magnetic field

	Composition (Volume %)						
Samples produced from bath	Ni	La	Sr	O	Mn	Al	P
SC 23	80.65	0.41	-	12.48	0.07	3.98	2.07
SC 24	28.75	1.85	-	32.13	0.57	34.07	2.62
SC 26	10.03	11.96	-	55.50	13.53	4.67	-

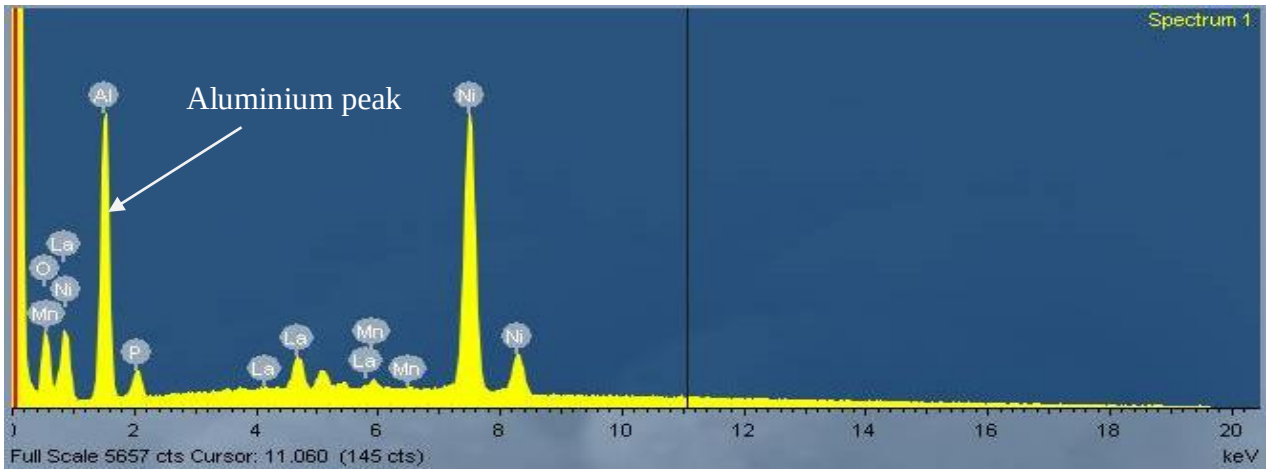

Figure 81. EDXA spectrum of an acidic electroless nickel – LSM coating deposited from bath SC 24

As can be seen from the spectrum and confirmed by the dominant aluminium peak – originating from the alumina substrate, the coating obtained from bath SC 24 was very thin.

6.3.3.4 Coating adhesion and composition versus magnetic field strength

Figure 82 shows the EDXA of a coating manufactured from bath SC 26 i.e under the influence of a magnetic field strength of 200 mT. When compared to the EDXA of coatings produced from bath SC 24 (Figure 81 above), the strong lanthanum peak distinctively confirmed a high LSM content in the coating and provided a substantive base for the composition of coatings bath SC 26 detailed in Table 18.

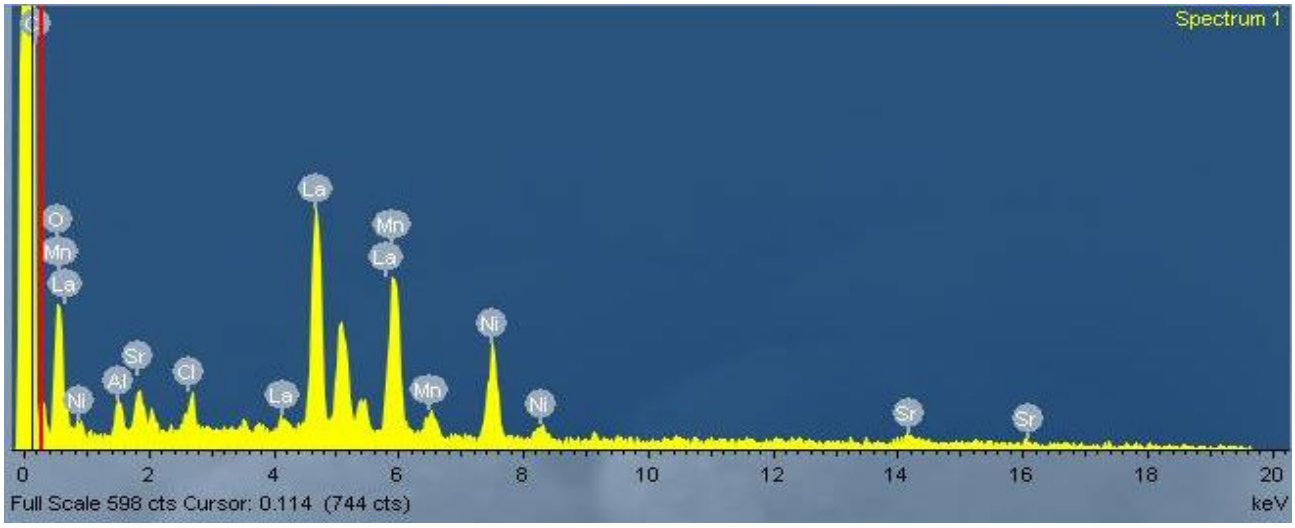

Figure 82. EDXA spectrum of an acidic electroless nickel – LSM coating deposited from bath SC 26. Sample has not been washed and dried

Though coatings with nickel content as low as 10.03 volume % were achieved from bath SC 26, to determine the possibility of their use as electrodes for SOFC technology, it was necessary to examine their quality and durability. To achieve this, a mild peel off test was carried out and Figure 83 shows the outcome of the test. It was observed that although the coatings were dark and high in LSM content (Figure 83a), after washing, drying and subjecting them to mild peeling by physically rubbing their surfaces with a soft sponge, large scale flaking occurred (Figure 83b) with most occurring during the washing stage.

(a) (b)

Figure 83. Image of an acidic electroless nickel – LSM coating deposited under the influence of a 200 mT magnetic field. (a) Just coated (b) after washing, drying and rubbing. The mid section of the coating can be seen to have washed off.

To investigate further, coatings manufactured under 150 mT magnetic field strengths (SC 25) were subjected to the same test. In the same vein as those manufactured under 200 mT (SC 26), the coatings equally peeled off but had on a positive note, less flake off and more force required to peel the surface.

With the trend occurring mostly in higher magnetic strength coatings, it became apparent that the presence of a high magnetic field strength must have distorted the traditional ionic nucleation and bonding of nickel onto a substrate and consequently hindered strong bonding in the coating. The outcome, as observed in high magnetic strength coatings, was that when the electromagnet was switched off and the coating rinsed, the particles dropped off.

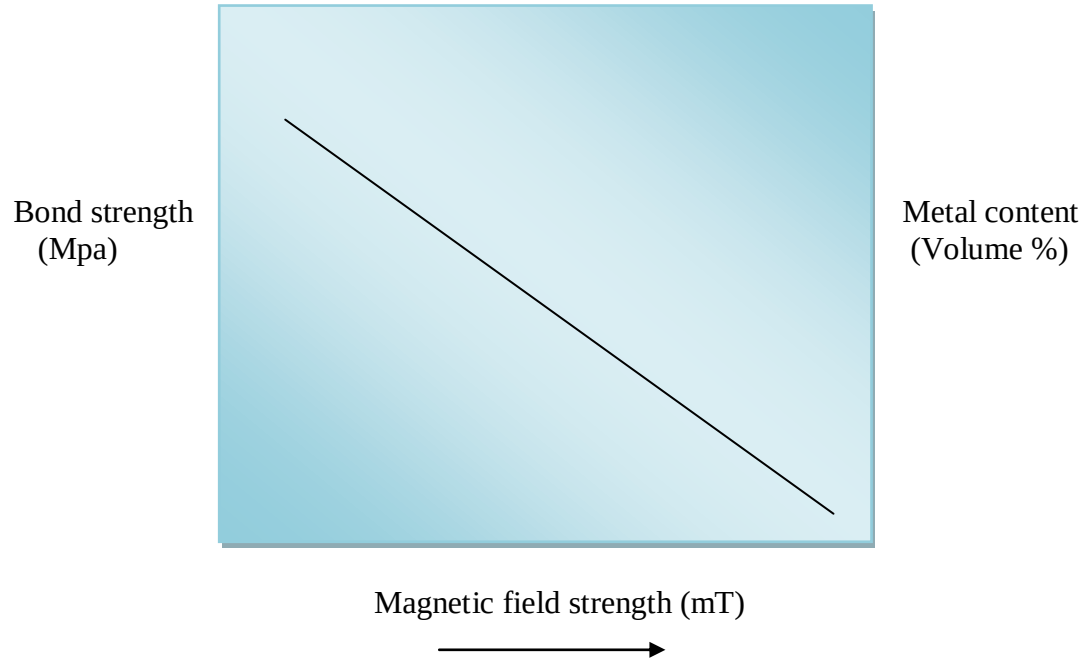

Figure 84. Typical relationship between the coating composition, bond strength and strength of magnetic field used during the co-deposition process.

Figure 84 depicts the possible relationship between the bond strength, coating composition and strength of an external magnetic field acting on particles during the co-deposition process. While the inverse trend between the bond strength, nickel content and magnetic field strength is shown, it is worthy to note that not all the co-depositions carried out (12 runs with 3 runs at each magnetic field strength) produced a coating and as such the figure represents a general rule which is still open to further research.

6.3.3.5 Agitation rate and magnetic field

With a lower magnetic field strength of 65mT consistently producing thin but uniform coatings, it was believed that the variation of other plating parameters in combination with the 65mT magnetic field strength might improve the nature of coatings obtained.

As discussed in section 4.3.3, studies have shown that the rate of agitation during ECD strongly influences the nature of deposits obtained by the process. To this end, the effect of rate of agitation was investigated before a conclusion was drawn on coatings manufactured from acidic baths. Experiments were repeated in baths according to the conditions of bath SC 24 with the exception of the rate of agitation which was varied between 300 rpm and 500 rpm.

6.3.3.5.1 Result V: Effect of agitation rate on the nature of coatings manufactured under the influence of a magnetic field

Figures 85, 86 and 87, highlight the effect of varying the rate of agitation rate during ECD while exposing the substrate/ bath solution to a magnetic field. It is evident from the images that at lower or higher than 400 rpm rate of agitation, poor coatings are manufactured. Coatings manufactured at a stirring rate of 300 rpm appeared to coat better than those co-deposited at 500 rpm – results which appeared to be well in line with the earlier stated report of Balaraju et al., 2003. In line with the work of the researchers, it is believed that on one hand, irrespective of the influence of the magnetic field on the motion or location of ceramic.

Figure 85. Image of acidic electroless nickel – LSM coating manufactured under 65 mT magnetic field strength at an agitation speed of 300 rpm.

Figure 86. Image of acidic electroless nickel – LSM coating manufactured under 65 mT magnetic field strength at an agitation speed of 400 rpm.

Figure 87. Image of acidic electroless nickel – LSM coating manufactured under 65 mT magnetic field strength at an agitation speed of 500 rpm.

particles in the solution, too fast a rate of agitation would have allowed the particles less time to get attached to the surface of the substrate. Conversely, slower rates of agitation such as 300 rpm, it is believed, must have also by and large, promoted particle agglomeration in the solution which consequently resulted in particle sedimentation under the influence of gravity. As seen the consequence of such interactions is the poor coatings observed.

Further experiments attempted to reproduce coatings from bath SC 24 at 400 rpm – which had earlier yielded relatively positive results, subsequently returned unsuccessful results. As such experiments with an acidic bath were discontinued.

It was concluded that the degree of alkalinity of LSM had to be considered if control was to be achieved at all over the nature of Ni – LSM deposits obtained.

6.3.3.6 Effect of alkaline baths

The conditions outlined in Table 17 were reproduced in alkaline EN baths. This is detailed in Table 19. In a similar manner to the experiments conducted in an alkaline EN solution

Table 19. Setup V: Experimental setup for alkaline electroless Ni-LSM coating under the influence of a magnetic field.

Bath	Magnetic field strength (mT)
SC 27	10
SC 28	30
SC 29	65
SC 30	150
SC 31	200

without the magnetic field, it was observed that the coatings readily plated. However under the influence of a high magnetic field (150 – 200 mT), the coatings appeared to form distinctive patterns which appeared to suggest that the nucleation of nickel on the substrate was hindered in some areas (Figure 88). The detection of aluminium (Table 20) confirms this occurrence. In

Figure 88. Image of 2 alkaline electroless nickel – LSM coatings manufactured under the influence of 200 mT magnetic field strength

terms of composition, the effect of the magnetic field was marginal. This is detailed in table 20.

The results confirmed that all the coatings manufactured from all the solutions were successful. Of concern though was that the nickel content averaged at about 80 volume %. Since an SOFC cathode region provides a highly oxidising environment, further work is still needed to attempt to reduce the nickel content of the coating in order to avoid oxidation of nickel to nickel oxide which is unstable in such environments and has a lower conductivity than nickel.

Table 20. Composition of alkaline electroless nickel – LSM coatings manufactured under the influence of a magnetic field

		Composition (Volume %)					
Samples produced from bath	Ni	La	Al	Sr	O	Mn	P
SC 27	79.03	0.86	-	-	13.63	0.43	6.06
SC 28	89.11	0.11	-	-	3.79	-	6.99
SC 29	81.54	0.27	-	-	8.38	0.17	9.47
SC 30	82.88	0.95	-	-	10.08	0.87	4.43
SC 31	88.23	0.29	0.67	-	5.53	-	5.28

6.3.3.7 Effect of powder composition

Since the composition of LSM determines its physical characteristics, of which its magnetic property is one, the effect of the use of an alternative powder was studied. Table 19 previously used to co-deposit nickel and LSM_{20} in an alkaline solution was similarly adopted. 2 runs were attempted at every magnetic field strength.

On the introduction of LSM_{18}, no difference of ceramic content in the coating was observed from those obtained in Table 20. As such, no further tests were conducted with LSM_{18} and it was subsequently concluded that the composition of LSM had no effect on the level of LSM particle incorporation during ECD.

6.3.3.8 Effect of plating duration

Further attempts made to increase the ceramic content of the coatings involved plating for 2 and 3 hrs. Thus far, with 65mT appearing to be most appropriate magnetic field strength for the studies, the experiments were conducted in baths prepared in a similar manner to SC 29.

Besides producing very uniform coatings, the results yielded no additional ceramic content as can be seen from Table 21 where nickel contents were again above 80 volume %.

Table 21. Variation of the composition of alkaline electroless nickel – LSM coatings with time. Solutions subjected to 65mT magnetic field strength

	Composition (Volume %)					
Samples produced from bath	Ni	La	Sr	O	Mn	P
SC 32 (65mT/2hrs)	92.65	-	-	-	-	7.35
SC 33 (65mT/3hrs)	81.39	0.39	-	10.13	0.16	7.93

6.3.3.9 Effect on surface topography

Atomic force microscopic (AFM) examination of a selection of coatings highlighted some correlations which may be exploited during the use of ECD as a method of manufacturing SOFC electrodes.

Coatings obtained from plain EN nickel baths, when compared to the alumina tile used as substrates, appeared to suggest that EN coatings were generally smooth (Figures 89 & 90). The

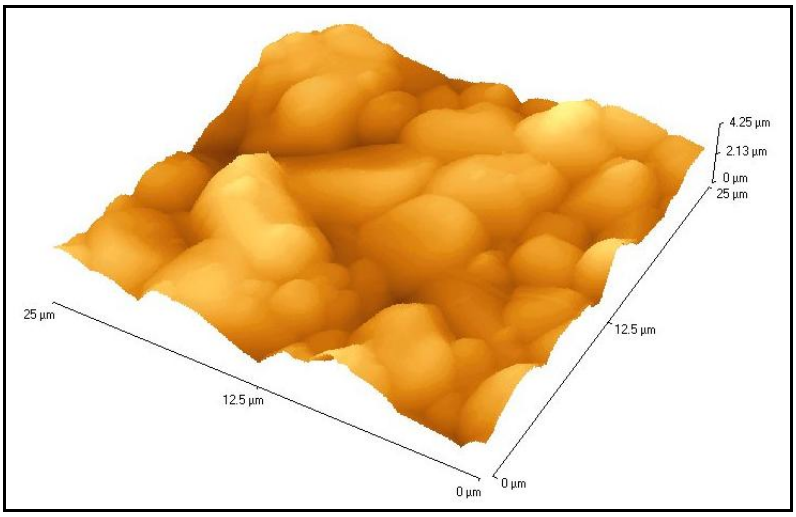

Figure 89. AFM topographical scan of the surface an AD 96 alumina tile

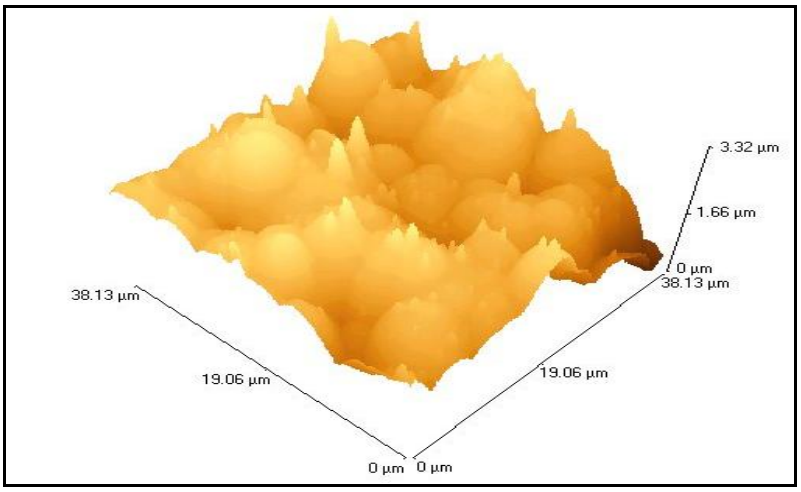

Figure 90. AFM topographical scan of the surface a plain electroless nickel coating – Bath SC 10.

former had an Ra value of 304.512 µm while the latter was 538.340 µm. However with the introduction of ceramic particles and under the influence of a magnetic field, there appeared to be a re-organisation of structure. Under the influence of low magnetic field strength, the average surface roughness of the coatings increased. With increasing field strength, the roughness slightly dropped (Table 22). Time though appeared to suggest a different trend, as with increasing number of hours of co-deposition, the coatings progressively became rougher – a desired property of SOFC electrodes (Figures 86 – 88).

Table 22. Effect of magnetic field on the average surface roughness of alkaline electroless nickel – LSM coatings

Samples produced from bath	Average surface roughness (µm)	Deposition time (hrs)
No plating (Al substrate)	304.512	-
Control run (plain Ni)	538.340	1
SC 27 (10 mT)	626.663	1
SC 29 (65mT)	577.733	1
SC 32 (65mT)	508.070	2

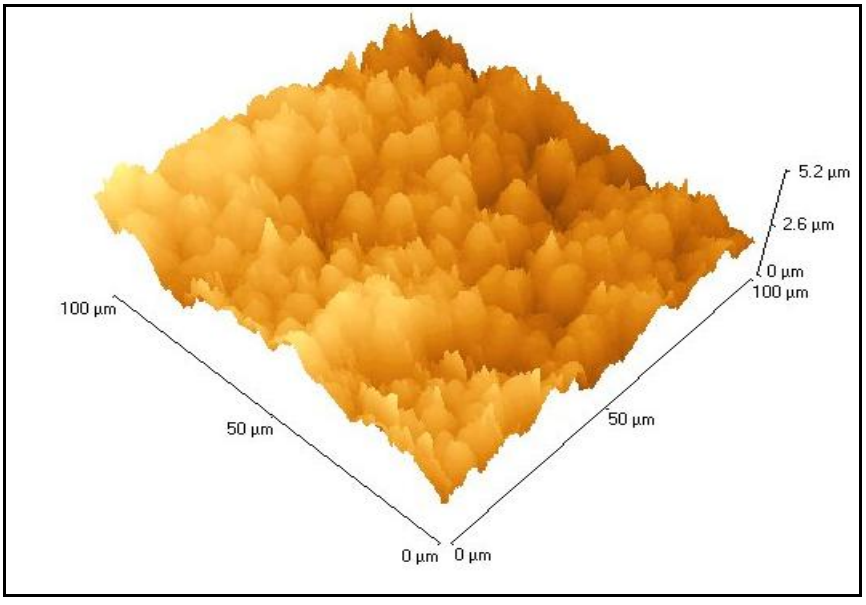

Figure 91. AFM topographical scan of the surface an Ni-LSM coating from SC 27.

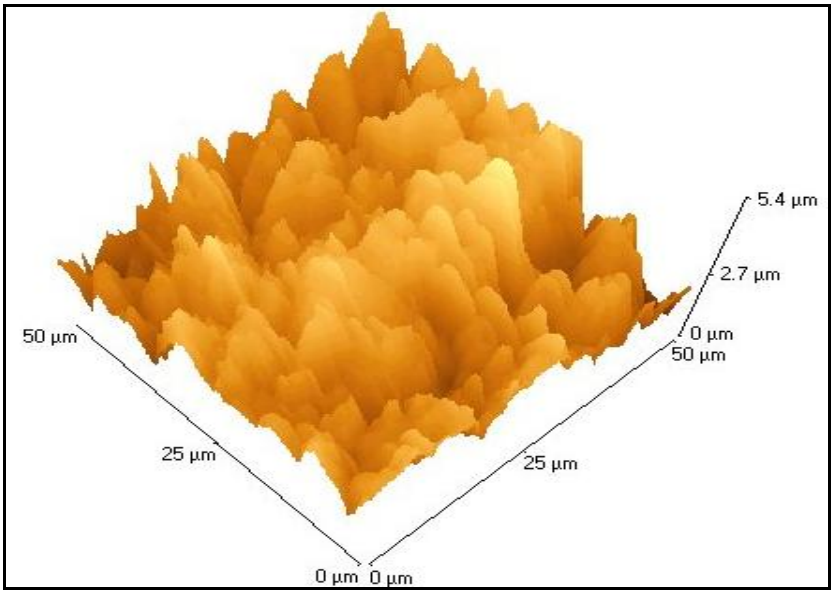

Figure 92. AFM topographical scan of the surface an Ni-LSM coating from bath SC 29.

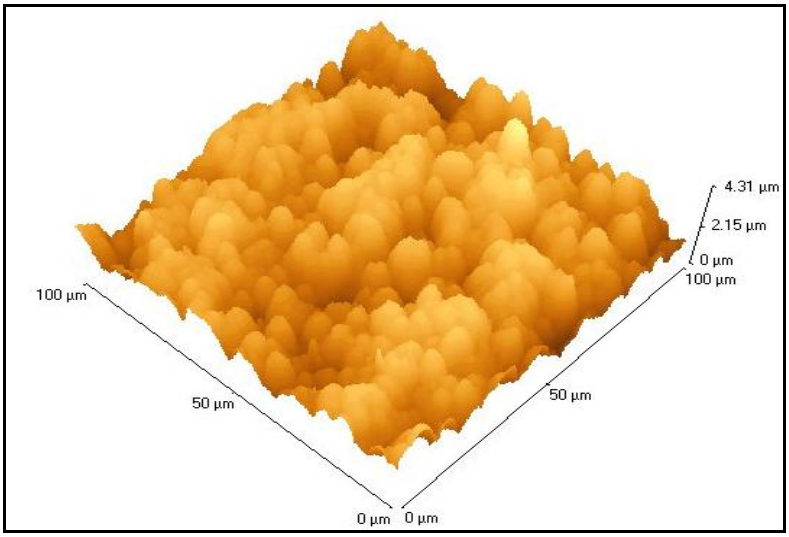

Figure 93. AFM topographical scan of the surface an Ni-LSM coating from bath SC 32.

7. Conclusion

The integrity, performance, durability and reliability of an SOFC are largely dependent on the composition of its component parts. As a result of this, establishment of defined variables that will aid the achievement of the required composition is vital.

This research primarily investigated the effect of external agents on the composition of electrodes (especially the cathodes), manufactured by the electroless nickel ceramic co-deposition (ECD) technique. With the aim of increasing the ceramic content of the electrodes, the effects of surfactants and magnets as enhancers were further studied.

Optimum parameters such as the desired powder loading, particle size, interaction between the particles and the solution, surfactant type, magnetic field strength and rate of agitation were established in the process. Factors such as coating thickness, bond strength, surface roughness, coating coherence and surface morphology, which would amongst other factors indicate the suitability of the end product to satisfy the requirements of an SOFC electrode were routinely monitored during the research in a bid to determine the suitability of the co-deposits to operate within the constraints of SOFC technology.

Free from surfactants, it was observed that the maximum particle incorporation into the nickel matrix was achieved at a powder loading of 50 g/l. Beyond this stated powder loading, the ceramic content in the coating diminished and varied directly with the coating thickness which was found to drop to as low as 2 μm. Whilst the observed reduction in the amount of ceramic entrapped in the coating, it is suggested, may have been associated with the phenomenon of saturation, the finding that the coating thickness steadily decrease with increase of the ceramic content in the bath was viewed to be based on the dynamics of electroless nickel plating (ENP) and the properties of YSZ. It is known that ENP is an

autocatalytic isotropic process that relies on continuously deposited nickel metal to provide a platform for further deposition of nickel metal that is reduced from an ionic state (Ni^{2+}) to a zero valent metallic state (Ni^{0}). Thus with un-activated YSZ particles providing less reactive insulating facets that do not encourage the autocatalytic deposition process, it can be understood that the increasing ceramic content in the bath will tend to shield active sites for the zero-valent Ni to adsorb onto. If this occurs, as can be seen from the available evidence, the result is a continuous decrease of the coating thickness. At 50g/l, the coating thickness observed was 14 µm and the ceramic to metal ratio measured via energy dispersive x-ray analysis technique was 41 to 59, ceramic to metal ratio.

Attempts to further increase the ceramic content of the coatings witnessed the use of surface active agents (surfactants) and a variation of magnetic field strengths.

Based on their lyophilic-lyophobic tendencies and with the right selection criteria observed, surfactants possess excellent wetting, emulsifying, solubilising and dispersing characteristics. On the principle of dispersion possibly providing better availability of particles to be entrapped during the plating process, it was believed that surfactant usage could enhance the nature of co-deposits obtained. After a selection process that involved observing both particle precipitation ratios in electroless nickel solution and water, and determining the zeta potential of YSZ and LSM particles in both solutions, the surfactant sodium dodecyl sulphate (SDS) was selected for use during the plating process.

With respect to surfactant usage, it was conclusively found that as long as the surfactant's (SDS) critical micelle concentration had been exceeded, the ceramic content of a deposited Ni – YSZ electrode varied directly with the surfactant's concentration in the bath with a ceramic content of as high as 60 volume % achieved. This finding was of immense importance as it uniquely offered an opportunity to have effective control over the amount of metal in SOFC

electrodes co-deposited by the technique. A high nickel content is unwanted in SOFC electrodes as it is an inherent indication of a tendency of the cell to crack whilst in operation.

A drawback though was observed with the use of surfactants with the loss of coating thickness found to occur. When compared with available literature on the dynamics of surfactants, the finding was found to agree with the work of Janczuk et al. (1994) who found that as the concentration of surfactants increases in a solution, a monolayer gradually forms and gradually becomes stable. As with increased ceramic content impeding co-deposition, the surfactant generally follows the same trend with the formation of a barrier to the coating.

Thermal cycling, an expected frequent occurrence in SOFC technology, will tend to amongst other things, encourage cell delamination. To this end, excellent bond strengths will at a minimum, be required for SOFC units manufactured by ECD. Whilst the coatings manufactured using YSZ particles appeared to display good bonding between the coating and the substrate, the reverse was the case for coatings obtained from baths containing LSM particles. Experiments conducted showed that whilst YSZ was more comfortable in an acidic electroless nickel solution, LSM completely caused a pH shift which inherently spontaneously destabilised the bath and prevented deposition. The magnetic nature of LSM furthermore it is proffered, also had a strong negative effect on nickel ions in the solution which is known to drive the reaction. Evidence for both conclusions arises from the finding that when bath solutions were changed from acidic to alkaline, electroless Ni-LSM deposits were readily obtained.

Although LSM appeared to readily co-deposit in alkaline environments – a position supported by its natural inclinicity due to strontium oxide's alkaline disposition, results obtained under a magnetic field in an acidic bath provided one of several tangentials for future research. It was found that under high magnetic field strengths (as high as 200 mT), the coating was saturated

with high amounts of LSM. However due to the underlying electroless nickel ionic bonding mechanism being overridden by the magnetic field, the particles were found to tend to flake off after the deposition process. It is believed that, if a mechanism is developed – even if binders can be applied after plating, the technique may hold a lot of promise for use in the manufacture SOFC cathodes by electroless nickel ceramic co-deposition technique in the future.

The search for an optimum magnetic field strength whereby the bond strength appeared to be qualitatively good, with maximum ceramic incorporation also observed, witnessed the co-deposition process occurring at lower magnetic field strengths. The optimum flux density was found to be 65mT.

In conclusion, it was found that acidic electroless nickel solutions tend to provide suitable conditions for the manufacture of SOFC anodes by ECD technique while due to the alkaline nature of the LSM powder, alkaline EN solutions are more appropriate for cathodes.

Attempts to increase the ceramic content of the coating also witnessed variations in the level of particle agitation during the manufacturing process. It was found that under the influence of a magnet field, the best results were produced at a stirring rate of 400 rpm.

8. Contribution to knowledge

Electroless nickel ceramic co-deposition is a new and patented method of manufacturing solid oxide fuel cell electrodes. Determining the exact variables that will yield the required composition of the SOFC electrodes has been investigated by several researchers since its conception (Waugh, 2009; Baba, 2010), but none has studied the effect of external agents.

Surfactants (surface active agents) are readily available. The interaction of SDS with YSZ particles has never been studied by any previous researcher and the findings in this work show that the compounds possess immense potentials for use during the co-deposition process. In fact a long list of other types of surfactants such as cetyl trimethyl ammonium bromide (CTAB) exist of which due to their intrinsic differential natures, may even provide better results.

The use of magnetic field during the co-deposition of second phase particles by electroless nickel plating, to the best of my knowledge has not be reported in literature, let alone fuel cells. The subtle support provided by the external agent holds a lot of promise not only for use during the SOFC manufacture, but also for the co-deposition of other materials of a magnetic nature. The success achieved and documented in this thesis, means that the technique may not just only be applied in SOFC technology, but may find use in anti-corrosion and wear resistance coatings where materials of the nature of iron, constitute the particulate matter.

9. Future work

Electroless nickel plating, the platform on which electroless nickel ceramic co-deposition operates is largely influenced by several variables – the effect of some of which has been studied in this research. While it is clear that by altering these variables in combination with external agents such as surfactants and magnets, the ceramic content of ECD coatings deposited for use as solid oxide fuel cell electrodes can be further increased, it is believed that more research can build on the nature of results obtained in this work. The following are factors that may positively influence the results;

1. Alternative reducing agent: In this study, the efficient and effective hypophosphite reducing agent has been relied upon for the reduction of nickel ions prior to its nucleation on the surface of the substrate. However, the corresponding co-deposition of phosphorus as a result of using the reducing agent provides a cause for concern in fuel cell technology. Not only has phosphorus been found to poison the cell, its formation of a liquid phase with nickel at temperatures above 850^{o}C must also be considered.

   Thus it is recommended that research into alternatives such as the borohydride ion or hydrazine be attempted. While they may have less deleterious effects on the cell, the use of the borohydride ion during electroless nickel plating is known to produce porous coatings which may be of use in the need to create pores for gas transportation to the triple phase barrier.

2. As external agents have been used, it might be necessary to study their effect on the performance of the cell so as to ensure that the conditions required for optimum cell performance are met.

3. For co-deposition of cathodes, the possibility of utilising an electroless lanthanum deposition process to augment the current technique may possibly further improve the nature of deposits manufactured. It is believed that if Lanthanum can be anodised, it may form an initial cathode layer before the ECD process is used to form a cathode conducting layer.

4. Though nickel has been co-deposited in the SOFC electrodes manufactured, and as such guarantees that the required electrical conductivity can be achieved, it is necessary for the performance of these coatings i.e stability, durability and reliability, be investigated in all entirety.

5. The orientation of the substrate has been found to have an effect on the level of particle incorporation into the nickel matrix during ECD by several researchers (Sheela and Pushpavnam, 2002; Waugh, 2009). Since during the use of magnets, the field is concentrated greatly on a particular side, extensive study on the contribution of this effect on the nature of deposits obtained may provide better insights to the overriding phenomenon which could subsequently be exploited to maximise the ceramic content of the coatings.

10. Publications

Published works in the form of Journal and conference publications are detailed below. Posters and internal articles submitted within the university are also outlined within.

- Peer reviewed journal papers

1 Effect of SDS on the dispersion stability of YSZ particles in an electroless nickel solution. N.Nwosu, A. Davidson, N. Shearer. Chemical Engineering Communications, 2013, Vol. 200, No.12, 1623 – 1634.

2 On the influence of surfactant incorporation during electroless nickel plating, N. Nwosu, A. Davidson, C. Hindle, M. Barker. Industrial & Engineering Chemistry Research, 2012, Vol.51, 5635 – 5644.

3 Effect of sodium dodecyl sulphate on the composition of electroless nickel – yttria stabilized zirconia coatings. N. Nwosu, A. Davidson, C. Hindle. Advances in Chemical Engineering and Science, 2011, Vol.1, No.3, 118 – 124.

- Peer reviewed conference paper

4 Characterisation of solid oxide fuel cell cathodes manufactured by traditional and novel (low cost) techniques. N. Nwosu, A. Davidson, W. Waugh. Proceedings of the 1st international conference on materials for energy, Germany.

- Inter-faculty university papers

5 Electroless Nickel-LSM Co-deposition: Bringing solid oxide fuel cells to the market. N. Nwosu. Edinburgh Napier University FECCI Research conference 2010.
(Awarded best 1st year research student paper and presentation).

- Inter-faculty university posters

6 Composition of surfactant incorporated solid oxide fuel cell anodes (Poster). N. Nwosu. Edinburgh Napier University SEBE Research poster event 2011.
(Poster awarded 1st prize).

7 Manufacture of low cost solid oxide fuel cells utilising gas produced from municipal solid waste. N. Nwosu, A. Davidson. Edinburgh Napier University SEBE Research poster event 2010.
(Poster awarded 2nd prize).

REFERENCES

Aleksinas, M.J. (1990). Troubleshooting electroless nickel plating solutions. In Electroless plating: fundamentals and applications; Mallory, G. O., Hajdu, J. B., Eds.; American Electroplaters and Surface Finishers Society: FL, USA, pp108.

Alsari , A.M.; Khulbe, K.C.; Matsuura, T. (2001). The Effect of Sodium Dodecyl Sulfate Solutions as Gelation Media on the Formation of PES Membranes. *Journal of Membrane Science*, 188, 279 – 293.

Baba, N.B. (2010). Novel processing of solid oxide fuel cell anodes. PhD thesis, Edinburgh Napier University. Edinburgh U.K.

Balaraju, J.N.; Sankara Narayanan T.S.N; Seshadri, S.K. (2003). Electroless Ni-P Composite Coatings. Journal of Applied Electrochemistry, 33, 807 - 816.

Boehm, E.; Bassat, J. M.; Steil, M. C.; Dordor, P.; Mauvy, F.; Grenier, J. C. (2005). Oxygen diffusion and transport properties in non-stoichiometric $Ln_{2-x}NiO_{4+\delta}$ oxides. Solid State Ionics, 176, 2717-2725.

Brenner, A.; Riddel, G. (1950). Nickel plating by chemical reduction. U.S. Patent 2,532,282; ibid,. J. Res. Natl. Bur. Stand. 1946, 37, 1

Burova, L.I.; Perov, N.S.; Semisalov, A.S.; Kulbachinskii, V.A.; Kytin, V.G.; Roddatis, V.V; Vasiliev, L.A.; Kaul, A.R. (2012). Effect of the nanostructure on room temperature ferromagnetism and resistivity of undoped ZnO thin films grown by chemical vapor deposition. *Thin solid films*, 520, 4580 – 4585.

Chen, B. H.; Hong, L.; Ma, Y.; Ko, T. M. (2002). Effects of surfactants in an electroless nickel-plating bath on the properties of Ni-P alloy deposits. Ind. Eng. Chem. Res., 41, 2668 − 2678.

Chen, F.; Liu, M. (2000). Preparation of yttria-stabilized zirconia (YSZ) films on $La_{0.85}Sr_{0.15}MnO_3$ (LSM) and LSM-YSZ substrates using an electrophoretic deposition (EPD) process.

Chiba, R.; Fumikatsu Y.; Sakurai Y. (1999). An investigation of $LaNi_{1-x}Fe_xO_3$ as a cathode material for solid oxide fuel cells. *Solid state ionics*, 124, 281 – 288.

Choi, S.H. (2007). Development of SOFC anodes resistant to sulphur poisoning and deposition. *Doctoral thesis submitted to Georgia Institute of Technology*.

Datta, P.; Bronin, D.I.; Majewski, P; Aldinger, F. (2008). Cermet cathodes for strontium and magnesium-doped LaGaO3 - based solid oxide fuel cells. *Materials chemistry and physics* , 356-361.

Davidson, A.M.; Waugh, W. (2008). Method of Manufacture of an Electrode for a fuel cell. New international (PCT) patent application claiming priority from United Kingdom application no. 0719260.2.

Derjaguin, B. V.; Landau,J. D. (1941). Theory of the stability of strongly charged lyophobic sols and of the adhesion of strongly charged particles in solution of electrolytes. Acta Physicochim. URSS. 14, 633−662; Ibid, Verwey, E. J. W.; Overbeek, J. T. G.(1948). Theory of the stability of lyophobic colloids; Elsevier: Amsterdam.

Dukhin, A. S.; Goetz, P. J. (2002). Ultrasound for characterizing colloids: Particle sizing, zeta potential, rheology; Elsevier: Boston, 308.

Fergus, J. W. (2006). Electrolytes for solid oxide fuel cells. *Journal of Power Sources* , 30 – 40.

Gabrielson L.; Edirisinghe M.J. (1996). On the dispersion of fine ceramic powders in polymers. Journal of materials science letters. 15, 1105 – 1107.

Ger, M.D.; Hwang, B.J. (2002). Effect of Surfactants on Co-Deposition of PTFE Particles with Electroless Ni-P Coating. *Materials Chemistry and Physics*, 76, 38 – 45.

Gutzeit G. (1959). Catalytic Nickel Deposition from Aqueous Solution. I-IV. *Plating surface finishing*, 46, 1158-1164.

Hawkes A.; Exarchakos L.; Hart D.; Leach M.; Haeseldonckx D.; Cosijns L.; D'haeseleer W. (2006). Fuel cells, Proceedings of European sustainable electricity meeting.

Hart, N.; Brandon, N.; Shemilt, J. (2000). Environmental evaluation of thick film ceramic fabrication techniques for solid oxide fuel cells. Mat. Manuf. Proc., 15, 47 - 64.

Horne, C.R.; Jaiswal, A.; Lynch, R.; Zhang, J.; McGovern, W. (2007). Low-Cost Manufacturing of solid Oxide Fuel Cell Components Using Laser Reactive Deposition (LRD™). Society of vacuum coaters, 505

Hunter, **R.J.** (1981). Zeta potential in colloid science: Principles and applications, Academic press, ISBN: 0123619602.

Imai, T.; Sasaura, M.; Nakamura, K.; Fujiura, K. (2007). Crystal growth and electro-optic properties of $KTa_{1-x}Nb_xO_3$. *NTT Technical Review*, 5, 1– 8.

Jakob, C.; Erler, F.; Nutsch, R.; Steinhauser, S.; Wielage, B.; Zschunke, A. (2000). Metalloberflache. 54, 50.

Janczuk, B.; Bruque, J.M.; Gonzalez-Martın, M.L.; Moreno del Pozo, J. (1994). The surface free energy of fluorite in presence of sodium dodecyl sulfate. *Powder Technol.* 80, 127 – 131.

Jonker, G.H.; Van santen, J.H. (1950). Ferromagnetic compounds of manganese with perovskite structure. Physica XVI, 337 – 349.

Jørgensen, M. J. (2001). *Lanthanum Manganate Based Cathodes for Solid Oxide Fuel Cells.* Doctor of Philosophy thesis submitted to Keele University, Risø-R-1242(EN), Materials Research Department.

Karakoussis, V.; Brandon N.P.; Leach, M; Van der Vorst, R. (2001). The environmental impact of manufacturing planar and tubular solid oxide fuel cells. *J. Power Sources*, 101, 10 – 26.

Krotz, D. (2002). Almost there: a commercially viable fuel cell, Lawrence Berkeley National Laboratory U.S.A, http://www.lbl.gov/Science-Articles/Archive/MSD-fuel-cells.html, accessed on 29/07/2010.

Landolt-Bornstein. (1986). Numerical Data and Functional Relationships in Science and Technology, New Series, II/16, Diamagnetic Susceptibility, Springer-Verlag, Heidelberg.

Lautrey, J. (2009). Manufacture of nanoparticles of polystyrene or polymethyl methacrylate for use in fuel cells, BEng tnterim project report submitted to Edinburgh Napier University's School of Engineering and Built Environment, pg 10-12.

Mallory, G.O. (1990) [a]. The Electroless Nickel Plating Bath: Effect of Variables on the Process. In Electroless plating: fundamentals and applications; Mallory, G. O., Hajdu, J. B., Eds.; American Electroplaters and Surface Finishers Society: FL, USA, pp 57 – 99.

Mallory, G.O. (1990) [b]. The fundamental aspects of electroless nickel plating. In Electroless plating: fundamentals and applications; Mallory, G. O., Hajdu, J. B., Eds.; American Electroplaters and Surface Finishers Society: FL, USA, pp 55.

Marton, J. P.; Schlesinger, M. (1968). The nucleation, growth and structure of thin Ni-P films. J. Electrochem. Soc. 115, 16.

McCarroll, W.H.; Ramanujachary, K.V.; Fawcett I.D.; Greenblatt, M. (1999). Electrical and magnetic properties of strontium substituted lanthanum manganate perovskite crystals prepared using fused salt electrolysis. Journal of solid state chemistry. 145, 88 – 96.

Millar, L.; Taherparvar, H.; Filkin, N.; Slater, P.; Yeomans, J. (2008). Interaction of $(La_{1-x}Sr_x)_{1-y}MnO_3$-$Zr_{1-z}Y_zO_{2-D}$ cathodes and $LaNi_{0.6}Fe_{0.4}O_3$ current collecting layers for solid oxide fuel cell application, Proceedings of the 2008 conference for the engineering doctorate in environmental technology.

Mitterdorfer, A.; Gauckler, L.J.,(1998). $La_2Zr_2O_7$ formation and oxygen reduction kinetics of the $La_{0.85}$ $Sr_{0.15}$ Mn_y O_3, O_2 (g) YSZ system, Solid state ionics, 185 – 218.

Moon, J-W.; Hwang, H.J.; Awamo, M.; Maeda, K. (2003). Preparation of NiO-YSZ tubular support with radially aligned pore channels. *Materials letters, Vol.57, no.8* , 1428-1434.

Natividad, E.; Lataste, E.; Lahaye, M; Heintz, J.M.; Silvain, J.F. (2004).Chemical and morphological study of the sensitisation, activation and Cu electroless plating of Al2O3 polycrystalline substrate. Surface science, 557, 129 – 143.

Newberry, J.E. (1979). Surface interactions of micelles and divalent metal ions, J. Colloid and interface science. 74, 483 – 488.

Nwosu, N. (2010). Electroless nickel – LSM co-deposition: Bringing solid oxide fuel cells to the market. Proceedings of the Edinburgh Napier University FECCI Research conference.

Nwosu, N.; Davidson, A.; Hindle, C.; Barker, M. (2012). On the Influence of Surfactant Incorporation during Electroless Nickel Plating. Industrial & Engineering Chemistry Research. 51, 5635 − 5644.

Nozawa, k.; Orui, H.; Komatsu, T.; Chiba, R.; Arai, H., (2008). Development of highly efficient plannar solid oxide fuel cells, NTT technical review vol.6 No.2

Odekerken, J.M. 1966. Use of Co-Deposited Non-Conducting Materials to Improve the Corrosion Resistance of Nickel- Chromium Electrodeposits. British Patent 1041753, U.S. Patent 3644183 and DDR Patent 414061964.

Rao Y.; Takahashi A.; Wong C.P. (2003). Di-block copolymer surfactant study to optimize filler dispersion in high dielectric constant polymer-ceramic composite, composites (Part A: applied science and manufacturing). 34, 1113 – 1116.

Riddick, T.M. (1968). Zeta-Meter manual, Zeta-Meter Inc., New York.

Rudin, A. (1999). The elements of polymer science and engineering. 2nd edition, Academic press.

Shao, Z.; Kwak, C.; Haile, S.M. (2004). Anode-supported thin-film fuel cells operated in a single camber configuration 2T-I-12. *Solid state ionics*, 175, 39 – 46.

Sheela, G.; Pushpavanam, M. (2002). Diamond-dispersed electroless nickel coatings, Journal of Metal finishing, 45 – 47.

Singhal, S. C. (2007). Solid Oxide Fuel Cells. *The Electrochemical Society Interface• Winter 2007* , 41.

Sisti, M.J.; LaPlante, J. (2001). EN process performance. *Products finishing*, 66, 46.

Skinner, S.J.; Kilner, J.A. (2000). Oxygen diffusion and surface exchange in $La_{2-x}Sr_xNiO_{4+\delta}$. Solid State Ionics, 135 (1-4), 709 – 712.

Tables de Constantes et Donnees Numerique, Volume 7, Relaxation Paramagnetique, Masson, Paris, 1957.

Tsai, T.; Barnett, S. (1996), Effect of LSM-YSZ cathode on thin-electrolyte solid oxide fuel cell performance, Solid state ionics, 207 – 217.

Ullmann, H.; Trofimenko, N.; Tietz, F.; Stover, D.; Ahmad-Khanlou, A. (2000). Correlation between thermal expansion and oxide ion transport in mixed conducting perovskite-type oxides for SOFC cathodes . *Solid state ionics*, 79-90.

Wang, S.; Jiang, Y.; Zhang, Y.; Yan, J.; Li, W. (1998). The role of 8 mole% yttria stabilized zirconia in the improvement of electrochemical performance of lanthanum manganite composite electrodes. J. Electrochem. Soc., 145, 1932 - 1939.

Watanabe H. (1961). Magnetic Properties of Perovskites Containing Strontium, II. Lanthanum-Strontium Manganites. Journal of the physical society of Japan. 16, 433 – 439.

Watanabe, K.; Imai, S.; Mori Y.H. (2005). Surfactant effects on hydrate formation in an unstirred gas/liquid system: An experimental study using HFC-32 and sodium dodecyl sulfate, *Chem. Eng. Sci.*, 60, 4846–4857.

Waugh, W. (2009). Development of a new manufacturing method of electrodes for solid oxide fuel cells. PhD thesis, Edinburgh Napier University. Edinburgh U.K.

Xianguo, L. (2006). *Principles of fuel cells.* New York: Taylor and Francis Group.

Yeong-Shyung, C., Armstrong, T.R. (1999). Lattice expansion induced stresses in Calcuim-doped Yttrium Chromite interconnect materials under reducing environment. *Processing and characterization of electrochemical materials and devices*. Ceram.Trans., 95 – 104.

Zener C. (1951). Interaction between the d-shells in the transition metals. American physical society. Phys. Rev. 81, 440 – 444.

APPENDIX A

Comparative assessment of the manufacture of SOFC cathodes: Electroless nickel co-deposition vs Screen printing

A.1 Required equipment

- Electroless Nickel Co-deposition (ECD)

(i) Hot plate (480 watts): Heating electroless nickel and other pre-treatment chemicals to required temperature. Hot plate ramp rate is 5^{o}C per min.

(ii) Overhead stirrer* (70 watts): To avoid LSM attraction to the magnetic stirrer during deposition

** Not required for anode manufacture as YSZ is not ferromagnetic.*

- Screen printing

(i) Heating furnace (4,800 watts): Organic vehicle burn off and sintering of produced cathode. Furnace ramp rate is 20^{o}C per min.

(ii) Hot plate (480 watts): To dissolve polymer prior to mixing with organic vehicle.

(iii) Ball milling machine (3,840 watts): Mixing of polymer, organic vehicle & ceramic to form screen printing ink.

(iv) Screen printing machine (non-visual alignment) (1,800 watts): Coating of the electrolyte with the cathode (or anode).

(v) Vacuum pump (1/2hp (373 watts)): Holds the substrate in place. A vacuum pump capable creating at least 25 inhg (12.27 psi) vacuum is needed for the above screen printer type.

(vi) Compressor (3hp (2,238)): Supplies air pressure to drive the screen printer's hydraulics. A compressor capable of supplying 6scfm (169.92 ltr/min) of air at a pressure of 80 psi (5.5bar) to a Semi-automatic screen printer (e.g. Presco model 465) is required.

A.2 Material & Equipment cost

(a) ECD

	General cost	Amount required	Cost for quantity required
Material			
LSM powder	£612 per kg	5g	£3.06
4-step pre-treatment chemicals	£5.07per litre	400 ml	£2.40

Equipment

Overhead stirrer *	£ 937	-	£937
Heater	£ 358.20	-	£358.20

Total cost of materials and equipment required for ECD £ 1,300.66

**can be substituted with an air bubbler or completely removed if LSM can be deposited without being attracted to the magnetic stirrer*.

(b) Screen printing

	General cost	Amount required	Cost for quantity required
Material			
LSM powder	£612 per kg	6g	£4.92
Ethyl cellulose	£14 per 5g	0.48g	£1.34
Terpineol	£44 per 1kg	7.52g	£ 0.33

Equipment

Heating furnace	£1,060	-	£1,060
Heater and magnetic stirrer	£358.20	-	£358.20
Ball milling machine	£1,796.40	-	£1,796.40
Screen printing machine*	£12,000	-	£12,000
Vacuum pump	£373	-	£373
Compressed air (compressor)	£489.96	-	£489.96

Total cost of materials and equipment required for screen printing £16,078

***** *This price reflects a low cost non-visual aligning screen printer as visually aligned and more accurate screen printers could range even higher than £120,000.*

A.3 Manufacturing process energy consumption

This step is determined from the length of time an equipment is used. Energy used up in the cathode manufacturing process is determined from equations (i) and (iv) below.

- Useful equations

Equipment wattage X usage time = minimum energy input _____ i

1 Kw.hr = 3.6 MJ _____ ii

1 Horse power = 0.746 kw _____ iii

Minimum energy input X cost per Kw.hr (£/kw.hr) = cost of energy _____ iv

Approx. cost of energy = 0.23 per Kw.hr _____ v

- Calculations

ECD

Equipment	Total time used	Energy consumption from equ.(i),(ii) and table A.2(a)	Cost of energy from equ.(iv) & (v)
Overhead stirrer	60 mins	0.252 MJ	£0.02
Heater	130 mins	3.744 MJ	£0.24
Total		3.99 MJ	£0.26

Screen printing

Equipment	Total time used (Minutes)	Energy consumption (MJ) from equ.(i),(ii)(iii) and table A.2(b)	Cost (£) of energy from equ.(iv) & (v)
Heater	7	0.2	0.2
Heating furnace	269	77.47	4.99
Ball milling machine	5	1.152	0.074
Screen printer	3	0.32	0.021
Vacuum pump	5	0.11	0.007
Compressor	5	0.67	0.043
Total		79.9 MJ	£5.15

A.5 At a glance

	Electroless nickel co-deposition	Screen printing
Process manufacturing energy	4MJ	79.9MJ
Energy cost to manufacture single electrode	£0.26	£5.15
Minimum material and equipment cost for first electrode	£1,311	£16,079
Time taken to manufacture first electrode	2 hrs	5 hrs

APPENDIX B

COSHH assessment for pre-treatment chemicals and plating solution

---

(i) Process details

- Storage, handling and disposal of pre-treatment chemicals, ceramic powders and plating solution

(ii) Equipment used for the processes

- Large beakers, plastic tubs, gloves, safety glasses, laboratory coats and face masks.

(iii) Substances disposed of

- Cuprolite, pre-catalyst, catalyst and Niplast at 78 and electroless nickel plating solution.

(iv) Notes

Chemical	MSDS source and date	Colour & state of substance	Comments	Main hazardous compound(s) (if any)
Cuprolite	Alfachimici S.p.A, 08/02/2006, Version 7	Colourless liquid	- Toxic in nature and is a threat to the environment - Not easily biodegradable - Is bioaccumulable - Low skin irritation	- 90% - 100% Alkyl amine ethoxylate
Uniphase PHP A salt	Alfachimici S.p.A, 20/12/1996, Version 2	White powder	No specific hazards associated with this product under normal use.	- Does not contain substances with significant toxicology
Chemical	MSDS source and date	Colour & state of substance	Comments	Main hazardous compound(s) (if any)

Uniphase PHP B	Alfachimici S.p.A, 29/06/2005, Version 5	- Dark brown solution -Colourless when expired	- Product is corrosive. - Can cause irritation of the airway. - may generate flammable gases on contact with dithiocarbamates, mercaptans and other organic sulphides, elementary metals (alkalis, alkaline earth, powder alloys, vapours), and powerful reducing agents - may generate toxic gases on contact with inorganic fluorides, halogenated organic substances, sulphides, nitrides, nitriles, organophosphates and powerful oxidising agents. - may catch fire on contact with dithiocarbamates, elementary metals (alkali, alkaline earth, powder alloys, vapours, sheets or bars), and nitrides.	- 27% hydrochloric acid
Electroless nickel plating solution	Schloetter plating technology 06/10/2005	Green	- Limited evidence of a carcinogenic effect - Toxic to aquatic organisms. - Causes burns - Irritating to respiratory system	N/A

(iv) Control measures

- Respiratory protection, personal protection equipment (e.g Safety glasses, gloves and laboratory coat)

(v) Emergency procedures.

Before seeking medical assistance the following processes may be adhered to

- If contact is made with the skin, wash the area suspected of having made contact with the toxic solution immediately

- If contact is made with the eyes, wash immediately and thoroughly with running water, keeping eyelids raised, for at least 10 minutes. Following this, protect the eyes with sterile gauze or a clean, dry, handkerchief.

- if swallowed, do not induce vomiting. Seek medical help immediately.

- In the event of a fire, use extinguishers based on water, CO2, foam or chemical powders

(vi) Overall assessment of risk

- Can the process or any hazardous substance be eliminated at all – No
- Can the process or substance be substituted with a less hazardous alternative - No
- Will any of the process present significant risks to health if no controls were in place – yes
- Are the control measures presently in place adequate - yes

(vii) Conclusion

The risk associated with the process is high due to the hazardous nature of the substances used. However with the use of standard personal protection equipment, the risks can be adequately controlled.

Appendix C:

Risk assessment of electroless nickel ceramic co-deposition of solid oxide fuel cell electrodes

Hazards identified	Nature of possible harm	Steps required to prevent harm
Highly corrosive and toxic nature of pre-treatment and plating solutions (See COSHH page)	- Can cause damage to the skin or burns of varying degrees of severity if contact is made with them. - Risk of serious damage to the eyes	- Always use personal protective equipment such as gloves, laboratory coat and safety glasses, when handling the chemicals.
Hydrogen evolution during plating	Inhalation of dangerous gases which may be carcinogenic.	- Use of fume cupboard is mandatory during plating. - Face mask is recommended but not essential during plating and solution preparation.
Spill during plating due to bubbling and expansion of the solution as a result of applied heat and trapped gases/air.	Can cause damage to the skin or eyes.	- Use of personal protective equipment during plating.
Ingestion	Possibility of provoking strong corrosion of the buccal cavity and of the pharyns with risk of esophagus and stomach perforation.	- Do not consume and avoid consuming any edible substance while in the laboratory as this might get contaminated before consumption.
Very hot surface of hotplate during plating (about 125^{o}C)	Burns to the skin	Operator must be fully alert and well trained on how to operate any hotplate being

		used.
Explosion	Extensive damage to the skin and organs	Avoid pressure build in storage containers by leaving storage container covers slightly open. This prevents build up of hydrogen gas which continues to evolve after and plating and may cause explosion at high pressures.